Polarization measurement of synchrotron radiation with use of multilayers in the soft x-ray region

Hiroaki Kimura

Doctor of Philosophy

Department of Synchrotron Radiation Science
School of Mathematical and Physical Science
The Graduate University for Advanced Studies

1992

Contents

I. Introduction 1

1-1. Background of the research 1

1-2. What has been done before the present research 2

1-3. Methods of polarization measurement 3

1-4. Aim of this research 4

II. Description of the polarization of light 5

2-1. The Stokes parameters 6

2-2. The Mueller matrices 8

2-3. The Poincaré sphere and the parameters of the polarization ellipse 10

2-4. The degree of linear and circular polarization 14

III. Principles of measurement in the present research 16

3-1. Principle of rotating-analyzer ellipsometry 16

3-2. Multilayer polarizer and analyzer 19

3-3. Principle of rotating-analyzer ellipsometry with phase shifter 22

3-4. Multilayer phase shifter 28

IV. How to minimize and evaluate the experimental error 33

4-1. Rotating-analyzer ellipsometry 33

4-2. Rotating-analyzer ellipsometry with phase shifter 34

V. Design and construction of ELLI 38

5-1. Specifications to meet the demands 38

5-2. Required accuracy of the mechanism 40

5-2-1. Azimuthal angle 40

5-2-2. Incident angle 40

5-3. Structure of ELLI 41

VI. Performance of ELLI 52
6-1. Mechanism 52
6-2. Vacuum 52
6-3. Control system 53

VII. Polarization measurements and the results 54
7-1. Beamline description 54
7-1-1. PF BL-28A 54
7-1-2. PF BL-18A 56
7-2. Characterization of the polarization elements 58
7-2-1. Measurement of the polarizance of the analyzer 58
7-2-2. Measurement of phase shifter 61
7-3. Rotating-analyzer ellipsometry with phase shifter (RAEP) 63
7-3-1. Linear undulator 63
7-3-2. Bending magnet 71
7-3-3. Helical undulator 75
7-4. Rotating-analyzer ellipsometry (RAE) at BL-28A 79
7-4-1. Linear undulator 79
7-4-2. Helical undulator 80
7-5. Rotating-analyzer ellipsometry (RAE) at BL-18A 83
7-5-1. Dependence on the vertical observation angle varied by moving the diaphragm 83
7-5-2. Dependence on the vertical observation angle varied by tilting the first mirror 85
7-5-3. Dependence on the acceptance of the vertical observation angle 87
7-5-4. Dependence on a portion of the beam cross section 87
7-6. Rotating-analyzer ellipsometry (RAE) at SOR-RING BL-1' 90

VIII. Discussion 92
8-1. The beamline ellipsometer ELLI 94
8-2. Multilayers as polarization elements 94
8-3. Analytical method of rotating-analyzer ellipsometry with phase shifter 95
8-4. The major axis of the polarization ellipse (δ) and the degree of linear polarization (P_L) of the light emerging from the monochromator at a bending magnet beamline 95
IX. Conclusion 98
X. Acknowledgements 100
XI. References 101

I. Introduction

1-1. Background of the research

Besides the two important features of synchrotron radiation (SR) namely the high brightness and the continuity of the spectrum from vacuum ultraviolet (VUV) to hard x-rays (HX), its polarization characteristic is also important. Utilization of polarized probe light, such as linearly or circularly polarized light, gives us further information on the symmetry of materials through the observed phenomena.

SR from a bending magnet section is linearly polarized in the plane of the electron or positron orbit. It is also well known that SR is elliptically polarized above and below the orbit plane. As circularly polarized SR, the off-axis SR[1A] from a bending magnet or SR from a special insertion device[1B] is provided. For quantitative analysis of experimental data using these light sources, it is indispensable to know accurate information about the actual polarization state of the light emerging from a monochromator.

In other words, the development of the polarization measurement can be associated with the development of polarization elements. Two types of polarization elements have been used so far for SR. A polarizer composed of several Au coated mirrors has been used in the VUV region. For example, typical values of throughput and polarizance (degree of polarizing power) of the polarizer are 5% and 0.85, respectively, for light with wavelength 30 nm[1C], and has no more effect in the x-ray region. In the HX region a crystal set at a 45° Bragg angle can work as a polarizer. The lattice constant of a good crystal is smaller than 20Å which is much smaller than the wavelength in the soft x-ray (SX) region. Therefore, it is very difficult to do a polarization measurement by use of conventional

VUV polarizers or crystals in SX region, because their throughput and polarizance become poor. Consequently polarization measurement of SR has been also very difficult in the SX region. Due to the lack of readily available SX polarizers, many polarization-sensitive SX experiments have been carried out by simply assuming that the results of theoretical calculations do not change so much in practical beamlines.

The above difficulty in polarization measurement in SX region could be overcome by utilizing soft x-ray multilayer polarizers[1D], because of the reason given in the following section.

1-2. What has been done before the present research

In the last years, multilayer mirrors for SX have been developed extensively. Their application to SX polarizers has been proposed, because they have high throughput and high polarizance in the vicinity of an angle of incidence of 45°. For example, typical values of throughput and polarizance of our Ru/Si multilayer are ~20% and 0.99 for wavelength of 17.0 nm[1E], respectively. Accuracy in the polarization measurement depends largely on the polarizance of an analyzer, which is a kind of polarizer. Therefore, multilayer polarizers would provide us with much more accurate results in the SX region than conventional VUV polarizers.

Khandar et. al[1F] and Gluskin et. al[1G] reported on the experiments of multilayer polarizer, although they presented just a typical polarization signal obtained by rotating the multilayer analyzers which were not characterized. Khandar et al.[1H,1I] measured, by rotating a Nb/Si-multilayer analyzer, the degree of linear polarization (P_L) of SR of 15.4-nm wavelength emerging from a grazing incidence monochromator at a beamline of the ACO storage ring. Their attempt had a limited success, giving only the minimum value of the degree of linear polarization for a

particular setting of the beamline optics used. Alexandrov et al.[1J] studied, at wavelengths 22–30 nm, the polarizance of a Mo/Si multilayer at angles of incidence around 45° by means of photographic detection, which is notorious for poor linearity.

Yamamoto et al[1K]. presented an example of a multilayer functioning as a phase shifter. Kimura et al.[1L] measured, with the use of Ru/Si–multilayer phase shifter and analyzer, the state of polarization of SR with 12.8–nm wavelength at the Photon Factory, obtaining full information concerning the state of polarization of SR at various different conditions.

1–3. Methods of polarization measurement

The polarization state of SR was measured in the visible region by Codling et al.[1M] using the Nicol prism at NBS. They measured the intensity of vertical and horizontal component of the light and reported that the agreement between theoretical distributions and observed experimentally is good.

Suitable quarter–wave plates in the VUV region have not been so far developed. Rosenbaum et al.[1N] used two conventional VUV polarizer (analyzer), and determined P_L of SR of wavelength 40–100 nm at DESY by measuring the transmitted intensity for four independent combinations of azimuth of polarizers. Heinzmann[1A,1O] measured P_L of SR of the same wavelength at BESSY by rotating–analyzer ellipsometry (RAE) using such a conventional VUV polarizer (analyzer). He calculated the degree of circular polarization (P_C) on the assumption $P_L^2+P_C^2 = 1$, which means the degree of polarization equals unity.

Schledermann et al.[1P] proposed to use a single mirror or a conven–tional VUV polarizer as a phase shifter by utilizing its retardation upon reflections. Westerveld et al.[1Q] created circularly polarized light from

linear polarization light using single mirror phase shifter and evaluated its polarization state by RAE using the single mirror analyzer. Gaupp et al.[1R] and Koide et al.[1C,1S] constructed their respective ellipsometers and carried out polarization measurements using such VUV polarizers at a wavelength of 80 nm and in a range of 15.5–49.6 nm, respectively. By measuring the intensity of transmitted light for several independent combinations of azimuthal angles of a phase shifter and an analyzer, they completely determined the state of polarization of light.

In the HX region, Ishikawa et al.[1T] carried out complete determination of the polarization states using a multiple crystal diffractometer. By means of RAE with phase shifter for different conditions of the phase shifter, states of the light beam emitted from the elliptical wiggler installed on the TRISTAN Accumulator Ring were measured at wavelengths of around 0.15 nm.

Kimura et al.[1J] performed polarization measurements in the SX region at wavelength 12.8 nm using two multilayers as a phase shifter and an analyzer. From the phase information, they determined parameters of the polarization ellipse except the degree of polarization.

1-4. Aim of this research

Our study on the polarization measurement to determine all the parameters of polarization state in the SX region, has the following goals:

(1)To develop a beamline ellipsometer using soft x-ray multilayer mirrors under ultra high vacuum.

(2)To develop and evaluate a method of polarization measurement with imperfect quarter-wave plate and imperfect analyzer.

(3)To study the polarization state of the light from a bending magnet and an undulator in the SX region.

II. Description of the polarization of light

There are several other cases in optics in which alternative conventions are possible and all of them are found in the literature. We obey here the convention suggested by Second International Conference on Ellipsometry, Nebraska convention[2A]. This convention is given in Table 2–1.

Table 2–1. Preferred Conventions for Optical Parameters

Electric field strength	$\mathbf{E}=\mathbf{E}_0\exp i(\omega t+\delta)\exp(-i\mathbf{k}\cdot\mathbf{r})\exp(-az/2)$
Complex index of refraction	$\tilde{n}=n-ik$
Complex relative amplitude attenuation on reflection	$\rho=\tilde{r}_p/\tilde{r}_s$
Relative phase change on reflection (Retardation)	$\Delta=\delta_p-\delta_s$

In Table 2–1, $\mathbf{E}$ is the electric field vector of a traveling wave, $\mathbf{E}_0$ is the amplitude of the wave, ω is the angular frequency of the wave, t is the time, δ is the phase angle, $\mathbf{k}$ is the wave vector, $\mathbf{r}$ is the position vector, a is the absorption coefficient, z is the direction of traveling of the wave, n is the index of refraction and k is the extinction coefficient, and $r_p(r_s)$ is the amplitude reflectance for p–(s–) component. Please note signs of ωt, $\mathbf{k}\cdot\mathbf{r}$, and k.

The most common forms to describe the polarization state of light are the Stokes parameters and the Jones parameters. Their matrix calculations are called Mueller calculation and Jones calculation, respectively. The Jones

parameters can describe only perfectly polarized light. The Stokes parameters can also describe partially polarized light. In this paper, we use the Stokes parameters (vector), the Mueller matrices, the Poincaré sphere, and the parameters of polarization ellipse for easy understanding.

The history of these polarization calculation techniques is presented in the following[2B].

1852 The Stokes parameters were proposed by the English physicist George G. Stokes.

1892 The Poincaré sphere was invented by the French mathematician Henri Poincaré to describe a polarization state.

1940 The Jones vector and Jones matrix calculation were invented by the American physicist Robert Clark Jones.

1942 Using matrices of 4×4, the American physicist, Hans Mueller, explained well the problem related to polarization or partial polarization.

2-1. The Stokes parameters

The Stokes parameters have four components, S_0, S_1, S_2, and S_3. All of them have the dimension of an intensity of light and can be measured using a perfect quarter-wave plate and a perfect analyzer. The perfect quarter-wave plate is an element in which phase retardation equals 90° and the reflectances or transmittances for s- and p-component equal unity. The perfect analyzer is an element in which the reflectance or transmittance for s- component equals unity and that for p-component equals zero.

We measure here the intensity of the light through the analyzer in which the major transmitting axis is along an azimuth η and the intensity through the quarter-wave plate in which the slow axis is horizontal. The azimuth is measured counterclockwise (CCW) from the horizontal plane when an

observer faces the beam. In the following equations $I(\eta,0°)$ denotes the intensity of the light measured through the analyzer set at azimuth η and $I(\eta,90°)$ denotes the intensity measured through the quarter-wave plate and the analyzer. $I(0°,0°)$ equals the sum of the intensity of horizontally linearly polarized component and a half of the intensity of unpolarized component. $I(-45°,90°)$ equals the sum of the right-handed circularly polarized component and a half of the intensity of unpolarized component. The Stokes parameters are thus obtained by

$$\begin{aligned} S_0 &= I(0°,0°) + I(90°,0°) \\ S_1 &= I(0°,0°) - I(90°,0°) \\ S_2 &= I(45°,0°) - I(-45°,0°) \\ S_3 &= I(-45°,90°) - I(45°,90°) . \end{aligned} \qquad (2\text{-}1\text{-}1)$$

Evidently S_0 represents the total intensity of the light beam. S_1 is equal to the excess in intensity of the light of the horizontally linearly (azimuth equal to 0°) polarized component over the light of the vertically linearly (azimuth equal to 90°) polarized component. S_2 has a similar interpretation with respect to the azimuths equal to 45° and –45°. Finally, S_3 gives the excess in intensity of light transmitted through a device which accepts right–handed circular polarization, over that transmitted by a device which accepts left–handed circular polarization. The right– (CW) or left–handedness (CCW) is defined with the direction of rotation of the electric vector of the light facing the light beam.

These components satisfy the following condition, when the light is perfectly polarized,

$$S_0^2 = S_1^2 + S_2^2 + S_3^2. \qquad (2\text{-}1\text{-}2)$$

If the beam is partially polarized,

$$S_0^2 > S_1^2 + S_2^2 + S_3^2. \qquad (2\text{-}1\text{-}3)$$

Then the ratio between the perfectly polarized component and the total intensity of light is defined, by the following equation, introducing the degree of polarization V,

$$V = \frac{\sqrt{S_1^2+S_2^2+S_3^2}}{S_0}. \qquad (2\text{-}1\text{-}4)$$

Evidently, the value of V of perfectly polarized light equals unity.

Since in many cases the polarization state is more important than the absolute intensity, it is convenient to use the normalized Stokes parameters by normalizing all parameters by S_0, which means that the normalized S_0 equals unity.

2-2. The Mueller matrices

Any polarization element can be described by a Mueller matrix which transforms the Stokes parameters of the incident light into other Stokes parameters.

The Stokes vector *S* is composed of the Stokes parameters,

$$S = \begin{pmatrix} S_0 \\ S_1 \\ S_2 \\ S_3 \end{pmatrix}. \qquad (2\text{-}2\text{-}1)$$

An azimuth rotator *R* is represented by

$$R(\theta)=\begin{pmatrix}1 & 0 & 0 & 0\\ 0 & \cos 2\theta & -\sin 2\theta & 0\\ 0 & \sin 2\theta & \cos 2\theta & 0\\ 0 & 0 & 0 & 1\end{pmatrix}, \qquad (2\text{-}2\text{-}2)$$

where θ is the azimuthal angle.

A partial polarizer P, in which the major transmitting axis (s– axis) is along S_1 direction, is represented by

$$P(\alpha)=\frac{1}{2}\begin{pmatrix}r_s^2+r_p^2 & r_s^2-r_p^2 & 0 & 0\\ r_s^2-r_p^2 & r_s^2+r_p^2 & 0 & 0\\ 0 & 0 & 2r_sr_p & 0\\ 0 & 0 & 0 & 2r_sr_p\end{pmatrix}$$

$$=\frac{r_p^2}{2}\begin{pmatrix}\alpha^2+1 & \alpha^2-1 & 0 & 0\\ \alpha^2-1 & \alpha^2+1 & 0 & 0\\ 0 & 0 & 2\alpha & 0\\ 0 & 0 & 0 & 2\alpha\end{pmatrix}, \qquad (2\text{-}2\text{-}3)$$

where α is the ratio of amplitude reflectances or transmittances of P between s– and p–components, and equals r_s/r_p. A polarizer and an analyzer are essentially identical polarization elements. In this paper the polarizer located just before the detector is called analyzer.

A phase shifter Q, in which the slow axis (s–axis) is along S_1 direction, is represented by

$$Q(\Delta)=\begin{pmatrix}1 & 0 & 0 & 0\\ 0 & 1 & 0 & 0\\ 0 & 0 & \cos\Delta & -\sin\Delta\\ 0 & 0 & \sin\Delta & \cos\Delta\end{pmatrix}, \qquad (2\text{-}2\text{-}4)$$

where Δ is the retardation angle upon reflection or transmission defined by the difference between the phase angles, $\Delta_p - \Delta_s$.

A complex element which works both as a polarizer and a phase shifter, such as a reflecting surface, can be written with the product of $P(\alpha)$ and $Q(\Delta)$ as

$$M(\alpha,\Delta) = \frac{r_p^2}{2}\begin{pmatrix} \alpha^2+1 & \alpha^2-1 & 0 & 0 \\ \alpha^2-1 & \alpha^2+1 & 0 & 0 \\ 0 & 0 & 2\alpha\cos\Delta & -2\alpha\sin\Delta \\ 0 & 0 & 2\alpha\sin\Delta & 2\alpha\cos\Delta \end{pmatrix} . \qquad (2\text{-}2\text{-}5)$$

For example, the Stokes vector S' of the light reflected by an optical element described by $M(\alpha,\Delta)$ set with the azimuth χ is expressed as

$$S' = R(\chi)\cdot M(\alpha,\Delta)\cdot R(-\chi)\cdot S \quad . \qquad (2\text{-}2\text{-}6)$$

2-3. The Poincaré sphere and the parameters of the polarization ellipse

The three components of the Stokes vectors S_1, S_2, and S_3 can be represented simply with right-handed three-dimensional Cartesian coordinates of a point on or in the Poincaré sphere, and S_0 is equal to the radius of the sphere. S_3 points toward the North (upper) pole of the sphere (See Fig. 2-1).

The vector S is described by using the radius S_0, the degree of polarization V, a latitude L_a and a longitude L_o,

$$\begin{aligned} S_1 &= S_0 V\cos L_a \cdot \cos L_o, \\ S_2 &= S_0 V\cos L_a \cdot \sin L_o, \\ S_3 &= S_0 V\sin L_a. \end{aligned} \qquad (2\text{-}3\text{-}1)$$

L_a and L_o can be expressed by the polarization ellipse with the following

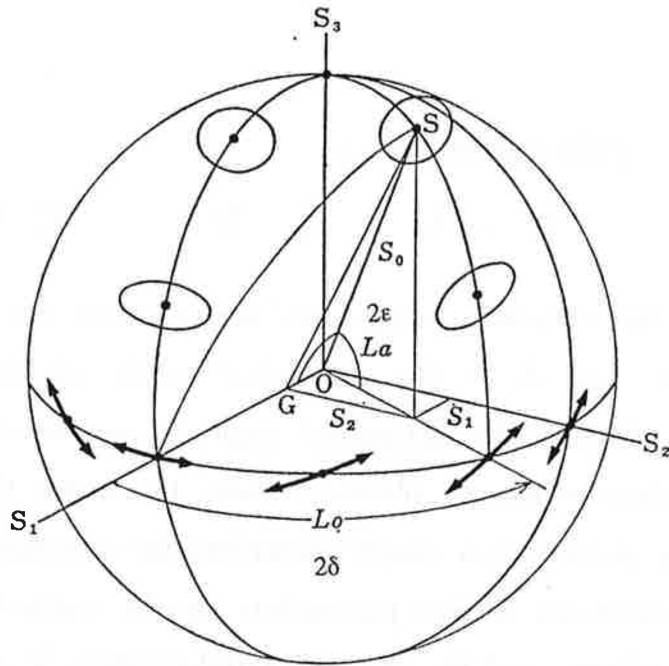

Figure 2–1. The Poincaré sphere. (V=1)

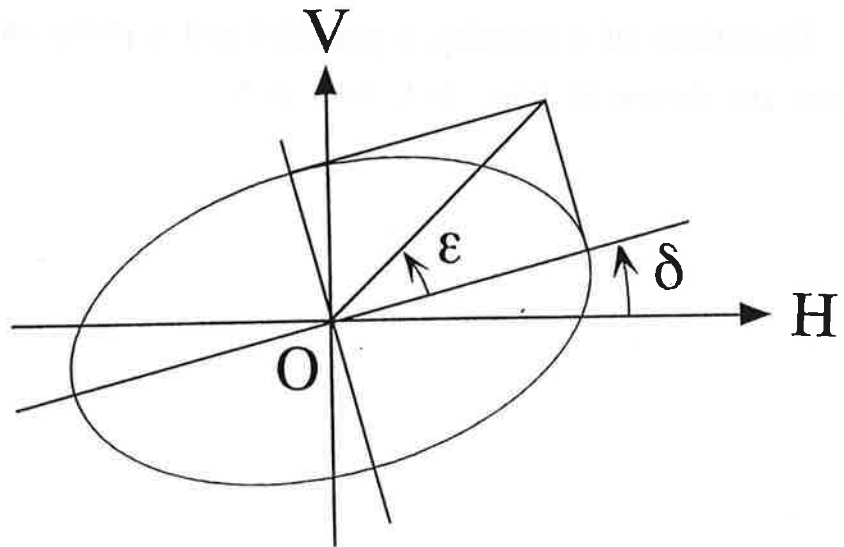

Figure 2–2. The polarization ellipse and the parameters of ellipse.

parameters of polarization ellipse,

$$L_a = 2\delta, \qquad L_o = 2\varepsilon, \qquad (2\text{-}3\text{-}2)$$

where ε is the ellipticity angle($-45° \le \varepsilon \le 45°$, $\varepsilon > 0$ for right-handed, $\varepsilon < 0$ for left-handed), and δ is the azimuthal angle of the major axis of the polarization ellipse. The azimuthal angle is measured CCW concerning the horizontal plane when an observer faces the beam (See Fig. 2-2). Please note that the polarization ellipse describes the polarized component only.

The normalized Stokes parameters can be expressed with parameters of polarization ellipse and the degree of polarization V as

$$\begin{aligned} S_0 &= 1, \\ S_1 &= V\cos2\varepsilon\cdot\cos2\delta, \\ S_2 &= V\cos2\varepsilon\cdot\sin2\delta, \\ S_3 &= V\sin2\varepsilon. \end{aligned} \qquad (2\text{-}3\text{-}3)$$

Operations of a retarder, a polarizer and a phase shifter on the Poincaré sphere are shown in Figs. 2-3, 2-4, 2-5.

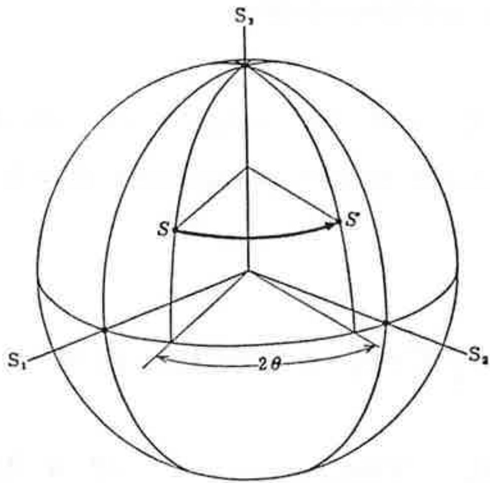

Figure 2–3.
The operation of a retarder having an azimuth θ.

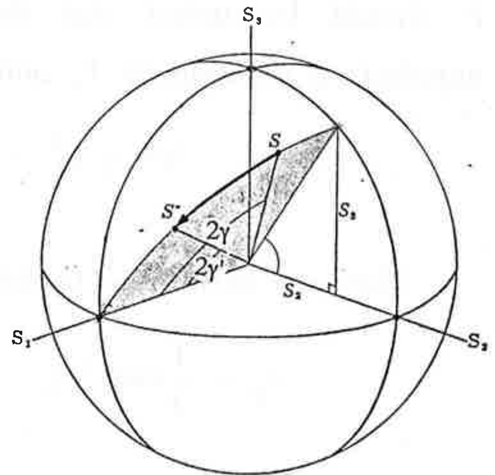

Figure 2–4.
The operation of a polarizer having an amplitude reflectance ratio α, r_s/r_p, in which the major transmitting axis (s– axis) is along S_1 direction.
α=tanγ/tanγ'.

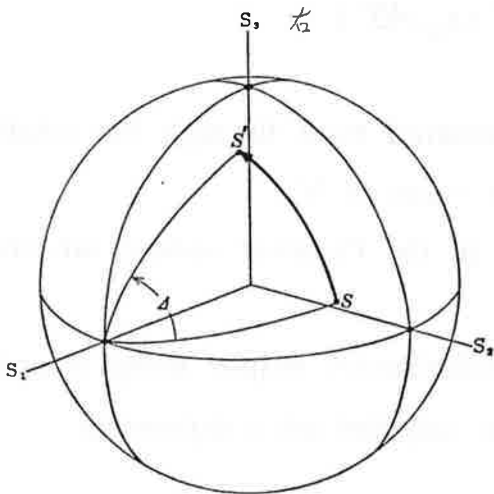

Figure 2–5.
The operation of a phase shifter having a retardation Δ, $\Delta_p-\Delta_s$, in which the slow axis is along S_1 direction.

2-4. The degree of linear and circular polarization

The degree of linear polarization P_L and the degree of circular polarization P_C are defined using the normalized Stokes parameters ($S_0=1$) as follows,

$$P_L = \frac{I(\delta,0°)-I(\delta+90°,0°)}{I(\delta,0°)+I(\delta+90°,0°)} = \frac{\sqrt{S_1^2+S_2^2}}{S_0} = \sqrt{S_1^2+S_2^2} = V\cos 2\varepsilon \ , \quad (2\text{-}4\text{-}1)$$

$$P_C = \frac{I(-45°,90°)-I(45°,90°)}{I(-45°,90°)+I(45°,90°)} = \frac{S_3}{S_0} = S_3 = V\sin 2\varepsilon \ . \quad (2\text{-}4\text{-}2)$$

It should be noted that these denominators involve the intensity of unpolarized component. P_L and P_C satisfy the relation as

$$V^2 = P_L^2 + P_C^2 \ . \quad (2\text{-}4\text{-}3)$$

Here we define the pseudo-ellipticity angle ε_p as follows,

$$\varepsilon_p = \frac{1}{2}\cos^{-1}P_L = \frac{1}{2}\cos^{-1}(V\cos 2\varepsilon) \ . \quad (2\text{-}4\text{-}4)$$

$$(0° \le \varepsilon_p \le 45°)$$

It is important to note that ε_p can be measured even through the rotating-analyzer ellipsometry without knowing the value of V.

The descriptions of these parameters in the Poincaré sphere are shown in Fig. 2-6.

Furthermore we define the pseudo-polarization ellipse using δ and ε_p, which describes both the polarized and the unpolarized components.

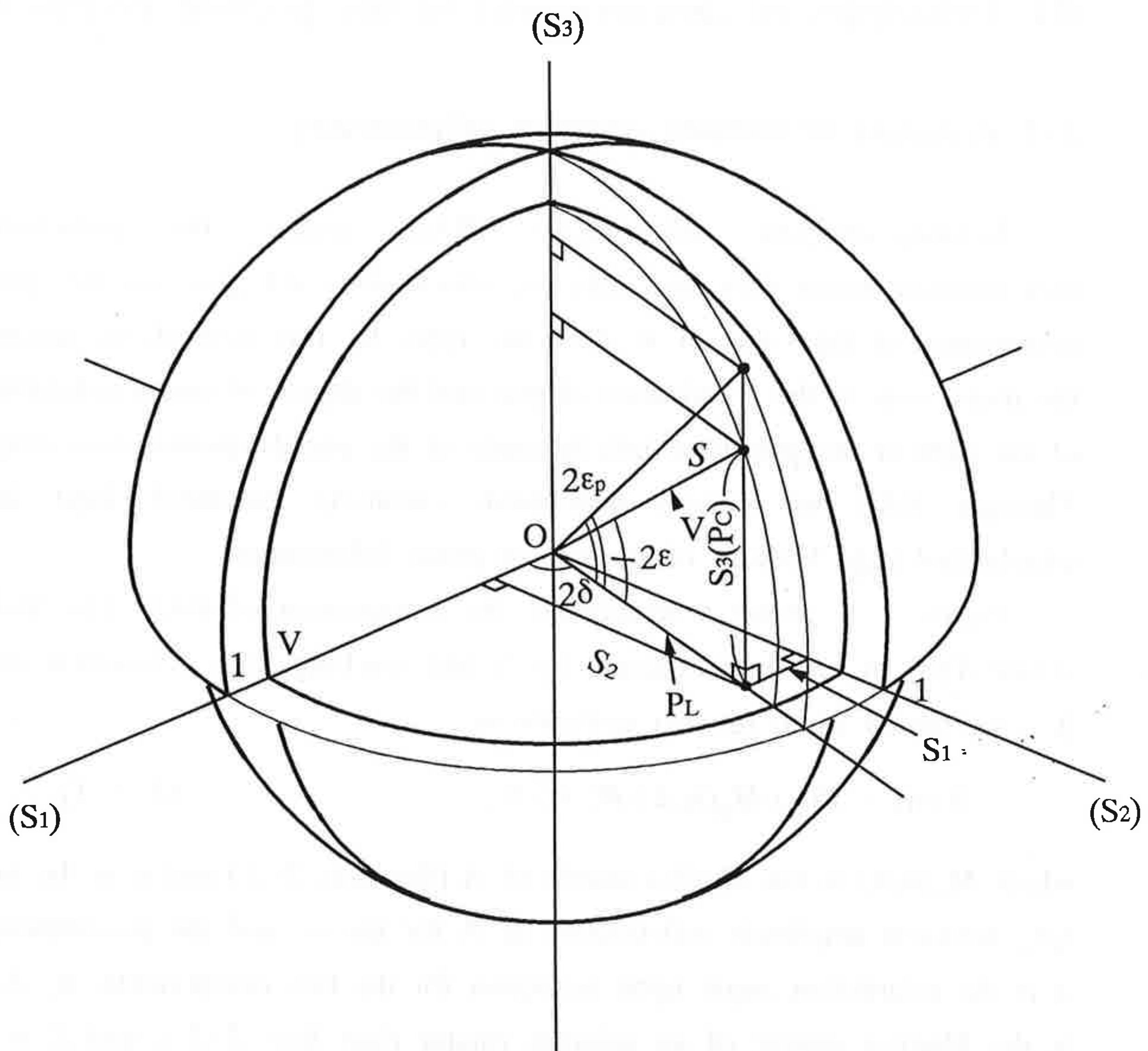

Figure 2-6. The descriptions of polarization parameters in the Poincare shere.

III. Principles of measurement in the present research

3-1. Principle of rotating-analyzer ellipsometry

Rotating-analyzer ellipsometry (RAE) means the polarization measurement using only an analyzer, which does not give us any phase information or the value of V about the light. By this method, we measure the major axis of the polarization ellipse and the degree of linear polarization of the light or the pseudo-ellipticity angle of the pseudo-polarization ellipse. Through RAE we cannot distinguish circularly polarized light from unpolarized light because of absence of phase information.

Figure 3-1 shows schematically the arrangement of RAE. The Stokes vector $S'(\eta)$ of the light reflected by A and reaching D is a function of η. It is expressed using Mueller matrices as

$$S'(\eta) = R(\eta)\cdot M_A(\alpha,\Delta)\cdot R(-\eta)\cdot S\ , \qquad (3\text{-}1\text{-}1)$$

where $M_A(\alpha,\Delta)$ is the Mueller matrix of A (See Sec. 2-2) and α is the ratio, r_s/r_p, between amplitude reflectances of A for the s- and the p-component, Δ is the retardation angle upon reflection for the two components, $\Delta_p-\Delta_s$, R is the Mueller matrix of an azimuth rotator (See Sec. 2-2), and S is the Stokes vector of the incident light.

The intensity $I(\eta)$ of the transmitted light is derived from Eq. (3-1-1),

$$I(\eta) \equiv S'_0(\eta) = \frac{r_p^2}{2}\{S_0(\alpha^2+1)+S_1(\alpha^2-1)\cos 2\eta+S_2(\alpha^2-1)\sin 2\eta\}\ . \qquad (3\text{-}1\text{-}2)$$

The far left matrix R of Eq. (3-1-1) has no effect to S'_0. Transforming the normalized Stokes parameters to the parameters of polarization ellipse and the degree of polarization V, the intensity can be written with

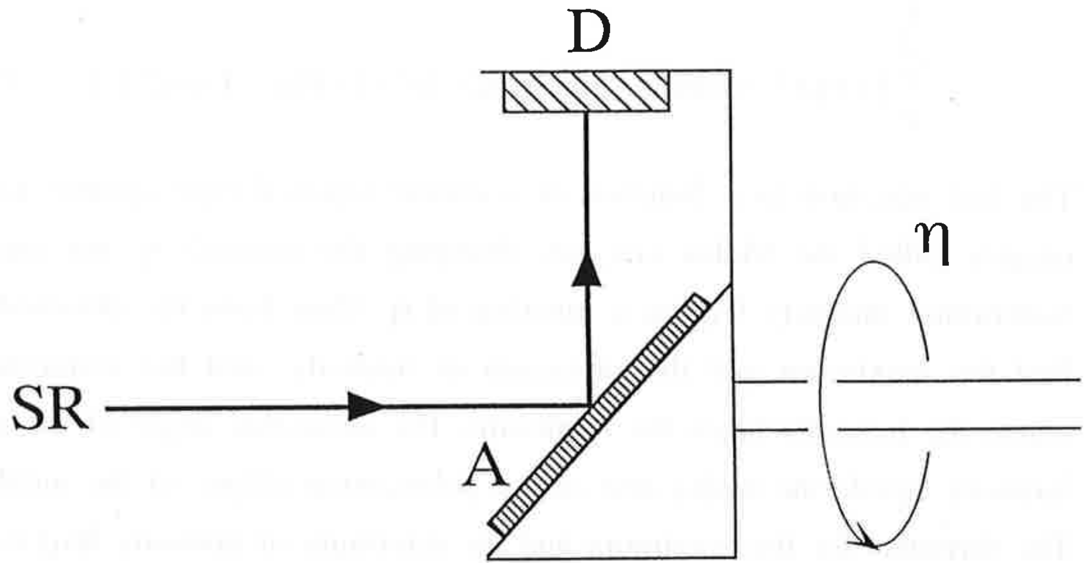

Figure 3-1. Side view of the setup of rotating-analyzer ellipsometry (RAE).

$$I(\eta) = \frac{r_p^2}{2}\{\alpha^2+1+V(\alpha^2-1)(\cos2\varepsilon\cdot\cos2\delta\cdot\cos2\eta+\cos2\varepsilon\cdot\sin2\delta\cdot\sin2\eta)\}$$

$$= \frac{r_p^2}{2}\{\alpha^2+1+V(\alpha^2-1)\cos2\varepsilon\cdot\cos2(\delta-\eta)\}$$

$$= \frac{r_p^2}{2}[2V(\alpha^2-1)\cos2\varepsilon\cdot\cos^2(\delta-\eta)+\{\alpha^2+1-V(\alpha^2-1)\cos2\varepsilon\}] \ . \qquad (3\text{-}1\text{-}3)$$

The last equation is a function of a cosine squared type against azimuth η, namely called the Malus law. By changing the azimuth η, we measure the transmitted intensity $I(\eta)$ as a function of η. Then from the obtained data we find the maximum and the minimum of intensity, and the azimuthal angles where the intensity takes the minimum. The azimuthal angle of the maximum intensity equals the major axis of the polarization ellipse of the incident light. The formulas for the maximum and the minimum of intensity $I(\eta)$ is obtained from Eq. (3–1–3) as follows

$$I_{Max} = \frac{r_p^2}{2}\{(\alpha^2+1)+V(\alpha^2-1)\cos2|\varepsilon|\} \ ,$$

$$I_{Min} = \frac{r_p^2}{2}\{(\alpha^2+1)-V(\alpha^2-1)\cos2|\varepsilon|\} \ . \qquad (3\text{-}1\text{-}4)$$

The contrast factor C_{ont} of the observed $I(\eta)$ is written as

$$C_{ont} \equiv \frac{I_{Max}-I_{Min}}{I_{Max}+I_{Min}} = \frac{(\alpha^2-1)V\cos2\varepsilon}{(\alpha^2+1)} \ . \qquad (3\text{-}1\text{-}5)$$

If we know the polarizance P_{zance}, $(\alpha^2-1)/(\alpha^2+1)$, of the analyzer (See Sec. 3–2), we can obtain the degree of linear polarization P_L or the pseudo–ellipticity angle ε_p of the incident light,

$$P_L = \frac{C_{ont}}{P_{zance}} = V\cos 2\varepsilon = \sqrt{S_1^2 + S_2^2}\ , \tag{3-1-6}$$

$$\varepsilon_p = \frac{1}{2}\cos^{-1}P_L = \frac{1}{2}\cos^{-1}\frac{C_{ont}}{P_{zance}}\ . \tag{3-1-7}$$

P_L and ε_p may involve the offset of unpolarized light component. Here it should be noted again that we cannot measure the value of V through RAE.

3-2. Multilayer polarizer and analyzer

Figure 3-2 shows a calculation s-polarization reflectance R_s, and p-polarization reflectance R_p of a multilayer mirror as function of the incident angle at a wavelength of 12.4 nm. For calculation, we assumed an ideally smooth 10.5 periods Ru/Si multilayer on a silicon substrate. The complex refractive index $\tilde{n}$ and the thickness d, (n–*i*k,d) used for the calculation are (0.9185–*i*0.0056, 3.95 nm) for Ru and (0.9985–*i*0.000433, 5.4 nm) for Si.

Around 45° incidence, a large difference between s- and p-reflectance is clearly seen. These simulation curves demonstrate the good polarization performances of multilayer mirrors in the soft x-ray region.

The polarizance P_{zance} which gives polarization power of polarizers is defined as follows,

$$P_{zance} = \frac{\alpha^2 - 1}{\alpha^2 + 1}\ . \tag{3-2-1}$$

where α is the ratio, r_s/r_p, between the amplitude reflectances for the s- and p-component.

Figure 3-3 shows the experimental setup used for the evaluation of the polarizance of a sample multilayer polarizer. Synchrotron radiation from a monochromator was reflected in the vertical plane by a pre-polarizing multilayer mirror P set at about 45° incidence. The sample multilayer

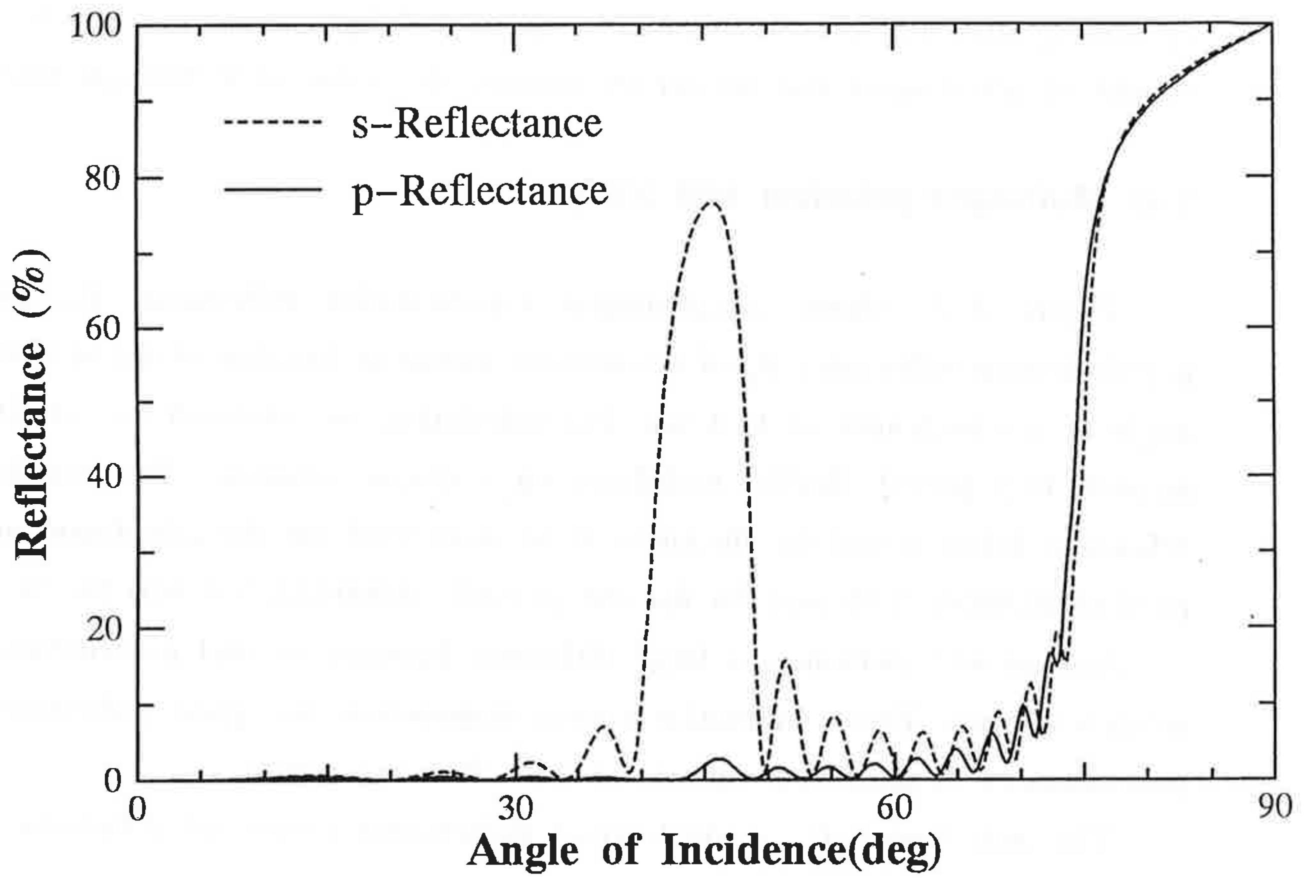

Figure 3–2. The calculating s– and p–reflectance of Ru/Si multilayer at a wavelength of 12.4 nm.

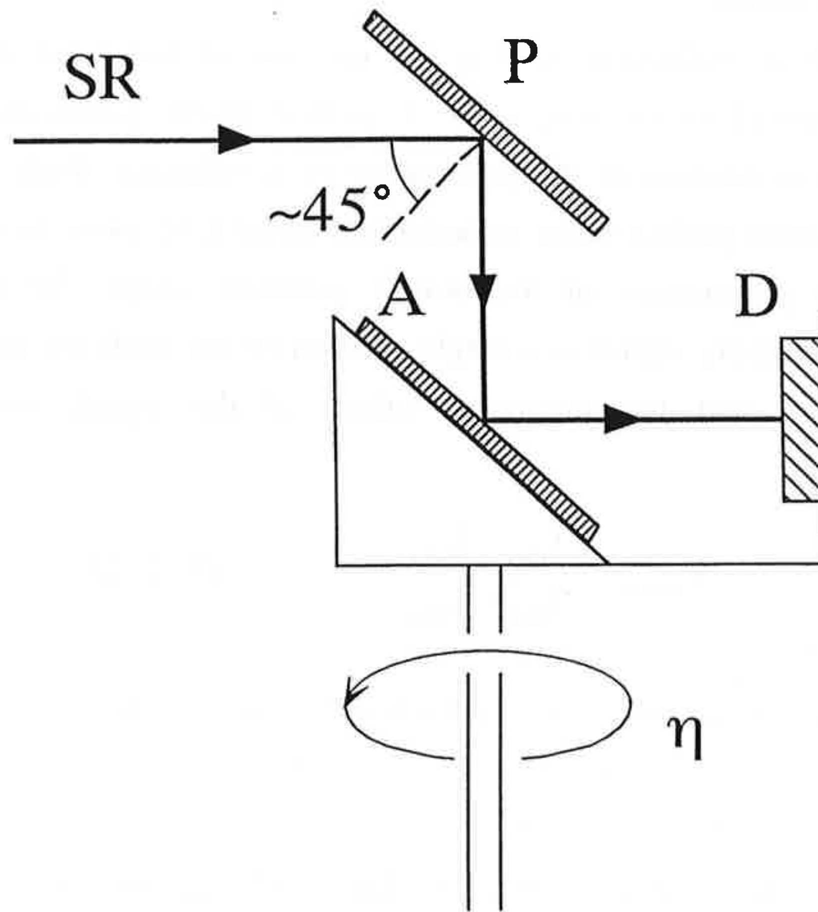

Figure 3-3. Side view of the setup of the polarizance measurement

polarizer is mounted at the analyzer assembly A. The assembly is rotatable around the incident beam from the pre–polarizer. A detector D is fixed to the analyzer assembly rigidly and receives the light reflected by the sample multilayer polarizer.

Through the reflection by P at 45°, the state of linear polarization of the light is improved to be very close to perfect linear polarization, which is essential for evaluation of the polarizance of a polarizer. With such a probe light with almost perfect linear polarization, namely, P_L close to unity, we can measure the polarizance of the sample polarizer simply by recording the sinusoidally varying signal in a single rotation of the analyzer assembly. With the maximum and the minimum values of the signal, we obtain the polarizance by

$$P_{zance} = \frac{I_{Max} - I_{Min}}{I_{Max} + I_{Min}} . \qquad (3-2-2)$$

When a sample polarizer with high polarizance is measured, we must use more highly linearly polarized probe light. The polarizance is always equal to or larger than the degree of linear polarization of the incident light.

The sensitivity of the detector to linear polarization can be described by multiplying a Mueller matrix for the polarizer at the left side of M_A (See Eq. 3–1–1), which is sandwiched between two Mueller matrices of the azimuth rotator. When the polarizance of the analyzer is sufficiently larger than the polarizance induced by the detector sensitivity, these successive operations to the light can be described with a single Mueller matrix of the polarizer. In this case, the effect of phase retardation of M_A does not appear on the measured data. Then the measured data can be fitted to Eq. (3–1–3), and we obtain the polarizance of the analyzer including the polarization sensitivity of the detector. We can use the above polarizance in other RAE measurements, as far as using the same analyzer and the same detector on the same arrangement.

3-3. Principle of rotating-analyzer ellipsometry with phase shifter

Rotating–analyzer ellipsometry with phase shifter (RAEP) means the polarization measurement using a phase shifter and an analyzer, which gives us the phase information as well as the intensity information of the light.

To study the polarization states and characteristics, we conveniently use the complex relative amplitude attenuation ρ defined by the ratio $\tilde{r}_p/\tilde{r}_s$. Figure 3–4 shows a set of complex values of ρ on the complex plane. In the figure the solid line shows ρ of the same multilayer of Sec. 3–2 and the dashed line shows the ordinary monolayer mirror whose complex refractive index is (0.9–*i*0.05), as function of the incident angle measured from normal. They are given by open circles plotted every one degree. In this figure, retardation Δ is the argument and the absolute transmittance ratio $r_p/r_s=1/\alpha$ is the distance from the origin.

Generally the ρ of multilayers have positive retardation in the grazing angle region. In the other region they have a complicate structure compared to monolayer mirrors. The polarization characteristics of multilayers are very much sensitive to the incident angle and to the practical structure of multilayers. Furthermore it is expected that they are also sensitive to the surface condition. Then it is difficult to evaluate them only from theoretical calculation or previously measured data.

In this section we propose a new analytical method. By this measurement, we can determine all the polarization parameters of the light and the polarization parameters of the phase shifter used through the phase information and the contrast factors of the observed sinusoidal signals. The signals are measured by a combination of RAE (See Sec. 3–1) and changes of the azimuth of the phase shifter.

Figure 3–5 shows schematically a side view of the experimental arrangement in RAEP measurement, where P is a phase shifter and A and D is an analyzer–detector assembly, both of which are installed in a vacuum

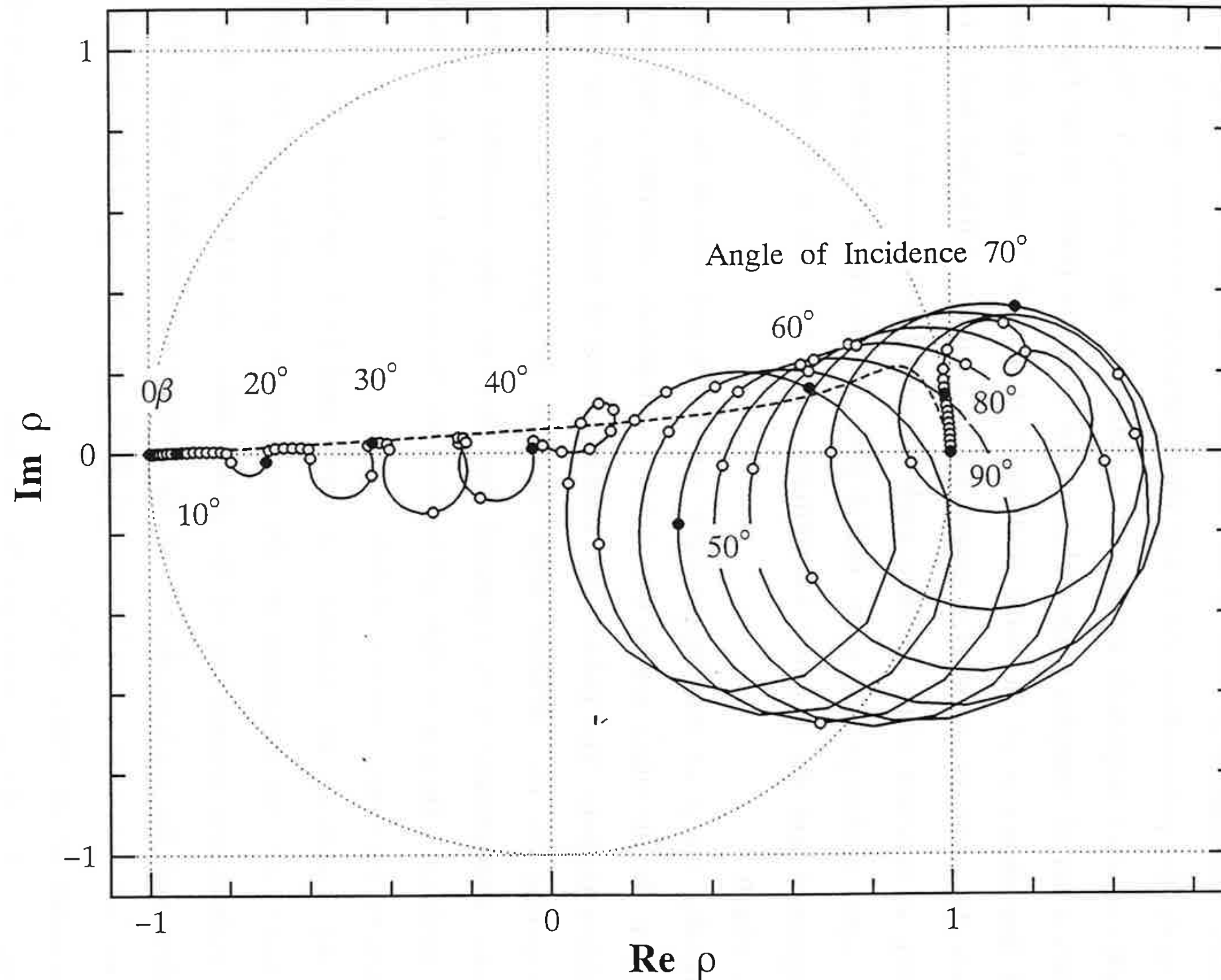

Figure 3–4. The complex relative amplitude attenuation ρ as function of the incident angle measured from normal. The solid line shows ρ of Ru/Si multilayer at a wavelength of 12.4 nm. They are given by open circles plotted every one degree. The dashed line shows ρ of an ordinary monolayer mirror

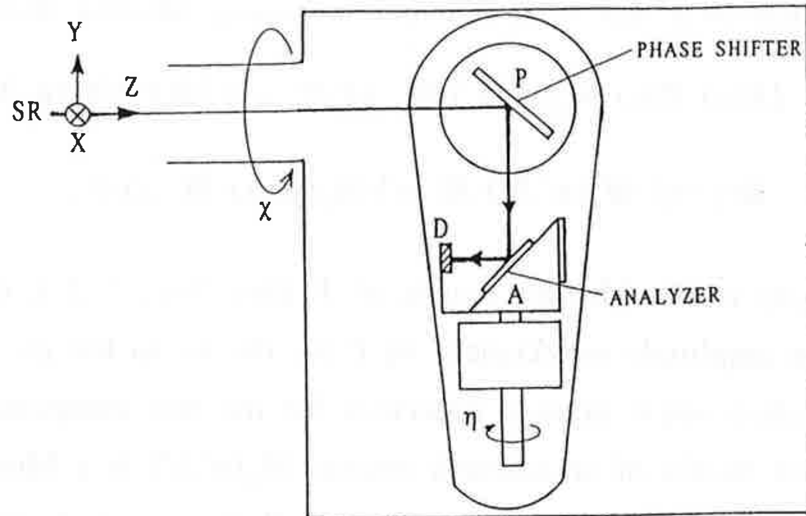

Figure 3–5. Side view of the setup of rotating–analyzer ellipsometry with phase shifter (RAEP).

chamber. The chamber and the analyzer assembly A are rotatable around the incident beam from a monochromator and around the reflected beam from P, respectively. The azimuthal angles χ of P and η of A are measured counterclockwise from the respective positions shown in Fig. 3–5.

The Stokes vector $S''(\chi,\eta)$ of the light reflected by P and A and reaching D is a function of χ and η. It is expressed using Mueller matrices as

$$S''(\chi,\eta) = [R(\chi)\cdot R(\eta)\cdot M_A(\alpha',\Delta')\cdot R(-\eta)\cdot R(-\chi)]\cdot[R(\chi)\cdot M_P(\alpha,\Delta)\cdot R(-\chi)]\cdot S$$

$$= R(\chi+\eta)\cdot M_A(\alpha',\Delta')\cdot R(-\eta)\cdot M_P(\alpha,\Delta)\cdot R(-\chi)\cdot S\ , \qquad (3\text{-}3\text{-}1)$$

where $M_P(\alpha,\Delta)$ is the Mueller matrix of P (See Sec. 3–2), α is the ratio, r_s/r_p, between amplitude reflectances of P for the s– to the p– component, Δ is the retardation angle upon a reflection for the two components, $\Delta_p-\Delta_s$. R is the Mueller matrix of an azimuth rotator. $M_A(\alpha',\Delta')$ is a Mueller matrix of A, $\alpha'=r'_s/r'_p$ where $r'_s(r'_p)$ is an amplitude reflectance of A for the s– (p–) component, and $\Delta'=\Delta'_p-\Delta'_s$. S stands for the Stokes vector of the incident light expressed by

$$S = \begin{pmatrix} S_0 \\ S_1 \\ S_2 \\ S_3 \end{pmatrix} = \begin{pmatrix} 1 \\ V\cos2\delta\cdot\cos2\varepsilon \\ V\sin2\delta\cdot\cos2\varepsilon \\ V\sin2\varepsilon \end{pmatrix}, \qquad (3\text{-}3\text{-}2)$$

where V is a degree of polarization, δ is the azimuth of the major axis of the polarization ellipse, and ε is the ellipticity angle of the ellipse, of the incident light.

The Stokes vector S' reflected from P is derived from Eq. (3–3–1), as

$$S' = M_P(\alpha,\Delta)\cdot R(-\chi)\cdot S$$

$$= \begin{pmatrix} S'_0 \\ S'_1 \\ S'_2 \\ S'_3 \end{pmatrix} = \begin{pmatrix} S_0(\alpha^2+1)+S_1(\alpha^2-1)\cos2\chi+S_2(\alpha^2-1)\sin2\chi \\ S_0(\alpha^2-1)+S_1(\alpha^2+1)\cos2\chi+S_2(\alpha^2+1)\sin2\chi \\ -2S_1\alpha\cos\Delta\cdot\sin2\chi+2S_2\alpha\cos\Delta\cdot\cos2\chi-2S_3\alpha\sin\Delta \\ -2S_1\alpha\sin\Delta\cdot\sin2\chi+2S_2\alpha\sin\Delta\cdot\cos2\chi+2S_3\alpha\cos\Delta \end{pmatrix} . \quad (3\text{-}3\text{-}3)$$

Substituting Eq. (3–3–2) into Eq. (3–3–3) , S' is rewritten using V, δ and ε,

$$S' = \begin{pmatrix} (\alpha^2+1)+V(\alpha^2-1)\cos2\varepsilon\cdot\cos2(\delta-\chi) \\ (\alpha^2-1)+V(\alpha^2+1)\cos2\varepsilon\cdot\cos2(\delta-\chi) \\ 2\alpha V(\cos2\varepsilon\cdot\cos\Delta\cdot\sin2(\delta-\chi)-\sin2\varepsilon\cdot\sin\Delta) \\ 2\alpha V(\cos2\varepsilon\cdot\sin\Delta\cdot\sin2(\delta-\chi)+\sin2\varepsilon\cdot\cos\Delta) \end{pmatrix} . \quad (3\text{-}3\text{-}4)$$

For a fixed azimuth χ^* of P, we do RAE measurement of the S' by changing η. Then we can obtain the azimuth of the major axis η^* and the pseudo–ellipticity angle ε_p^* of S' (See Sec. 3–1). η^* and ε_p are written using the Stokes parameters of S',

$$\tan2\eta^* = \frac{S'_2}{S'_1} , \quad (3\text{-}3\text{-}5)$$

$$\varepsilon_p^* = \frac{1}{2}\cos^{-1}\frac{\sqrt{S'^2_1+S'^2_2}}{S'_0} . \quad (3\text{-}3\text{-}6)$$

Substituting Eq. (3–3–4) into Eq. (3–3–5), we have the relation for η^*,

$$\tan2\eta^* = \frac{2\alpha V[\cos2\varepsilon\cdot\cos\Delta\cdot\sin2(\delta-\chi^*)-\sin2\varepsilon\cdot\sin\Delta]}{\alpha^2-1+V(\alpha^2+1)\cos2\varepsilon\cdot\cos2(\delta-\chi^*)} . \quad (3\text{-}3\text{-}7)$$

$$\eta^* = \frac{1}{2}\tan^{-1}\left(\frac{2\alpha V[\cos 2\varepsilon \cdot \cos\Delta \cdot \sin 2(\delta-\chi^*) - \sin 2\varepsilon \cdot \sin\Delta]}{\alpha^2 - 1 + V(\alpha^2+1)\cos 2\varepsilon \cdot \cos 2(\delta - \chi^*)}\right) \quad (-45^\circ \le \eta^* \le 45^\circ) \qquad (3\text{-}3\text{-}8)$$

Substituting Eq. (3–3–4) into Eq. (3–3–6), we have a relation including ε_p^*,

$$\varepsilon_p^* = \frac{1}{2}\cos^{-1}\frac{\sqrt{\{(\alpha^2-1)+V(\alpha^2+1)\cos 2\varepsilon \cdot \cos 2(\delta-\chi^*)\}^2 + \{2\alpha V(\cos 2\varepsilon \cdot \cos\Delta \cdot \sin 2(\delta-\chi^*) - \sin 2\varepsilon \cdot \sin\Delta)\}^2}}{(\alpha^2+1)+V(\alpha^2-1)\cos 2\varepsilon \cdot \cos 2(\delta-\chi^*)}$$

(3-3-9)

By fitting Eqs. (3–3–8) and (3–3–9) to the measured data set of $(\chi^*, \eta^*, \varepsilon_p^*)$ by means of the least squares method , we can determine the parameters V, ε, and δ for the incident light and α and Δ for the phase–shifting polarizer.

3–4. Multilayer phase shifter

In this section we describe a method to measure the polarization characteristics of a mirror using an analyzer and light of which the polarization state is known.

We should measure the polarization state of probe light in advance (See Sec. 3–3). The Stokes vector S of the light is expressed as

$$S = \begin{pmatrix} S_0 \\ S_1 \\ S_2 \\ S_3 \end{pmatrix} = \begin{pmatrix} 1 \\ V\cos 2\delta \cdot \cos 2\varepsilon \\ V\sin 2\delta \cdot \cos 2\varepsilon \\ V\sin 2\varepsilon \end{pmatrix}. \qquad (3\text{-}4\text{-}1)$$

We set a sample multilayer at the azimuthal angle to be $-45°+\delta$. Then the Stokes vector S''' of the light reflected by the multilayer is expressed as

$$S''' = R(-45°)\cdot M(\alpha,\Delta)\cdot R(45° - \delta)\cdot S$$
$$= R(-45°)\cdot M(\alpha,\Delta)\cdot R(45°)\cdot S'$$
$$= \frac{r_p^2}{2}\begin{pmatrix} S'_0(\alpha^2+1)-S'_2(\alpha^2-1) \\ 2\alpha(S'_1\cos\Delta - S'_3\sin\Delta) \\ -S'_0(\alpha^2-1)+S'_2(\alpha^2+1) \\ 2\alpha(S'_1\sin\Delta + S'_3\cos\Delta) \end{pmatrix}, \quad (3\text{-}4\text{-}2)$$

where $M(\alpha,\Delta)$ is the Mueller matrix of the multilayer (See Eq. (2–2–5)), R is the Mueller matrix of an azimuth rotator (See Eq. (2–2–2)). Setting the sample multilayer at ±45°+δ has an advantage in analysis because the Stokes parameters S'_2 of the incident light to the sample multilayer becomes zero.

Substituting Eq. (3–4–1) into Eq. (3–4–2), S''' is derived,

$$S''' = \frac{r_p^2}{2}\begin{pmatrix} 1+\alpha^2 \\ 2\alpha V(\cos 2\varepsilon\cdot\cos\Delta - \sin 2\varepsilon\cdot\sin\Delta) \\ 1-\alpha^2 \\ 2\alpha V(\cos 2\varepsilon\cdot\sin\Delta + \sin 2\varepsilon\cdot\cos\Delta) \end{pmatrix} = \frac{r_p^2}{2}\begin{pmatrix} 1+\alpha^2 \\ 2\alpha V\cos(2\varepsilon+\Delta) \\ 1-\alpha^2 \\ 2\alpha V\sin(2\varepsilon+\Delta) \end{pmatrix}, \quad (3\text{-}4\text{-}3)$$

where V is the degree of polarization of the probe light, ε is the ellipticity angle of the light, α is the ratio, r_s/r_p, of amplitude reflectances of the multilayer for the s– to the p–component, and Δ is a retardation for the two components, $\Delta_p-\Delta_s$.

When we make the rotating analyzer ellipsometry measurement of S''', we can obtain the azimuth of major axis ϕ and the pseudo–ellipticity angle ε_p of S''' (See Sec. 3–1). These two parameters are written using the Stokes parameters of S''',

$$\tan 2\phi = \frac{S'''_2}{S'''_1}, \qquad (3\text{-}4\text{-}4)$$

$$\cos 2\varepsilon_p = \frac{\sqrt{S'''^2_1 + S'''^2_2}}{S'''_0}. \qquad (3\text{-}4\text{-}5)$$

Substituting Eqs. (3–4–3) and (3–4–4) into Eq. (3–4–5), we can obtain the relation including α:

$$\cos 2\varepsilon_p = \frac{\sqrt{(1-\alpha^2)^2 \mathrm{cosec}^2 2\phi}}{1+\alpha^2} = \frac{1-\alpha^2}{(1+\alpha^2)\sin 2\phi}, \qquad (3\text{-}4\text{-}6)$$

$$\alpha^2 = \frac{1-\cos 2\varepsilon_p \sin 2\phi}{1+\cos 2\varepsilon_p \sin 2\phi}. \qquad (3\text{-}4\text{-}7)$$

The reason why the $(1-\alpha^2)\mathrm{cosec}2\phi$ is always positive originates from the fact that S'_2 equals zero (Consider the Poincarè sphere). α is written by the measured parameters,

$$\alpha = \sqrt{\frac{1-\cos 2\varepsilon_p \sin 2\phi}{1+\cos 2\varepsilon_p \sin 2\phi}} \qquad (3\text{-}4\text{-}8)$$

because α is positive.

Substituting Eqs. (3–4–3) and (3–4–8) into Eq. (3–4–5), we can obtain the following relation including Δ:

$$\tan^2(\Delta + 2\varepsilon) = \frac{V^2 - \cos^2 2\varepsilon_p (V^2 \sin^2 2\phi + \cos^2 2\phi)}{\cos^2 2\varepsilon_p \cos^2 2\phi}. \qquad (3\text{-}4\text{-}9)$$

Then Δ is expressed by the measured parameters,

$$\Delta = -2\varepsilon \pm \tan^{-1}\left(\frac{\sqrt{V^2 - \cos^2 2\varepsilon_p (V^2 \sin^2 2\phi + \cos^2 2\phi)}}{\cos 2\varepsilon_p \cos 2\phi} \right) . \qquad (3-4-10)$$

To determine the sign, we refer the expectation of theoretical calculation or we do two different measurements using two probe lights having different ε.

When V equals unity, Eq. (3–4–10) can be rewritten simply as

$$\Delta = -2\varepsilon \pm \tan^{-1}\left(\frac{\sin 2\varepsilon_p}{\cos 2\varepsilon_p \cdot \cos 2\phi} \right) , \qquad (3-4-11)$$

and these parameters are described using the Poincaré sphere in Fig. 3–6. In this figure the incident light S' is transformed to S'' by the function of polarization and transformed to S''' by the function of phase shift.

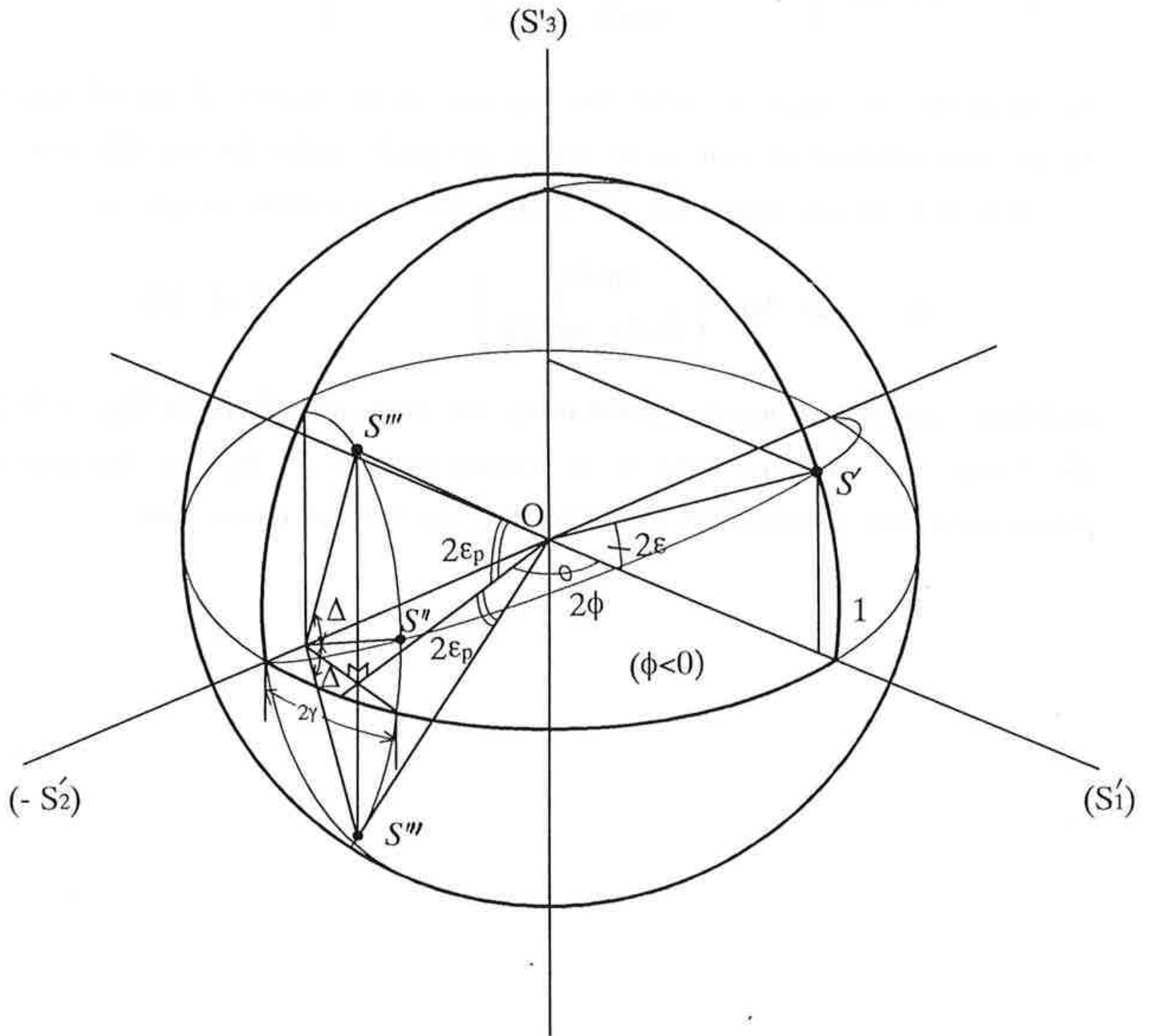

Figure 3-6. The operation of the phase shifter on the Poincaré shere, when V=1. $\alpha=\cot\gamma$

IV. How to minimize and evaluate the experimental error

4-1. Rotating-analyzer ellipsometry (RAE)

The sinusoidally varying signal in a single rotation of the analyzer can be expressed according to Malus' law by

$$I(\eta) = (I_{Max}-I_{Min})\cos^2(\eta-\delta)+I_{Min} \,. \qquad (4\text{-}1\text{-}1)$$

Possible vertical misalignment of the rotating axis of the analyzer causes difference between the two I_{Max} (when horizontally linearly polarized light is measured, these are I(0°) and I(180°)), and possible horizontal misalignment of the axis causes a difference between the two I_{Min} (I(90°) and I(270°)). Then we can realign the analyzer rotating axis according to the obtained data.

δ and C_{ont} which has no dimension as well as the ratio I_{Max}/I_{Min} are important for analysis. Therefore we use the logarithmic residual defined as

$$E = \sqrt{\frac{1}{n}\sum_{n}\{\log I_{data}(\eta_n)-\log I_{calc}(\eta_n)\}^2} \,, \qquad (4\text{-}1\text{-}2)$$

where

$$I_{calc} = (I_{Max}-I_{Min})\cos^2(\eta_n-\delta)+I_{min} \,. \qquad (4\text{-}1\text{-}3)$$

The most reliable values of δ, I_{Max}, and I_{Min} were determined with the least squares fitting using the residual.

In this paper each error for these parameters shown was evaluated as the value of this parameter when two times the minimum residual was obtained and when the other parameters were fixed to the most reliable values. The error of C_{ont} and ε *etc.* were calculated using the function of error propagation.

4-2. Rotating-analyzer ellipsometry with phase shifter (RAEP)

For the least squares fit to Eqs. (3-3-8) and (3-3-9), the most reliable values of η^* and ε_p^* are used. The problem is the weights distributed to these equations on the fitting procedure. When the polarization ellipse of S' is round, which means, when ε_p^* is close to 45°, the error in η^* is larger than in the case when ε_p^* is close to 0°. In this case, the error in ε_p^* is larger than for the case when ε_p^* is close to 45°, because P_L of S' is comparable with the analyzer polarizance. Then using the above values of η^* and ε_p^*, and calculating the position of S' on the Poincaré sphere in which the radius equals unity, the projection of the position on the S_1–S_2 plane (Show Fig. 4-1) is given by

$$(\cos 2\eta^* \cdot \cos 2\varepsilon_p^*,\ \sin 2\eta^* \cdot \cos 2\varepsilon_p^*) \quad . \qquad (4\text{-}2\text{-}1)$$

It was found that in all cases the points of Eq. (4-2-1) as a function of χ^* can be roughly fitted on a common ellipse. By means of a least squares method, we determine the parameters α and Δ for the phase-shifting polarizer and V, ε, and δ for the incident light, where the distance between the measured and the calculated points of Eq.(4-2-1) are minimized.

Here we consider the equation of η^* and ε_p^*.

$$\eta^* = \frac{1}{2}\tan^{-1}\left(\frac{2\alpha V[\cos 2\varepsilon \cdot \cos\Delta \cdot \sin 2(\delta-\chi^*) - \sin 2\varepsilon \cdot \sin\Delta]}{\alpha^2 - 1 + V(\alpha^2+1)\cos 2\varepsilon \cdot \cos 2(\delta-\chi^*)}\right) \quad . \qquad (3\text{-}3\text{-}8)$$

$$(-45^\circ \le \eta^* \le 45^\circ)$$

$$\varepsilon_p^* = \frac{1}{2}\cos^{-1}\frac{\sqrt{\{(\alpha^2-1)+V(\alpha^2+1)\cos 2\varepsilon \cdot \cos 2(\delta-\chi^*)\}^2 + \{2\alpha V(\cos 2\varepsilon \cdot \cos\Delta \cdot \sin 2(\delta-\chi^*) - \sin 2\varepsilon \cdot \sin\Delta)\}^2}}{(\alpha^2+1)+V(\alpha^2-1)\cos 2\varepsilon \cdot \cos 2(\delta-\chi^*)}$$

$$(3\text{-}3\text{-}9)$$

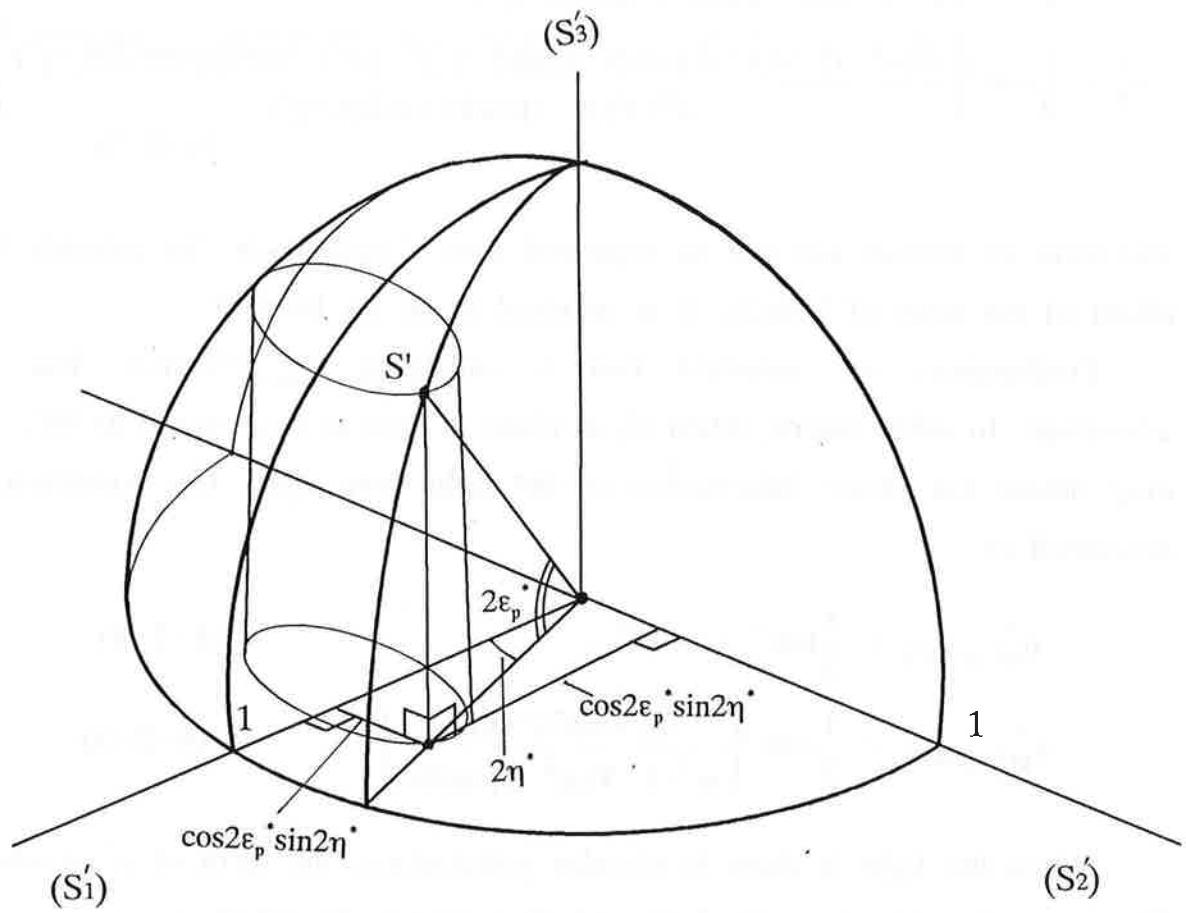

Figure 4-1. Projection of the point on the S_1'-S_2' plane.

Rotating analyzer ellipsometry with phase shifter is important for the determination of V and ε. When Δ equals 0°, Eqs. (3–3–8) and (3–3–9) are described as

$$\eta^* = \frac{1}{2}\tan^{-1}\left(\frac{2\alpha V\cos2\varepsilon\cdot\sin2(\delta-\chi^*)}{\alpha^2-1+V(\alpha^2+1)\cos2\varepsilon\cdot\cos2(\delta-\chi^*)}\right), \quad (4-2-2)$$

$$\varepsilon_p^* = \frac{1}{2}\cos^{-1}\left(\frac{\sqrt{\{(\alpha^2-1)+V(\alpha^2+1)\cos2\varepsilon\cdot\cos2(\delta-\chi^*)\}^2+4\alpha^2V^2\cos^22\varepsilon\cdot\sin^22(\delta-\chi^*)}}{\alpha^2+V(\alpha^2-1)\cos2\varepsilon\cdot\cos2(\delta-\chi^*)}\right). \quad (4-2-3)$$

The term of $V\cos2\varepsilon$ can not be separated into V and $\cos2\varepsilon$. To enhance the effect of the term of $V\sin2\varepsilon$, Δ is required to be far from 0°.

Furthermore we assumed that α satisfying $P_{zance} \approx V\cos2\varepsilon$ has an advantage. In other words, when S'_1 is close to zero at $\delta-\chi^*$ equal to 90°, we may obtain the phase information of the light very well. The condition is described as

$$\eta^*_{(\delta-\chi=90°)} = \frac{1}{2}\tan^{-1}\infty = 45°, \quad (4-2-4)$$

$$\varepsilon^*_{p(\delta-\chi=90°)} = \frac{1}{2}\cos^{-1}\left(\frac{2\alpha V\sin2\varepsilon\cdot\sin\Delta}{\alpha^2-1-V(\alpha^2-1)\cos2\varepsilon}\right). \quad (4-2-5)$$

When the light is close to circular polarization, the term of χ^* is small. The case of ε=45°, Eqs. (3–3–8) and (3–3–9) are described as

$$\eta^* = \frac{1}{2}\tan^{-1}\left(\frac{-2\alpha V\sin\Delta}{\alpha^2-1}\right), \quad (4-2-6)$$

$$\varepsilon_p^* = \frac{1}{2}\cos^{-1}\left(\frac{\sqrt{(\alpha^2-1)^2+4\alpha^2V^2\sin^2\Delta}}{\alpha^2+1}\right). \quad (4-2-7)$$

These equations do not include the term of χ^*. η^* and ε_p^* do not depend on χ^*. In such a condition, it is very difficult to get a reliable result by fitting analysis.

RAE to the incident light gives information on δ and P_L. From P_L, we get information about the minimum value for and the maximum value for ε. If P_L is close to zero, the possible ranges of values V or ε becomes larger.

Only the term $\sin 2\varepsilon \sin 2\Delta$ of ε and Δ is an odd function. To determine their signs, we must determine the sign of one of them by means of an other method. The maximum and the minimum values of $\tan 2\eta^*$ and the average of these are given by

$$\tan 2\eta^*_{Max} = \frac{2\alpha V[\cos 2\varepsilon \cdot \cos\Delta - \sin 2\varepsilon \cdot \sin\Delta]}{\alpha^2 - 1} , \quad (4\text{-}2\text{-}8)$$

$$\tan 2\eta^*_{Min} = \frac{2\alpha V[-\cos 2\varepsilon \cdot \cos\Delta - \sin 2\varepsilon \cdot \sin\Delta]}{\alpha^2 - 1} , \quad (4\text{-}2\text{-}9)$$

and

$$\tan 2\eta^*_{Ave} = \frac{-2\alpha V \sin 2\varepsilon \cdot \sin\Delta}{\alpha^2 - 1} . \quad (4\text{-}2\text{-}10)$$

Then from the sign of the average and the value of α, we determine the sign of $\varepsilon \cdot \Delta$. It is important information to determine the starting values of the fitting. The sign of Δ of multilayer is positive in the region of the total reflection, if theoretical calculation is right. In this point, using a simple monolayer phase shifter may be better than using a multilayer phase shifter, because the polarization characteristics of a monolayer is simple.

In this method we do not need to know the absolute intensity of the transmitted light but need to know the azimuthal angles of the intensity minimum and we need the contrast factors of the sinusoidal signals. Therefore, instability in incident beam intensity does not have serious influence on the accuracy of our method.

V. Design and construction of ELLI

5-1. Specifications to meet the demands

A beamline ellipsometer named ELLI (ELLIpsometer) has been designed and constructed. It consists of two polarization elements of soft x-ray multilayer mirrors. One works as a phase shifter (P) and the other as an analyzer (A). A schematic diagram of ELLI is shown in Fig 5-1 . To perform polarization measurements with the ellipsometer, we measure the intensity of transmitted beam passing through the polarization elements by changing the two azimuthal angles of each of the elements. The basic design principles of the apparatus are as follows.

(1)The azimuthal angles of P and A can be changed independently. The range of rotation is more than 360°.

(2)The incident angles at P and A can be changed independently. The angular range is from 90° to 20° measured from normal.

(3)ELLI can be used under ultrahigh vacuum (UHV) environment better than 10^{-7} Torr, which allows the apparatus to be connected to a vacuum ultraviolet (VUV) beamline without vacuum window.

(4)Easy on-line adjustment of the optical axis using the monochromatized beam is possible. It is important to match the rotating axis of azimuth of P with the light path to setup ELLI at the beamline. The path of the zero order (visible) light may not match with that of the monochromatized light in several beamlines.

(5)ELLI can measure the uniformity of the polarization state in the beam profile.

(6)By removing the optical elements the light can pass through the vacuum chamber to another experimental apparatus.

(7)ELLI can also use a transmission type phase shifter.

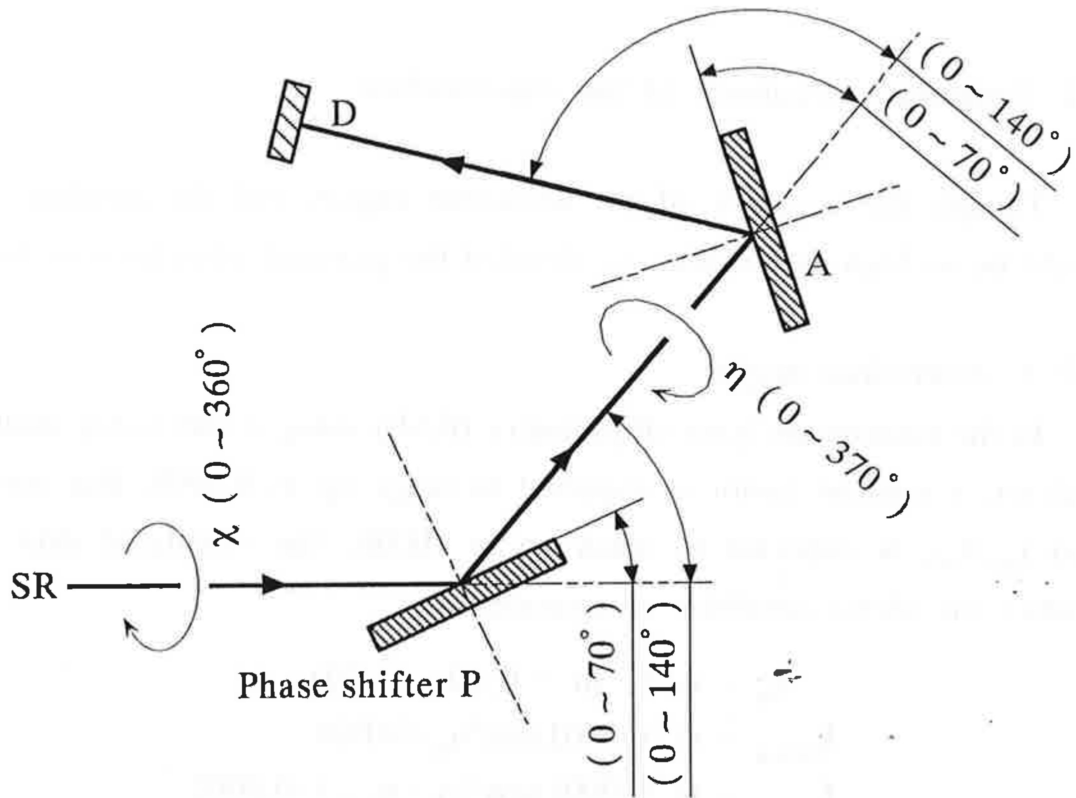

Figure 5-1. Schematical diagram of ELLI.

Then, the present ellipsometer can not only perform ellipsometry, but perform ellipsometry without a phase shifter and perform soft x–ray ellipsometry for mirrors.

5-2. Required accuracy of the mechanism

Though the accuracy of the azimuthal angles and the incident angles should be as high as possible, we decided the practical objectives as follows.

5-2-1. Azimuthal angle

In the rotating analyzer ellipsometry (RAE) using a soft x–ray multilayer analyzer, a contrast factor is expected to range up to 0.9998, that means, a ratio I_{max}/I_{min} is expected to reach up to 10000. The simulated data which satisfies the above condition is expressed as,

$$\eta_n = n \times 5^\circ \quad (n = 0,1,2,\cdot\cdot,72)$$
$$I_{ideal\,n} = (1-0.0001)\cos^2\eta_n + 0.0001$$
$$I_{error\,n} = (1-0.0001)\cos^2(\eta_n + \eta_{error}) + 0.0001$$

We define an average error ratio E as:

$$E = \sqrt{\frac{1}{73}\sum_{n=0}^{72}(\log I_{ideal\,n} - \log I_{error\,n})^2} \; .$$

We required E to be 2% and η_{error} was required to be 0.1466°. Then the minimum step of the azimuthal angle was required to be about 0.035°, and the error of the holding angle was required to be less than 0.015°.

5-2-2. Incident angle

The emerging beam from a VUV monochromator has a typical divergence about 2~5 mrad, 0.1~0.3°. Then the minimum step of incident

angle was required to be less than 0.05°, the error of holding the angle was required to be less than 0.03°.

5-3. Structure of ELLI

Figure 5-2 shows a drawing of the third quadrant projection of the inside mechanism of ELLI. Photographs of the mechanism are given in Figure 5-3. Figure 5-4 shows a drawing of the third quadrant projection of the chamber and the bench of ELLI. Their photographs are given in Figure 5-5 . The constituent elements of ELLi are as follows.

- Chamber
- Inside mechanism
  - Mechanism for changing the azimuth of P
  - Mechanism for changing the incident angle of P
  - Mechanism for changing the angle of analyzer arm
  - Mechanism for changing the azimuth of A
  - Mechanism for changing the incident angle of A
  - Holders for P and A
  - Detector
  - Exchangeable pinhole system and monitor mirror
  - System for setting origins of angles
  - Inside wiring layout
- Bench
- Control system

The functions and the detail of each part are given as follows.

Chamber

The Chamber is a vacuum chamber made of stainless steel (SUS304) and

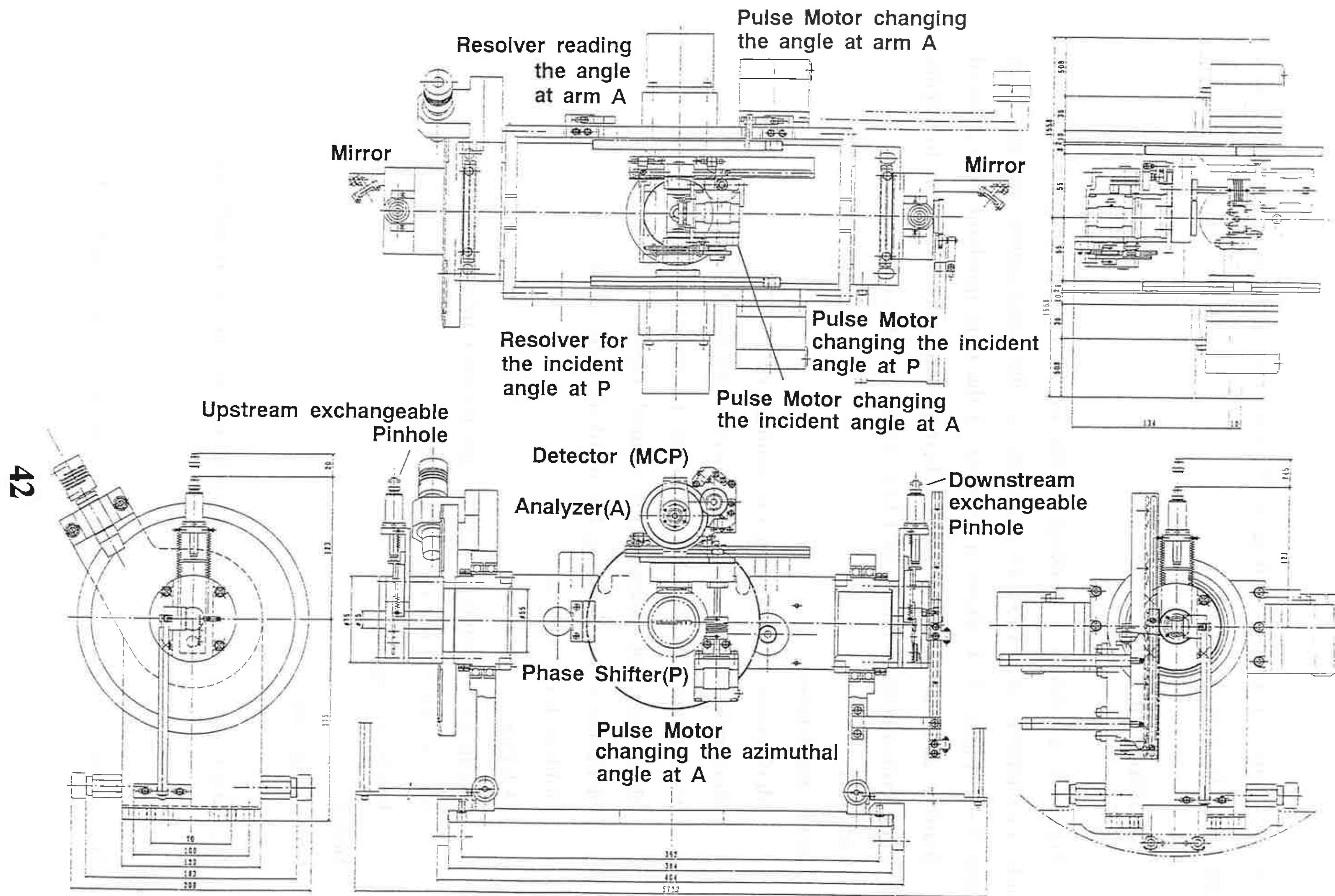

Figure 5–2. Drawing of the third quadrant projection of the inside mechanism of ELLI.

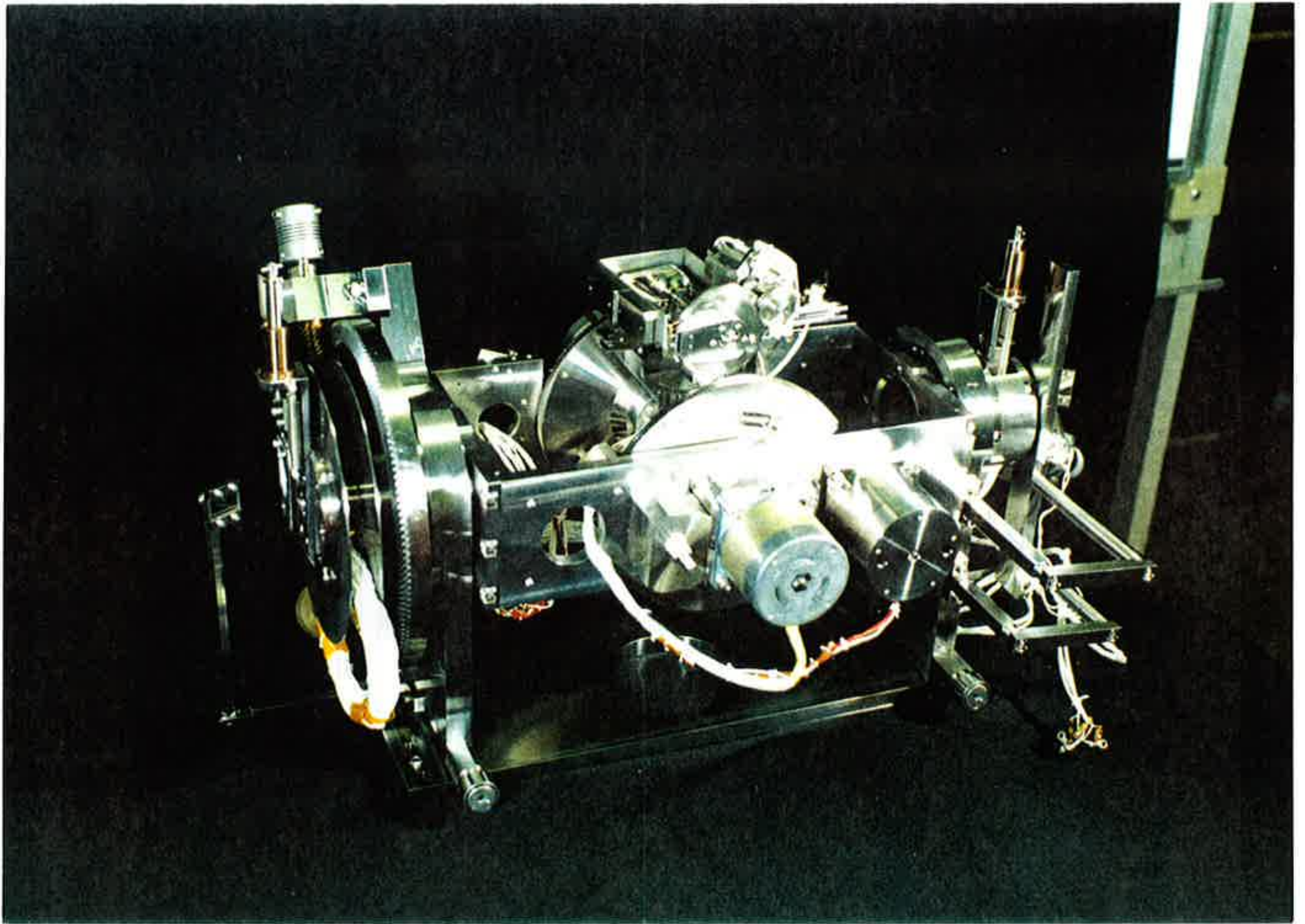

Figure 5–3. A photograph of the inside mechanism of ELLI.

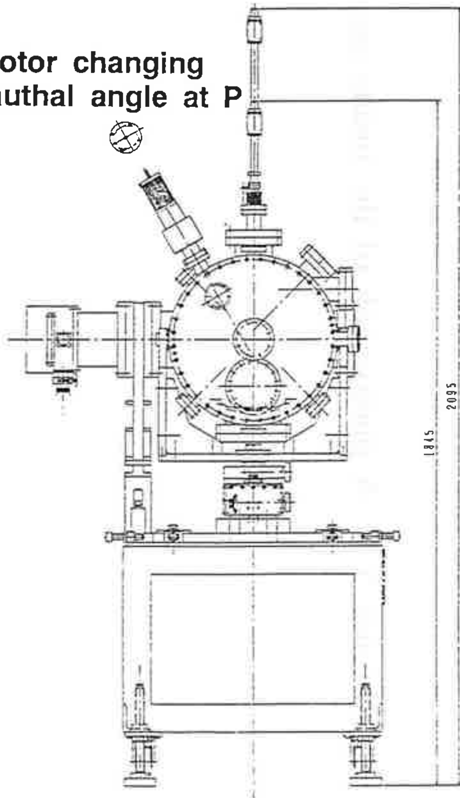

Figure 5–4. Drawing of the third quadrant projection of the chamber and the bench of ELLI.

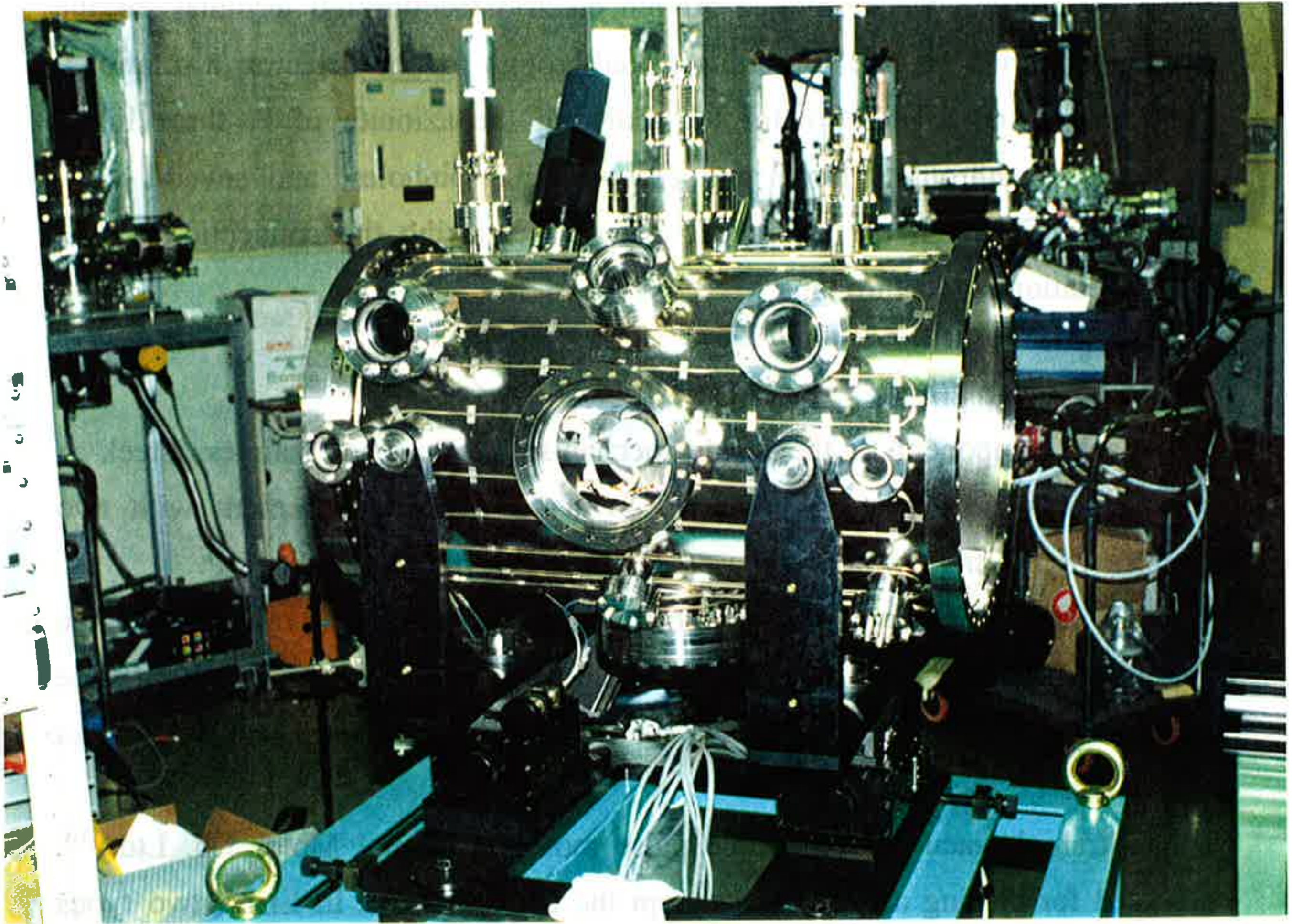

Figure 5-5. A photograph of the chamber of ELLI.

equipped with a turbo molecular pump (400 l/sec), a vacuum ion gauge, a valve for venting the system, a 50–pin electric feedthrough terminal for the inside electronics, a 4–BNC terminal feedthrough for the detector, a rotational feedthrough and a pulse motor for changing the azimuth of P, three linear rotational feedthroughs for P and exchangeable pinholes, and several view ports for adjustment of the optical axis and checking the connection of the linear rotational feedthroughs.

Inside mechanism

Each component of the inside mechanism is made of stainless steel. A rectangular main frame is supported by a "U" shaped basement with two couples of bearings which are used for changing the azimuth of P.

To keep reproducibility of positioning, a system of rails inside the chamber and four wheels were installed on the basement of the inside mechanism. The exact positioning is performed using two anchor blocks which can be locked by bolts.

Ultrahigh vacuum compatible pulse motors (Oriental Motor Co. Ltd.)[5A] are used for driving all rotations except the azimuth of P. In ELLI, two types of 5–phase pulse motors for UHV (UPH566–B and UPX534–B) are used, in which the minimum steps are 0.36° and 0.18°, respectively, and the stopping errors are 0.0833°. The motors are bakeable up to 180°C.

The power transmission system using UHV motors are simple and have negligibly small backlash as compared with that using motors in atmosphere. The friction is an important problem in vacuum, because the UHV motor does not have such a big power. Then for the transmission system, the flat gear system instead of the worm wheel system was adopted.

Two movements are monitored by two UHV compatible angle resolvers (EMR57–VAC–XC, Empire Magnetic Co. Ltd.), which work like a rotary encoder, whose resolution is 0.0879°. The resolvers are bakeable up to 165°C,

which limits a the baking temperature of ELLI.

Mechanism for changing the azimuth (χ) of P

The χ-rotation axis is fixed and is driven with a rotational feedthrough by a pulse motor which is placed outside the chamber. The hypoid gear system equipped with limit switches is adopted for the power transmission. The smaller gear is coated by titanium. The gear ratio is 1:18, and the minimum step is 0.02°.

Mechanism for changing the incident angle (θ_P) of P

This movement is driven by a UHV compatible pulse motor (UPH566-B). Because keeping this angle fixed is very important for ellipsometry, a scissors gear system was adopted and an UHV compatible resolver is directly connected to the shaft of the axis. The gear ratio of the transmission is 1:10, the minimum step is 0.036°, and the range of motion is not limited.

Mechanism for changing the angle (ϕ) of A arm

This movement is driven by a pulse motor (UPH566-B). A normal flat gear system equipped with limit switches was adopted. A counter weight is attached for keeping balance. For checking the movement with possible backlash, a resolver is connected directly to the shaft of the axis. The gear ratio of the transmission is 1:10, the minimum step is 0.036°, and the range of motion is 140° corresponding to an incident angular range of P from 90° to 20° measured from normal.

Mechanism for changing the azimuth (η) of A

This movement is driven by a UHV compatible pulse motor (UPX534-B). The normal flat gear system equipped with limit switches was adopted. The gear ratio is 1:5, the minimum step is 0.036°, the range of rotation is –

10°~370°. A counter weight is attached for keeping balance.

Mechanism for changing the incident angle (θ_A) of A

The incident angle of A and the angle of detector arm are driven by a pulse motor (UPX534–B). A θ–2θ mechanism is constructed by two couples of flat gear systems. The gear ratio for θ_A are 1:4, the minimum step is 0.045°, and the range of motion is from 90° to 20°.

Holders for P and A

P is mounted in a cassette, which is mounted on the phase shifter holder. The size of P mountable into the cassette is 20×10×1~4 mm^3. For the light to pass through ELLI or for the adjustment of the axis χ, the cassette can be detached from the phase shifter holder under vacuum with a linear rotational feedthrough. The center of the holder is cut out for a transmission type phase shifter.

A is mounted at analyzer holder. The size of A mountable at the holder is 20×10×1~4 mm^3.

Detector

A detector for polarization measurement using a multilayer is required to have a low polarization sensitivity (See Sec. 3–2), to have high efficiency, and to have uniformity in the sensitivity over the whole range of the detector area. Its size is an important problem for ELLI. A channeltron or an electron multiplier tube are too big and have some position sensitivity. A GaAsP photodiode is compact and has no polarization sensitivity but low efficiency. A microchannel plate (MCP) is satisfactory in all aspects. We use a MCP (X4655X, HAMAMATSU Co. Ltd.) in which the outer diameter is ϕ18 mm and the diameter of detective area is ϕ14.5 mm.

If small damages on the photocathode of the MCP are formed by

overload, then the MCP can be shifted slightly to an undamaged area.

Exchangeable pinhole system and monitor mirror

Two exchangeable pinhole plates are equipped at both ends of the χ axis for adjustment of this axis using monochromatized light. A pair of pinholes with 1-mm diameter are selected for the adjustment or as a small pinhole stop, that with 2-mm diameter is selected as a large pinhole stop, and that with 10-mm diameter is selected for the light to pass through. All these pinholes can be set on the χ axis using linear rotational feedthroughs. Luminescence powder is spread around both ϕ1-mm pinholes. The downstream one is made of thin transparent glass to watch the luminescence on the pinhole from the back side. Two mirrors are installed to watch the luminescence through the view ports.

System for setting origins of angles

After adjustment of χ axis, the origins of χ, η, and θ_P are adjusted with autocollimation technique using the reflection of laser-level light from P or A through a view port. Two mirrors for alignment of ϕ and θ_A are set on the analyzer arm and the detector arm. They are used for the tentative origins of ϕ and θ_A to be adjusted.

Inside wiring layout

Inside the chamber, wires covered with polytetrafluoroethylene (PTFE) (Zyunkousya Co. Ltd.) for insulation are used. Kapton foil is also used for insulation of wire connections. Shielded wires (PTFE) are used for the MCP. All the wires are laid out along the rotation axes for minimizing the excess wires, and are wound around a bobbin.

Bench

For easy adjustment of χ axis and for slight movement of the axis to measure the uniformity of the polarization state in the beam profile, a gimbals supports system whose pivot axes are on the upstream and the downstream exchangeable pinholes is installed on the bench. The horizontal and the vertical ranges for the adjustment by the system are ±5 mm and ±2.5 mm, respectively.

Control system

All the electric systems of ELLI are controlled by a personal computer (PC) (PC–9801DA, NEC). The whole control system is shown in Fig. 5–6. The pulse motor controller (PMC) controls the five stepping motors and gets the outputs of the resolvers and the limit switches. PMC can move the motors on the local mode without PC. The output of the MCP, the beam intensity monitor, and the storage ring current monitor are measured by electrometers (TR8652 ADVANTEST Co. Ltd). The PMC and the electrometers are controlled by the PC through a GPIB bus.

A mini controller can control all motors using the control software. It is convenient for adjustment of the optical axis using a telescope.

The software for ELLI is written in C++ (Borland Co. Ltd). The program is composed of 16 sub–programs, whose total list size including header files is 200 k bytes. The software has class libraries built for text screen control and data handling. It also has the capability to adjust the origins for the azimuthal and incident angles, various measurements, and cosine squares fitting. The extension of the software and debugging are very easy because of the easy handling of the C++ language.

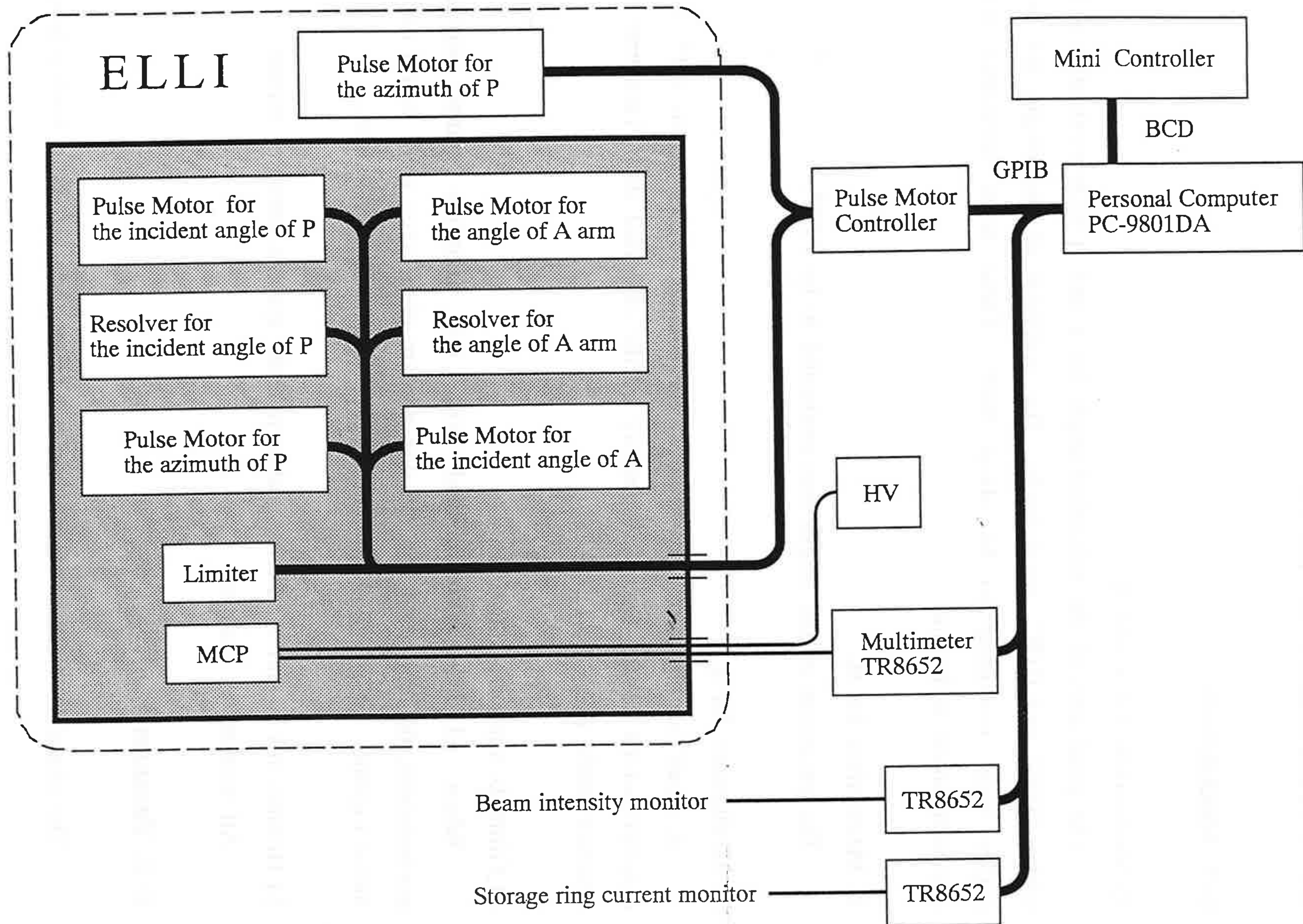

Figure 5-6. Block diagram of ELLI control system.

VI. Performance of ELLI

6-1. Mechanism

1) Mechanism for χ and η

The precisions of the azimuthal angle for χ and η were evaluated to be within 0.06° and 0.08°, respectively. The precision of the origin for both angles were evaluated to be about 0.02°. These were measured with autocollimation technique.

2) Mechanism for θ_P

The precision of the origin was evaluated to be 0.05°.

3) Mechanism for ϕ

A small backlash of ϕ, which was evaluated to be within 0.1°, was detected which results in an asymmetry of the obtained data. However the resolver could not detect it.

4) Gimbals support system

When ELLI was connected with the beamline under vacuum environment, the upstream and the downstream pivot axes were found not to move together for small movement of pivot axes within 0.5 mm.

5) Holders for P and A, exchangeable pinhole system, monitor mirror

All worked as planned.

6-2. Vacuum

The chamber of ELLI was baked out at around 150°C for twelve hours.

The temperature was measured on the outside wall of the chamber. A vacuum of 2.0×10^{-8} Torr was achieved after twelve hours baking. During operation of the motors, the vacuum rises up to 5×10^{-8} Torr. It is, however, good enough to connect ELLI with VUV beamline and to do the measurements without any differential pumping of a vacuum window.

6-3. Control system

The control system worked as planned.

VII. Polarization measurements and the results

7-1. Beamline description

We carried out polarization measurements for the monochromatized beam of synchrotron radiation (SR) from the Photon Factory (PF) storage ring at two different beamlines. The value of γ^{-1} derived from the energy of PF ring (2.5 GeV), which is the angular divergence of the bending magnet radiation at the critical wavelength, equals 0.2 mrad.

7-1-1. PF BL-28A

BL-28 is a beamline with an elliptic multipole wiggler[1B]. The wiggler was designed for four different modes: linear undulator, helical undulator, elliptic undulator, and elliptic multipole wiggler. Then the wiggler can emit either linearly polarized or circularly polarized light. In the present study, we carried out measurements in the linear undulator mode and the helical undulator mode. The helical undulator mode includes HUP submode and HUN submode. At the HUP mode or the HUN mode, electrons or positrons travel through the undulator with the motion of a left handed screw, and a right handed screw, respectively.

The whole optical arrangement of BL-28A is illustrated in Figure 7-1-1. The SR is confined by a water-cooled 4-blade diaphragms which has adjustable gaps and is placed at a distance of 14 m from the center of the wiggler. The SR through the diaphragms is deflected horizontally into the VUV branch (BL-28A) by a toroidal mirror M_0 and is led to a grating monochromator[7A]. The SR is pre-focused on the entrance slit (S1) by used of spherical mirrors M_1 and M_2 and is monochromatized and focused on the exit slit (S2). The monochromator, is of a constant deviation type and is equipped with five gratings G_1~G_5 and several mirrors. The monochromatized

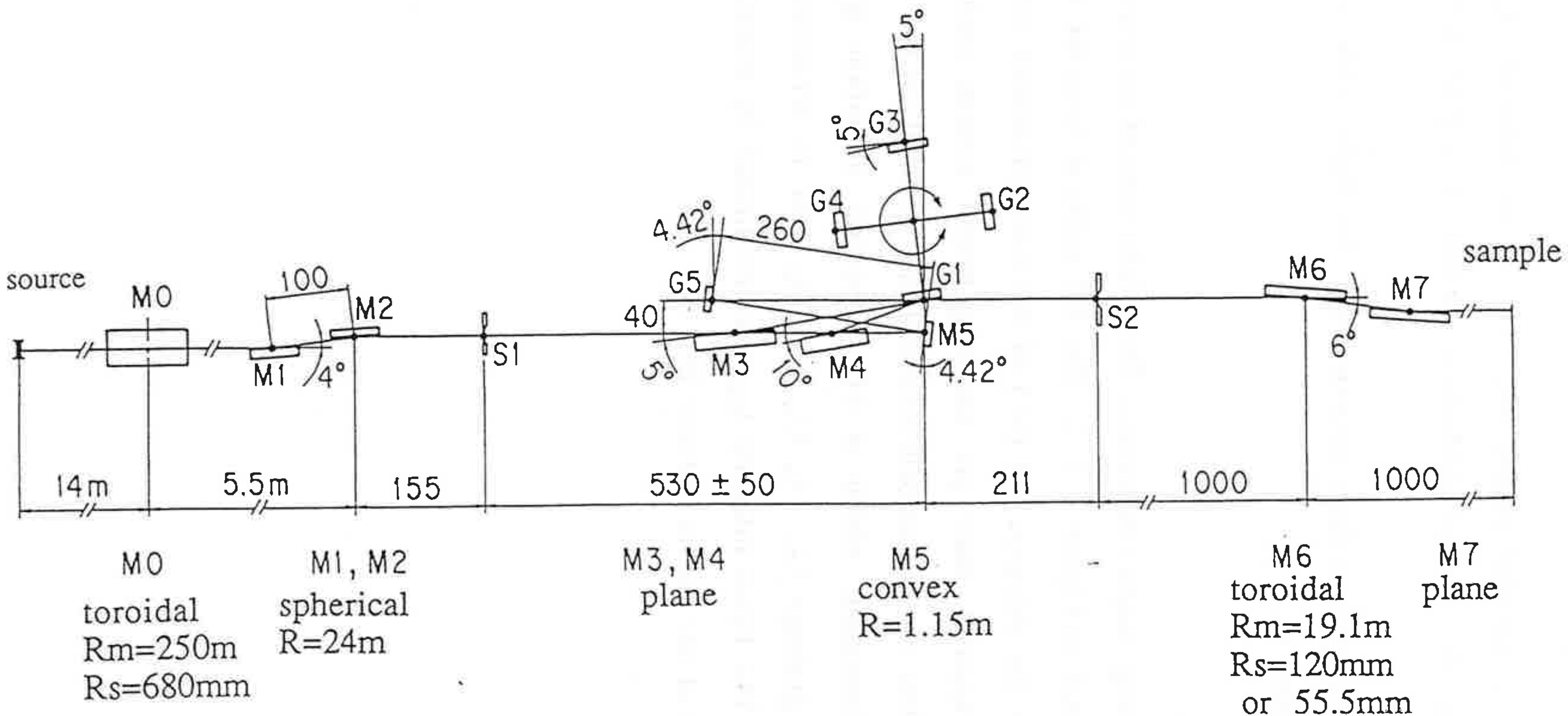

Figure 7-1-1. The whole optical arrangement of BL-28A. The units are given in mm if not specified.

SR is refocused by a toroidal mirror M_6. The beam intensity I_{Mon} was detected by measuring the total photoelectron current of a gold mesh after M_7.

We performed the polarization measurement for light with 12.8–nm wavelength using grating G_1.

7–1–2. PF BL–18A

BL–18 is a bending magnet beamline. The whole optical arrangement of BL–18A[7B] is illustrated in Figure 7–1–2. The SR emitted from the bending magnet is focused on the entrance slit (S1) of the monochromator through a diaphragm by a Kirkpatrick–Baez pre–focusing mirror system including a single plane mirror. The SR is monochromatized and focused on the exit slit (S2) by the monochromator, which is of a constant deviation type and equipped with four gratings G_1, G_2, G_3, and G_4, and is refocused by a toroidal mirror (M_f). The beam intensity I_{Moni} was monitored by recording the photoelectron current at the mirror surface M_f.

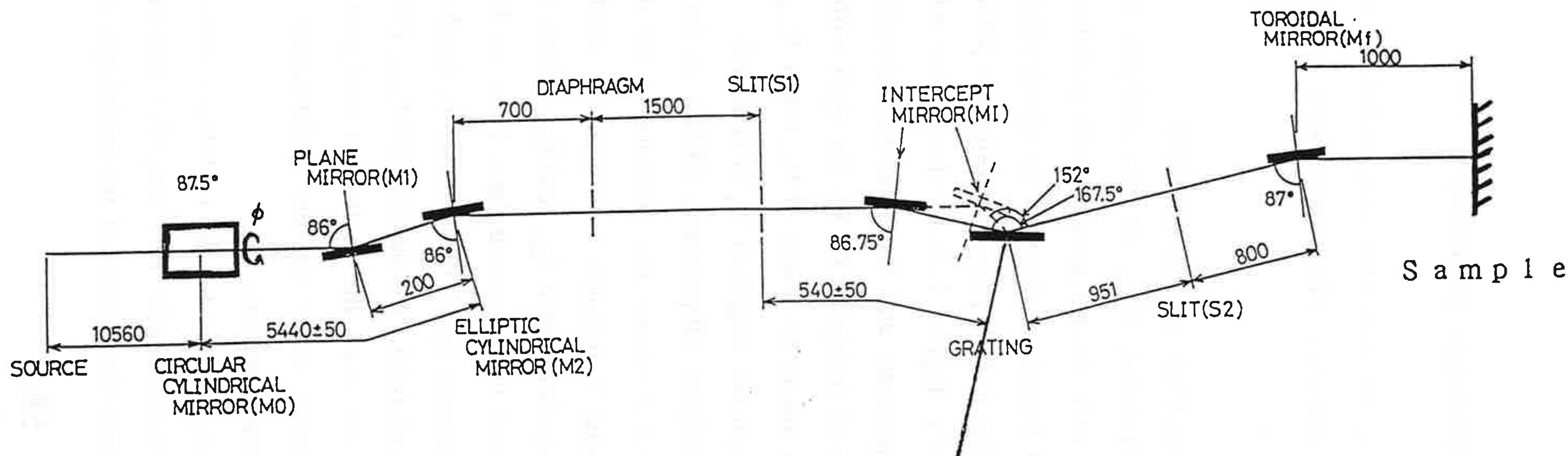

G_1: 500l/mm, R=6650.0mm deviation angle=167.5°

G_2:1200l/mm, R=2998.3mm deviation angle=152.0°

G_3: 600l/mm, R=2998.3mm deviation angle=152.0°

G_4: 300l/mm, R=2998.3mm deviation angle=152.0°

Figure 7-1-2. The whole optical arrangement of BL-18A. The units are given in mm if not specified.

7-2. Characterization of the polarization elements

A couple of 101-layer Mo/Si (3.19 nm/ 6.03 nm) multilayer mirrors were used as phase shifters and as analyzers. The mirrors were made on Si wafers using an RF sputtering system.

7-2-1. Measurement of the polarizance of the analyzer

At first we evaluated the polarizance, P_{zance}, of the analyzer A. The measurement was carried out at BL-18A. To get good linearly polarized light as a probe, we adjusted the optical beamline elements in advance(See Sec. 7-5), and reflected the light vertically with a phase shifting pre-polarizer P at 45° (the azimuth of P equals 0°). Figure 7-2-1 shows the reflective intensities of A for s- and p-components and the ratio α, between these components as function of the angle of incidence θ_A for the light with 12.8-nm wavelength. From this figure we found the value of θ_A, when P_{zance} takes the maximum, to be 41.085° in which the origin of θ_A is nominal.

Then we performed rotating-analyzer ellipsometry (RAE) at the above angle of incidence of A. Figure 7-2-2 shows the intensity at the detector obtained by rotating A. It took about 7 minutes to obtain the RAE data. Fitting these data to Eq. (4-1-1), we determined I_{Max} and I_{Min}. There is good agreement between the fitted curve and the measured data. Then we find that the effect of the linear polarization sensitivity of the detector is small enough compared to the polarizance of the analyzer. We determined P_{zance} (See. Sec. 3-1-2) to be 0.9971±0.0025, and we used the multilayer analyzer at the above incident angle and the above value of the polarizance in the measurement described in the following section.

To estimate the suitable wavelength range for the multilayer analyzer, we made measurements for the light at wavelengths 10.3 nm, 15.5 nm, and 20.6 nm. Figure 7-2-3 shows the reflective intensities of the multilayer analyzer

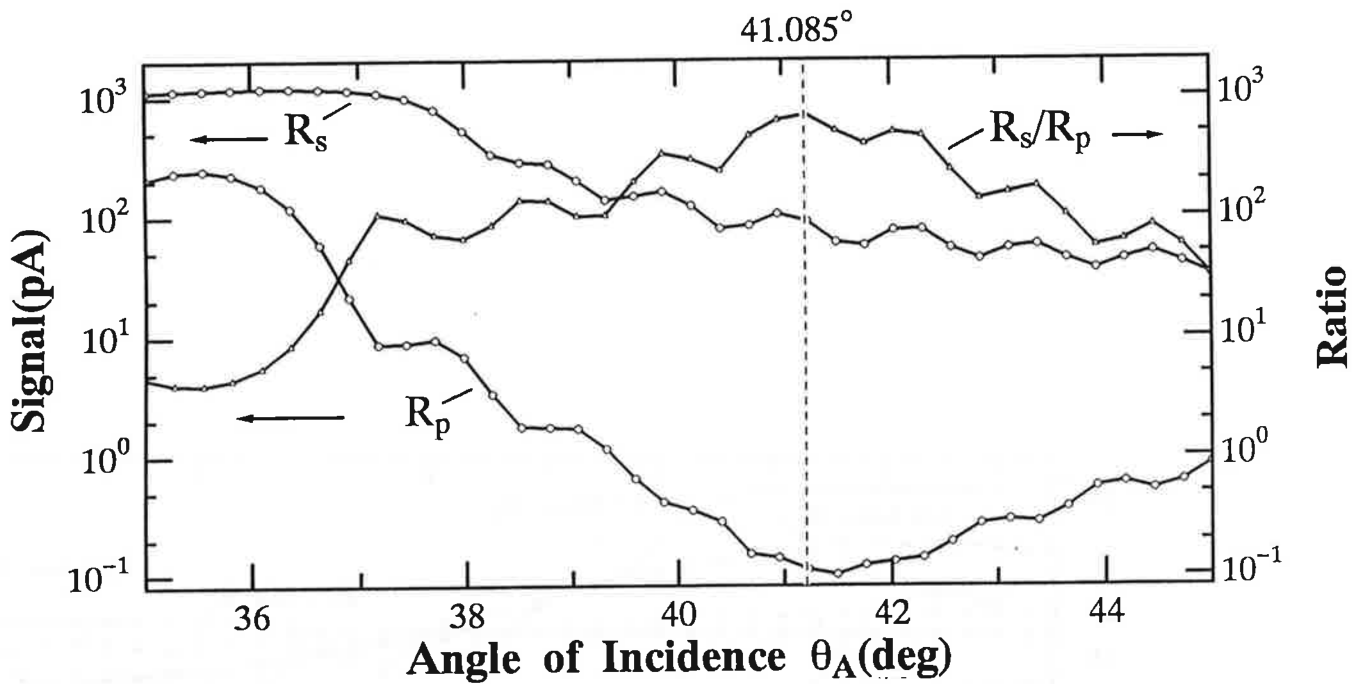

Figure 7-2-1. The reflective intensity and the ratio as function of the angle of incidence of the analyzer, θ_A. The origin of θ_A is nominal. $R_s(R_p)$ means the reflective intensity for s-(p-) component at a wavelength of 12.8 nm. R_s/R_p takes the maximum value at θ_A equal 41.085°.

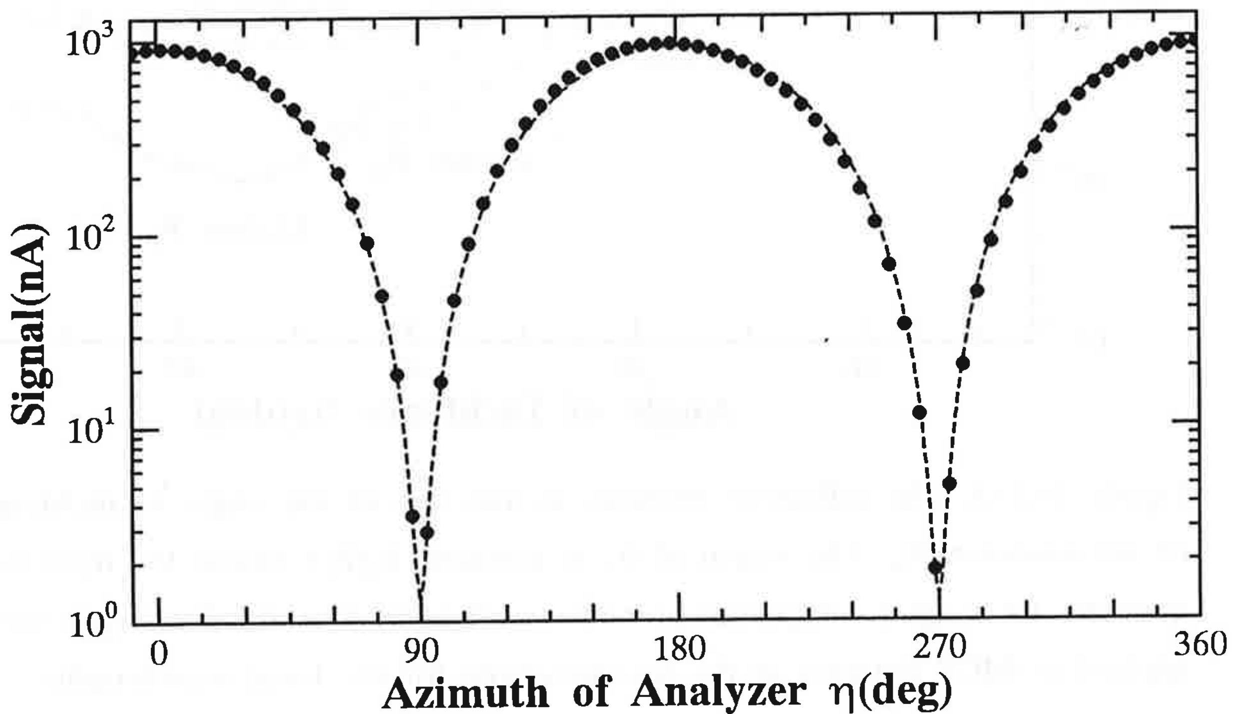

Figure 7-2-2. Intensity as function of the azimuth, η, of the analyzer at θ_A=41.085°. The solid circles show the measured data and the curve shows the result of fitting which evaluates C_{ont} to be 0.9971±0.0025.

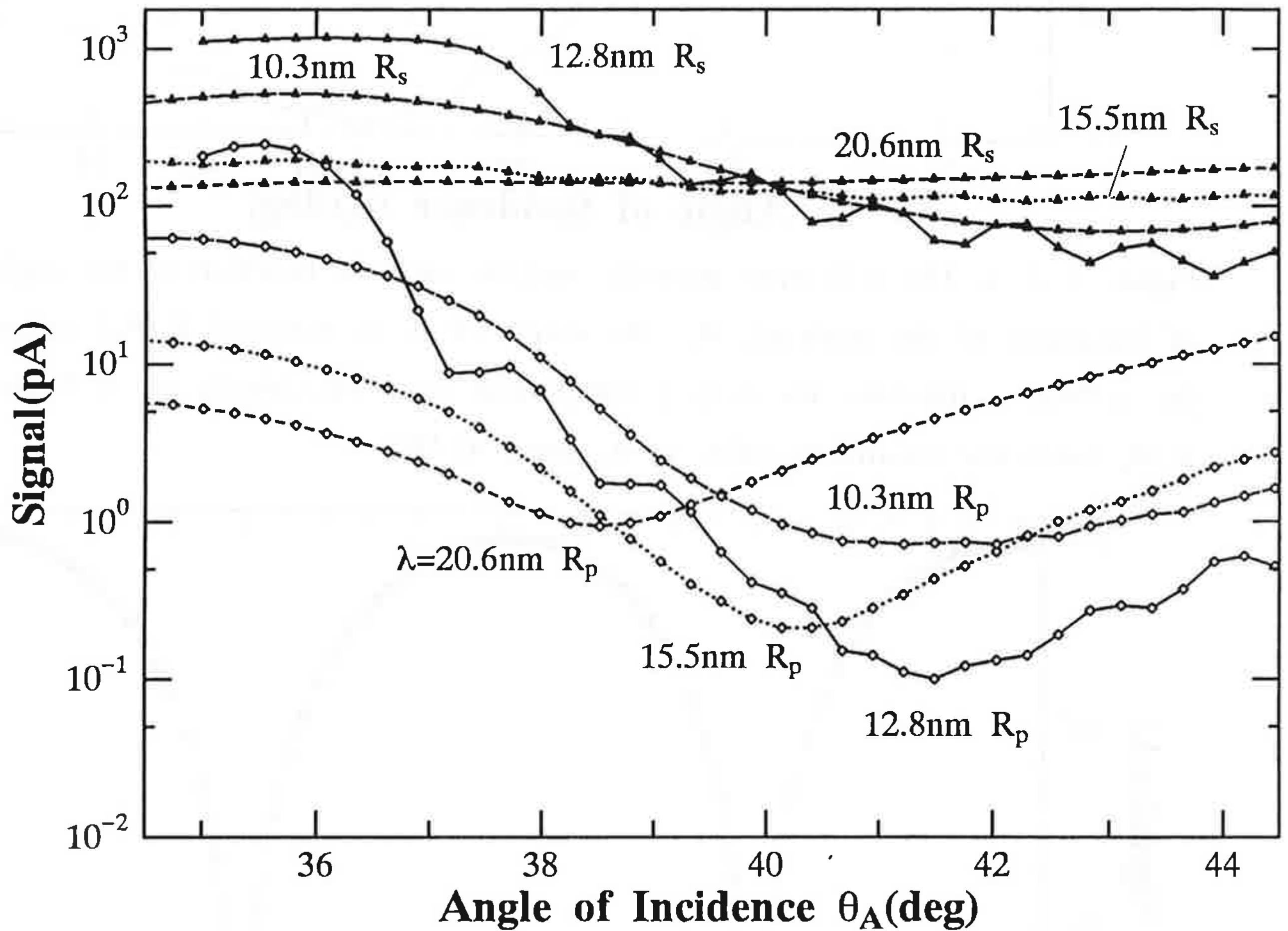

Figure 7-2-3. The reflective intensity as function of the angle of incidence of the analyzer, θ_A. The origin of θ_A is nominal. $R_s(R_p)$ means the reflective intensity for s-(p-) component at each wavelength. The fixed voltages were applied to MCP detector in the measurements for the fixed wavelengths.

for s– and p–components as function of θ_A. The fixed voltages were applied to MCP in the measurements for the fixed wavelengths. As shown in this figure, the reflective intensity for the light with 12.8–nm wavelength has fine structure due to the interference effect. This is because the wavelength is close to the optical path difference of this multilayer at this incident angle region.

At every wavelength, α is larger than over 100. Though the exact absolute value of the angle cannot be discussed, the θ_A for maximum α is close to the pseudo–Brewster angle of Mo. Therefore the analyzer can be used in the wavelength range between 10 nm and 20 nm.

7–2–2. Measurement of phase shifter

We measured the polarization characteristics of P in the glancing angle region. The measurement was carried out using ELLI at BL–28A. Before this measurement, we had evaluated the polarization state of the probe light (See Sec. 7–3–1 L46C). The parameters of the light are shown in Table 7–2–1.

Table 7–2–1. The parameters of the probe light.

V (Degree of Polarization)	ε(deg) (Ellipticity Angle)	δ(deg) (Azimuth of the Ellipse)
0.979	±0.8	-0.5

To transform S_2 to zero, We set the azimuth of P at χ=–45.5° (See Sec. 3–4). We performed RAE while keeping the angle of incidence of P (θ_P) fixed. From the measured sinusoidal signals, we obtained the azimuths of the ellipse (ϕ) and the pseudo–ellipticity angles (ε_p). These values, and the calculated values of r_s/r_p (α) and the retardation Δ are listed in Table 7–2–2.

Table 7-2-2. The fitted and calculated parameters.

θ_P(deg) Angle of Incidence	C_{ont} (Contrast Factor)	ε_p(deg) (Pseudo-Ellipticity Angle)	ϕ(deg) (Azimuth of the Ellipse)	α $\lvert r_s/r_p \rvert$	Δ(deg) (Retardation) (for $\varepsilon=-0.8°$ and $\varepsilon=0.8°$)
None (Probe light)	0.978	5.93	0		
85	0.968	6.90	-0.5	1.017	5.7, 8.9
83	0.967	7.01	-0.6	1.021	6.1, 9.3
81	0.964	7.31	-0.8	1.028	7.1, 10.3
79	0.961	7.72	-0.6	1.019	8.5, 11.7
77	0.961	7.66	-1.6	1.054	8.3, 11.5

In the table the errors of each value are not listed, because the evaluated errors of ε_p and ϕ of the light reflected from P were bigger than the differences of ε_p and ϕ against those of the probe light. For more accurate measurement, we should use the probe light to be close to perfect linear polarization by using a pre-polarizer.

Theoretically the multilayer has a positive retardation in this glancing angle region. That is used to determine the handedness of polarization ellipse.

7-3. Rotating-analyzer ellipsometry with phase shifter (RAEP)

We measured the polarization state of the monochromatized SR of 12.8-nm wavelength from several light sources and checked the method of analysis with RAEP. As polarization elements, the same multilayers were used as in sec. 7-2.

7-3-1. Linear undulator

The measurement was carried out using the undulator at BL-28A in the linear mode. The gap of the undulator was adjusted the 1st harmonic at 12.8-nm wavelength. The names of data sets, the corresponding conditions of measured light, and the angle of incidence at P are listed in table 7-3-1.

Table 7-3-1. The Condition of Data sets.

Name of Data Set	Incident Angle at P	Condition of light
L54A, L54B	54°	Linear mode, Peak of 1st
L46A, L46B, L46C	46°	

Figure 7-3-1 shows typical examples of MCP output obtained by rotating A while keeping P at several fixed angles χ^* plotted in logarithmic scale. Fitting these data to Eq. (4-1-1), we determine the azimuthal angles η^*, at which the intensity has a minimum value, and the pseudo-ellipticity angle ε_p^*. The values of η^* and ε_p^* are plotted against χ^* and the projection of these value on the S_1-S_2 plane are plotted for all data set, as shown in Figs. 7-3-2, 7-3-3, 7-3-4, 7-3-5, and 7-3-6. It took 3 hours to obtain each data set.

As described in Sec. 3-3, we could determine parameters α, Δ, V, ε,

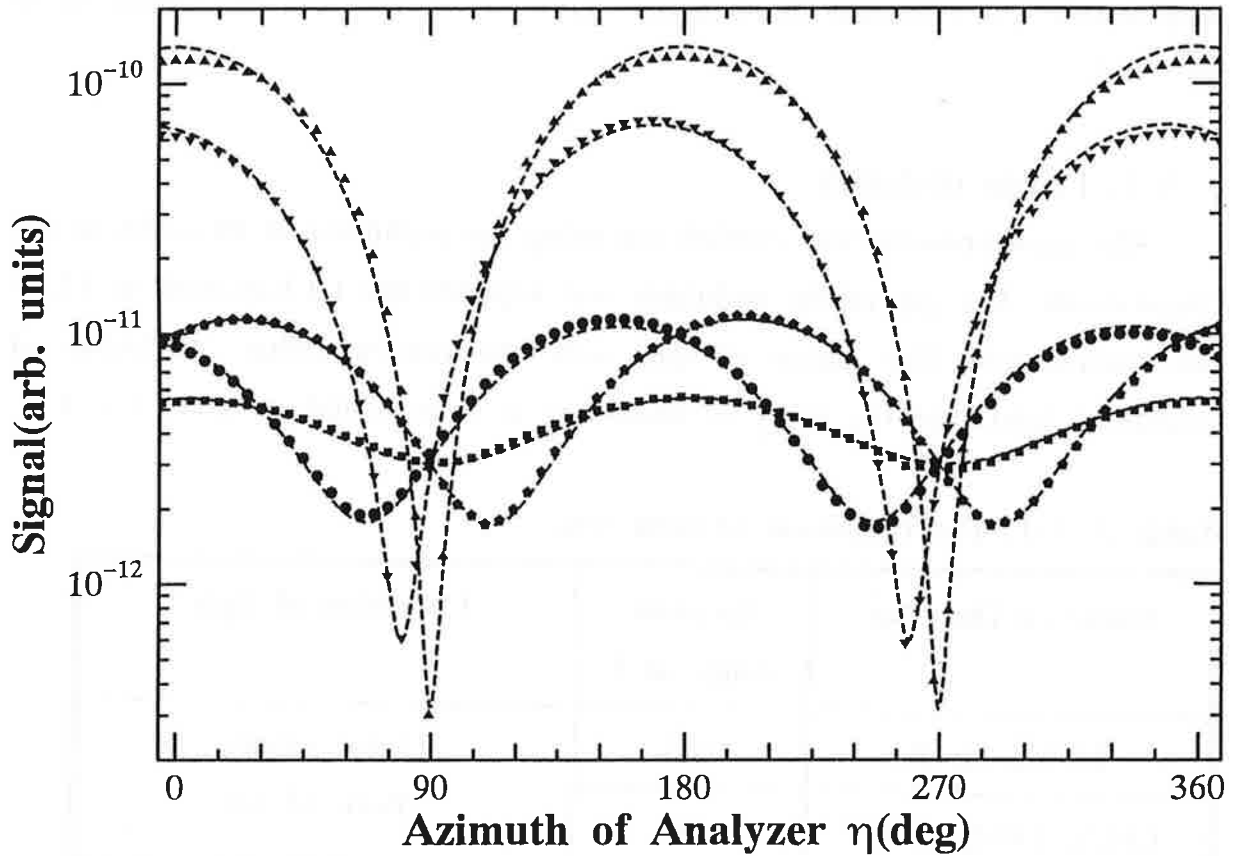

Figure 7-3-1. Typical examples of detector outputs while keeping phase shifter at several azimuths χ, and the data named L46C. The marks show the measured data and curves show the result of fitting.

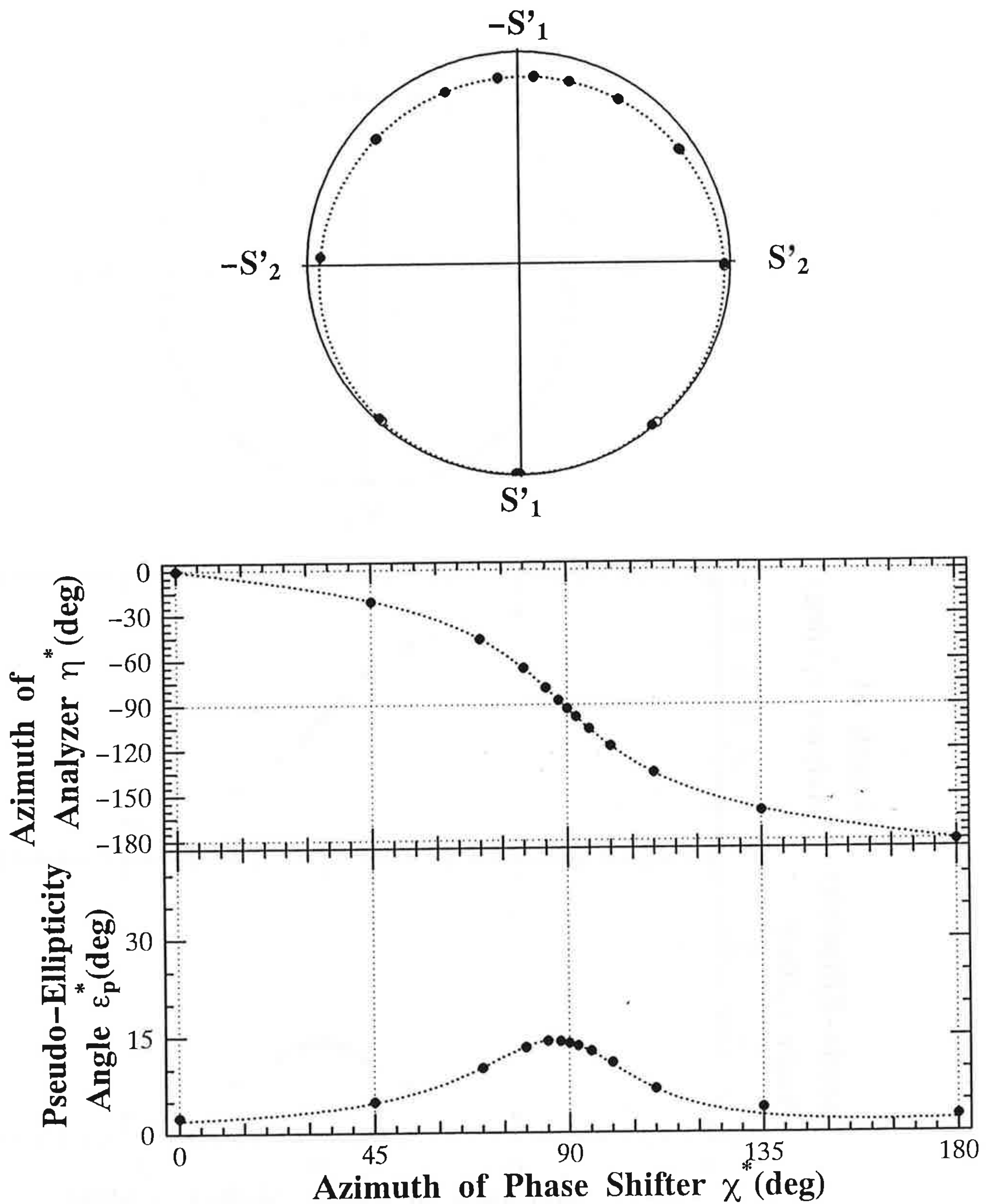

Figure 7–3–2. The values of η^* and ε_p^* of data **L54A** as function of χ^*, and the projection of these values on the S_1–S_2 plane. The solid circles show the measured data. The open circles and the curves show the fitted result.

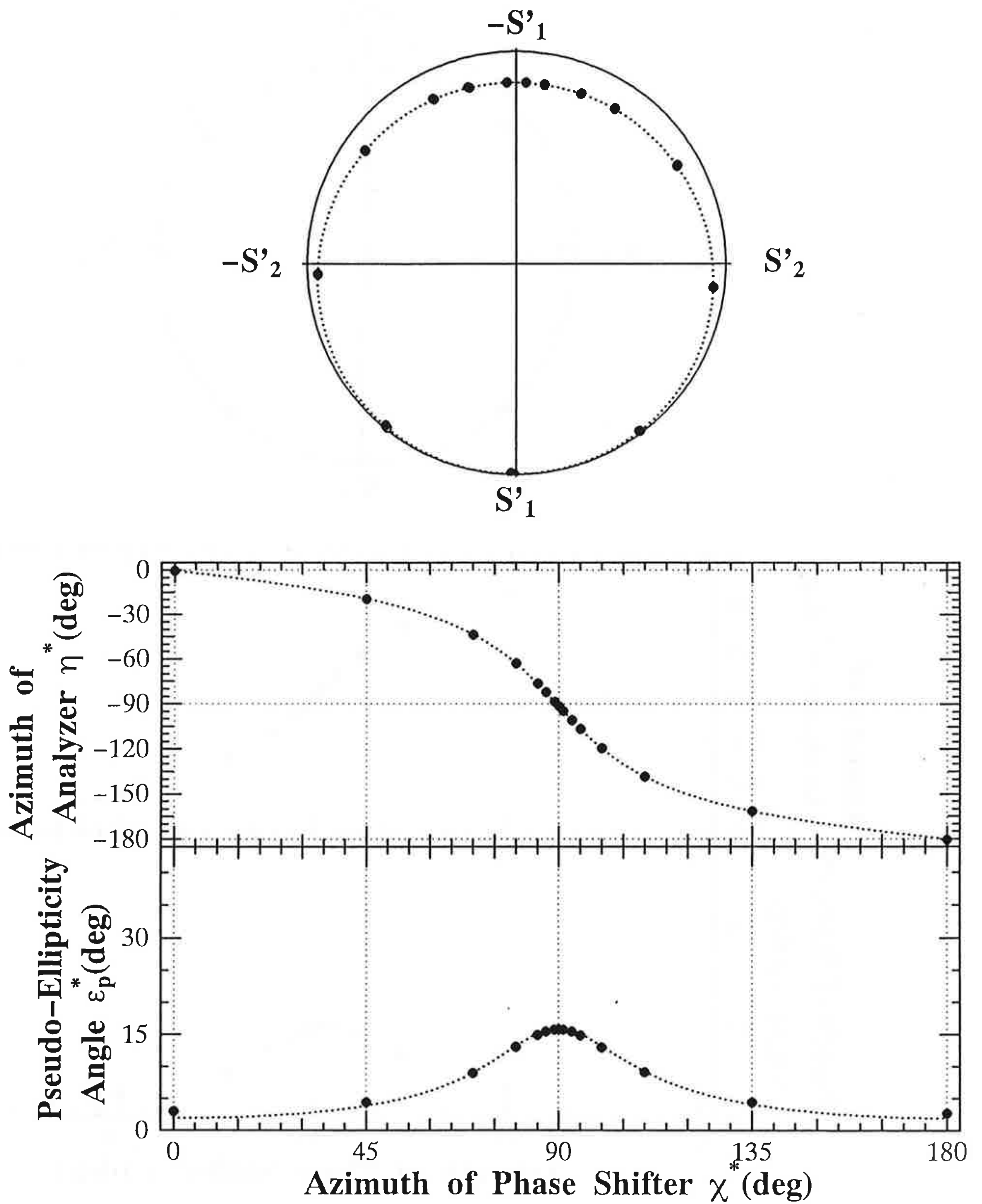

Figure 7-3-3. The values of η^* and ε_p^* of data **L54B** as function of χ^*, and the projection of these values on the S_1–S_2 plane. The solid circles show the measured data. The open circles and the curves show the fitted result.

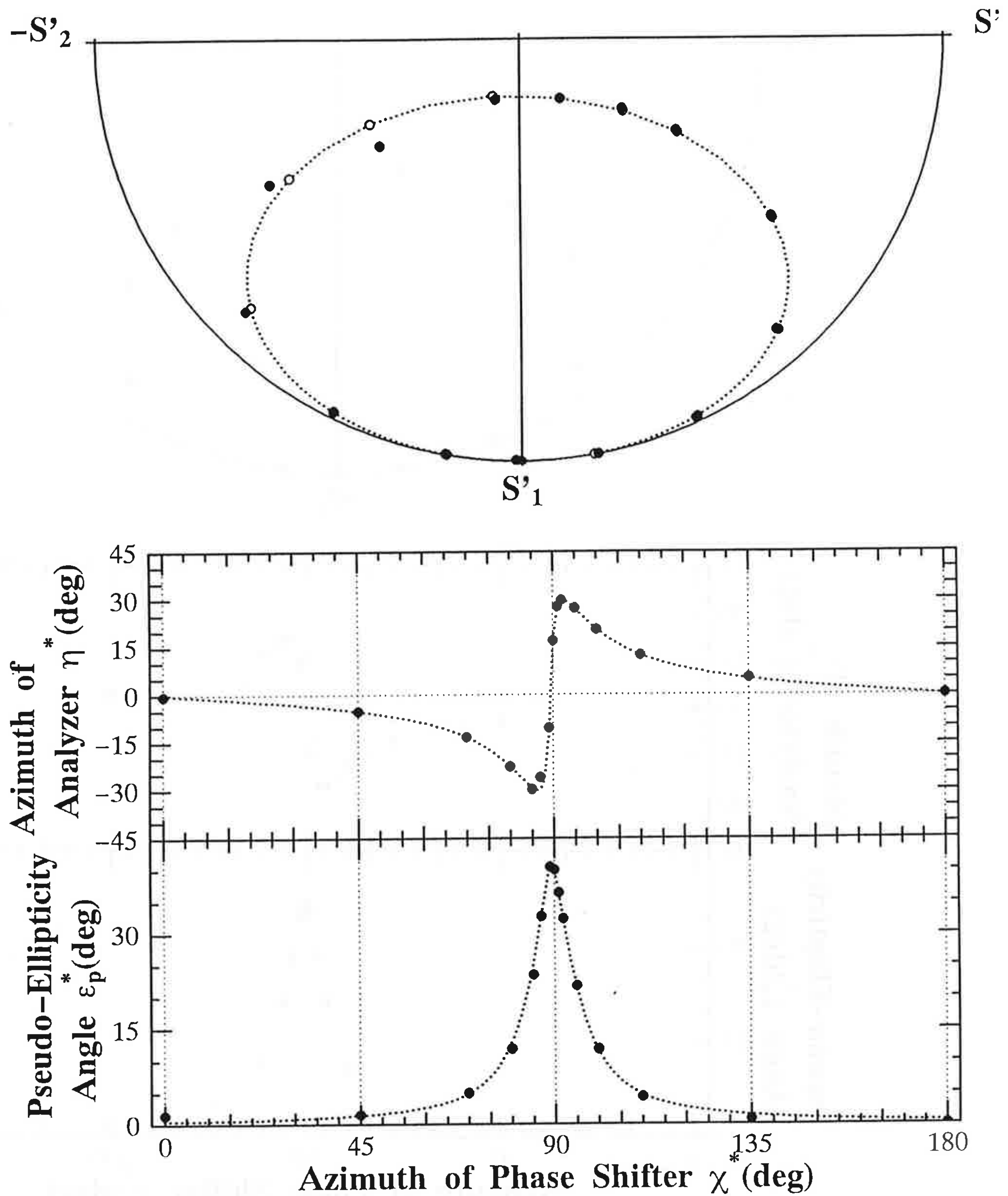

Figure 7–3–4. The values of η^* and ε_p^* of data **L46A** as function of χ^*, and the projection of these values on the S_1–S_2 plane. The solid circles show the measured data. The open circles and the curves show the fitted result.

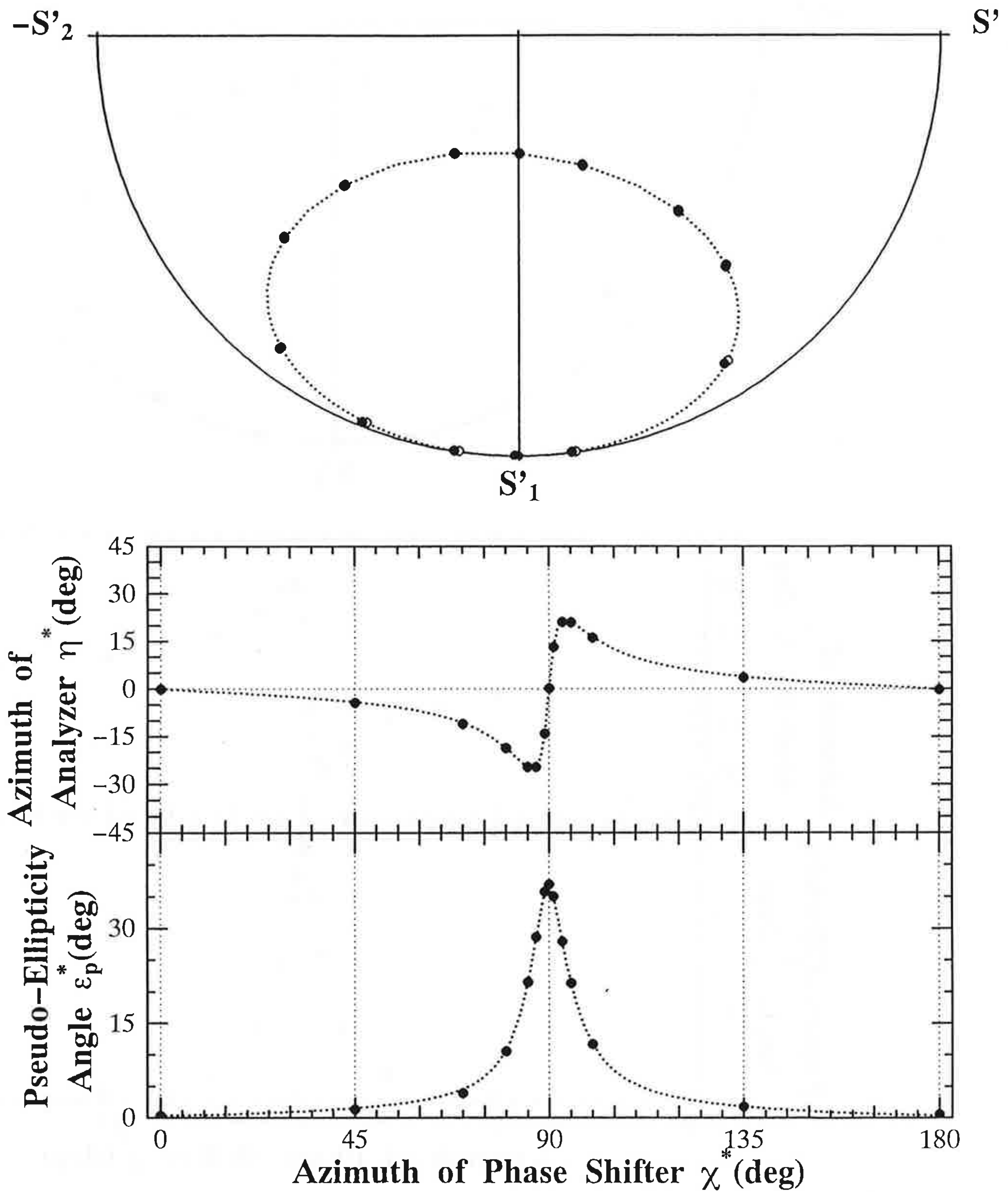

Figure 7–3–5. The values of η^* and ε_p^* of data **L46B** as function of χ^*, and the projection of these values on the S_1–S_2 plane. The solid circles show the measured data. The open circles and the curves show the fitted result.

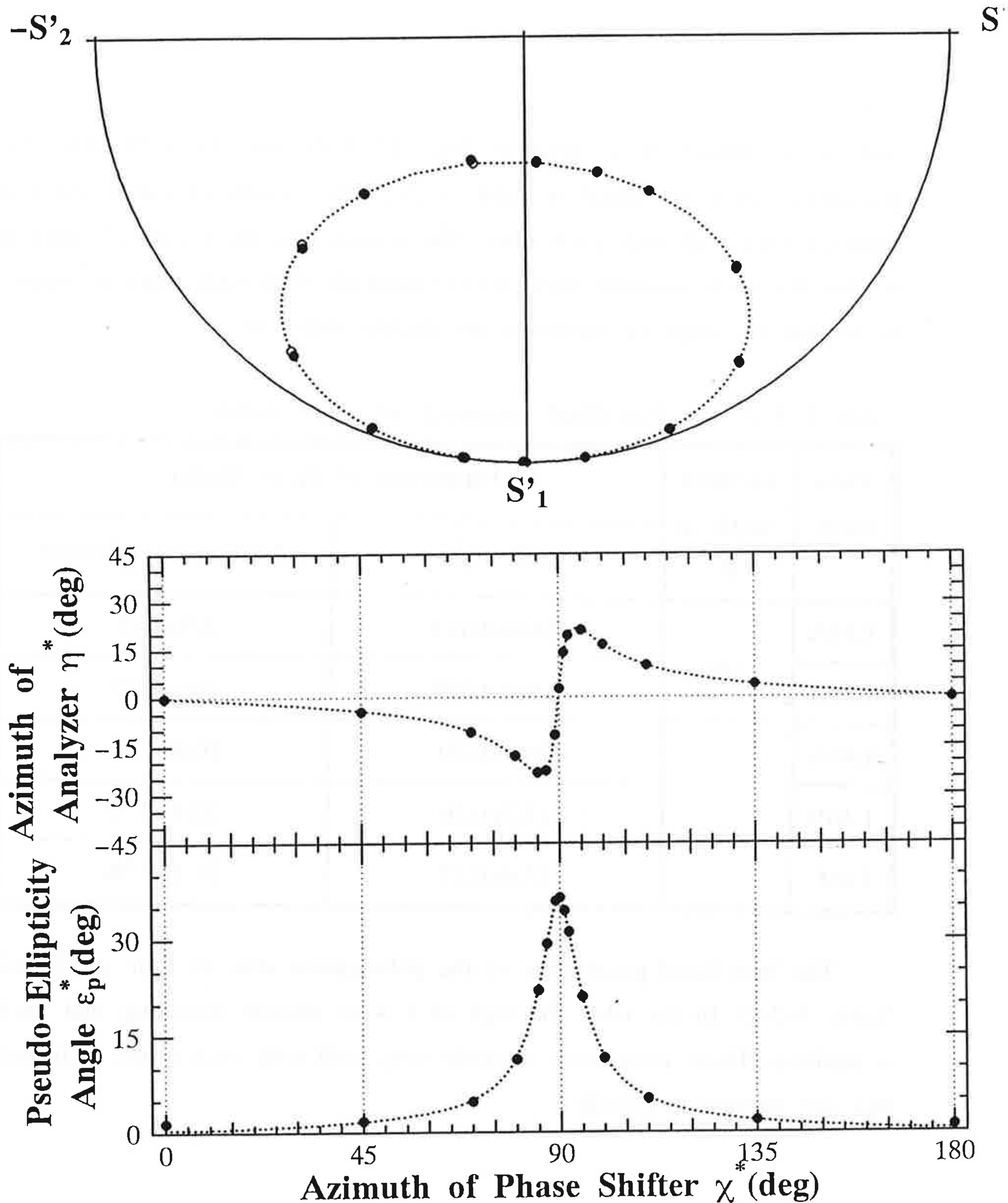

Figure 7-3-6. The values of η^* and ε_p^* of data **L46C** as function of χ^*, and the projection of these values on the S_1–S_2 plane. The solid circles show the measured data. The open circles and the curves show the fitted result.

and δ by fitting these data to Eqs. (3–3–8) and (3–3–9). The fitted parameters of P are listed in Table 7–3–2. The results of L46B and L46A coincide very well with each other. The reason why the results of other data set for the same incident angle do not coincide with each other is supposed to be that the angle of incidence are slightly different.

Table 7–3–2. The best fitted parameters of phase shifter.

Data Name	Incident Angle at P	Parameters of Phase Shifter	
		α ($\lvert r_s/r_p \rvert$)	$\lvert\Delta\rvert$(deg) (retardation)
L54A	54°	2.64±0.043	3.9±1.85
L54B		2.88±0.039	6.6±4.57
L46A	46°	10.9±0.20	10.8±1.34
L46B		13.2±0.20	20.4±2.77
L46C		13.0±0.15	21.2±2.76

The best fitted parameters of the polarization state of light are listed in Table 7–3–3. In the table the sign of ε were chosen assuming that each Δ is positive. These parameters coincide very well with each other. This means that our method is reliable.

Table 7-3-3. The best fitted parameters and the parameters of light

Data Name	Parameters of Light		
	V (Degree of Polarization)	ε(deg) (Ellipticity Angle)	δ(deg) (Azimuth of the Ellipse)
L54A	0.993±0.0031	−2.3±3.0	−0.6±0.14
L54B	0.981±0.0012	0.6±0.75	−0.6±0.09
L46A	0.978±0.0022	0.5±0.84	−0.7±0.19
L46B	0.981±0.0007	1.3±0.17	−0.5±0.07
L46C	0.979±0.0007	0.8±0.16	−0.5±0.08

7-3-2. Bending magnet

To study the degree of polarization of the on-axis and the off-axis SR from a bending magnet, we performed RAEP at BL-18A. We have changed the observation angle for SR by tilting the first mirror M_0 of the beamline (See Fig. 7-1-2).

Measurements were made for two different orientations of the mirror, $\phi=-0.075°$ and $-0.7°$, corresponding to vertical observation angles of, 0 mrad and −0.3 mrad, respectively. The nominal origin of ϕ was same as in Sec. 7-5-2. At $\phi=-0.075°$ the on-axis SR is observed. At $\phi=-0.7°$ the off-axis SR emitted below the plane of the positron orbit is observed. The names of data sets, the corresponding conditions and the angle of incidence at P are listed in Table 7-3-4.

The values of η^* and ε_p^* are plotted against χ^* and the projection of these values on the S_1–S_2 plane are plotted for these data set, as shown in Figs. 7-3-7, and 7-3-8. The results of the fitted parameters of P and for

the light are listed in Table 7-3-5, and 7-3-6.

Table 7-3-4. The Condition of Data sets.

Name	Incident Angle at P	The condition of measurement
on-Axis	47°	ϕ=-0.075°, 0 mrad
off-Axis	54°	ϕ=-0.7°, -0.25 mrad

Table 7-3-5. The best fitted parameters of phase shifter.

Name	Incident Angle at P	Parameters of Phase Shifter	
		α ($\lvert r_s/r_p \rvert$)	Δ(deg) (retardation)
on-Axis	43°	7.79±0.077	±20.6±3.0
off-Axis	54°	2.84±0.035	9.1±3.0

Table 7-3-6. The best fitted parameters and the parameters of light

Data	Parameters of Light		
	V (Degree of Polarization)	ε(deg) (Ellipticity Angle)	δ(deg) (Azimuth of the Ellipse)
on-Axis	0.970±0.008	±0.2±0.3	0.4±0.1
off-Axis	0.775±0.02	6.2±0.9	-10.8±0.3

In the measurement of the off-axis beam, the right handed circularly polarized light should be observed. From this fact we determine the signs of ε and Δ of this data set.

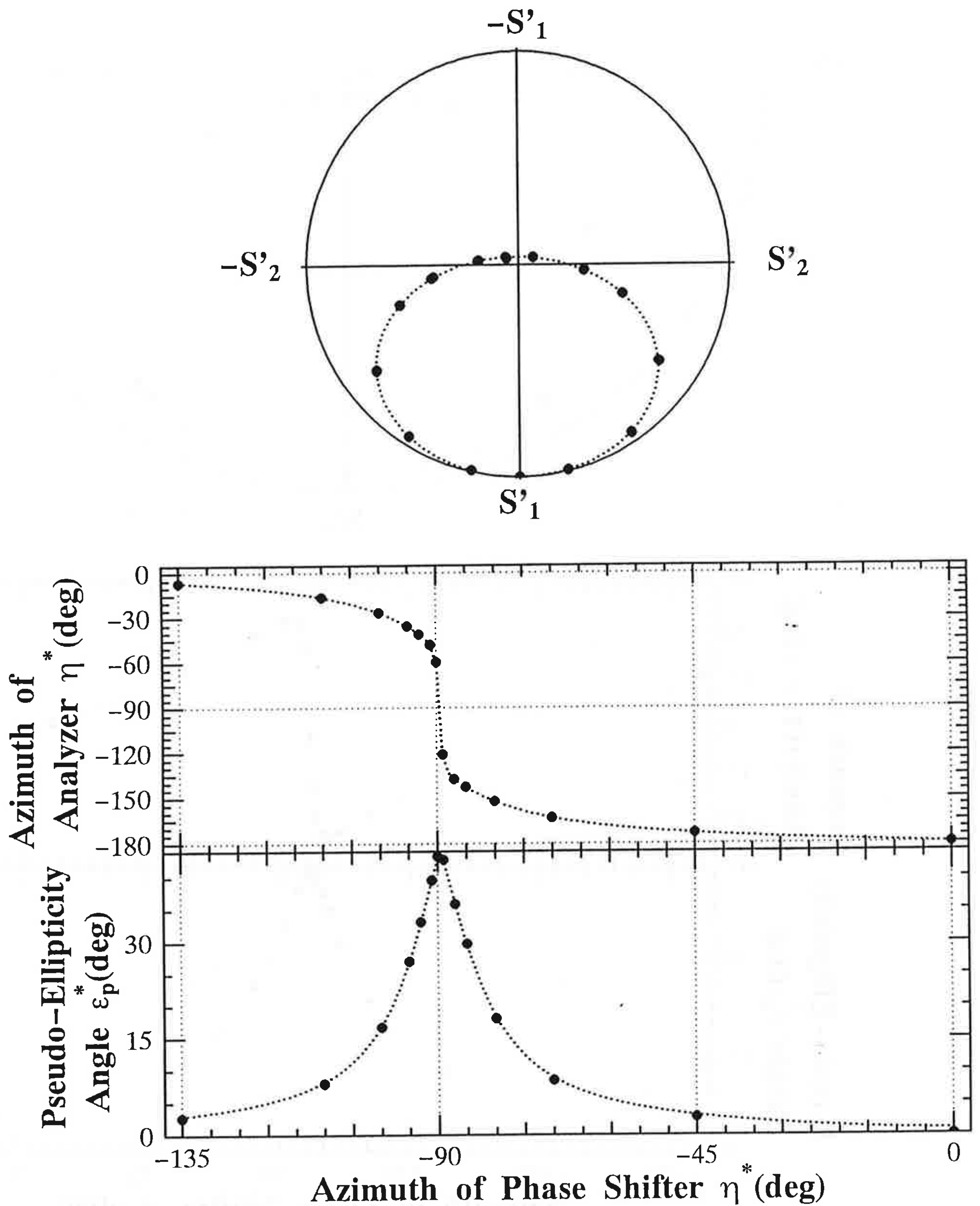

Figure 7-3-7. The values of η^* and ε_p^* of data **on-Axis** as function of χ^*, and the projection of these values on the S_1–S_2 plane. The solid circles show the measured data. The open circles and curves show the fitted result.

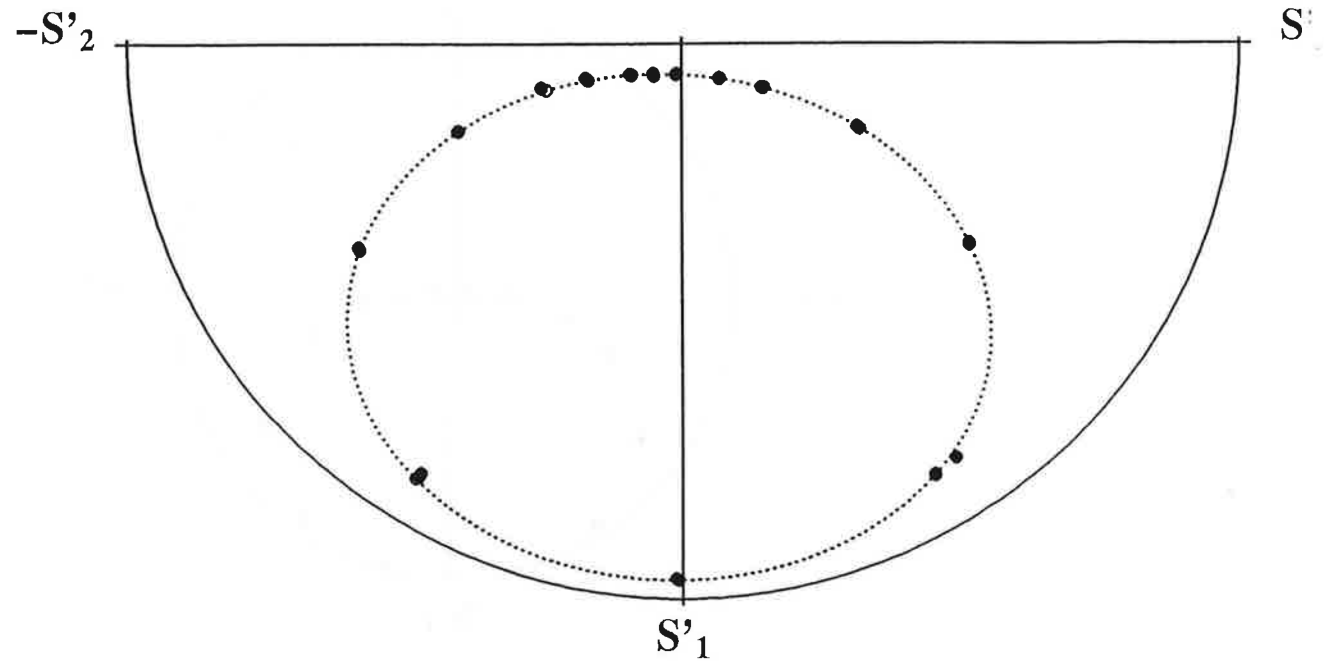

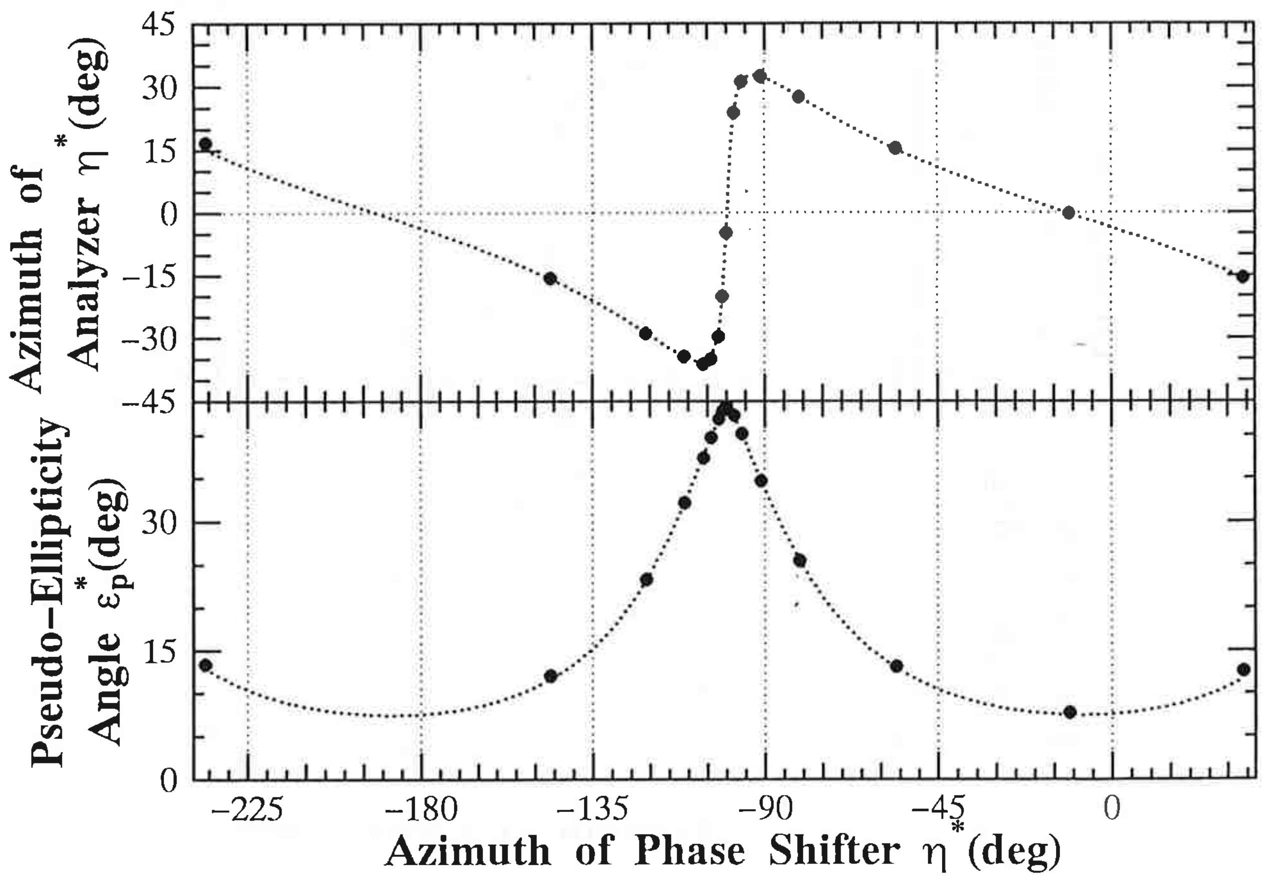

Figure 7–3–8. The values of η^* and ε_p^* of data **off–Axis** as function of χ^*, and the projection of these values on the S_1–S_2 plane. The solid circles show the measured data. The open circles and the curves show the fitted result.

Though V equals almost unity even for the off–axis beam from theoretical prediction, the observed V was far from unity. From this data, P_L and P_C were calculated to be 0.757 and 0.166, respectively.

7–3–3. Helical undulator

We performed RAEP with circularly polarized light. The gap of the undulator in the HUP mode was adjusted to emit the light with 12.8–nm wavelength in 1st harmonic. The angle of incidence at P was selected to 79°.

The values of η^* and ε_p^* are plotted against χ^* and the projection of these values on the S_1–S_2 plane are plotted for this data set, as shown in Fig. 7–3–9. As described in Sec. 3–3, we could determine five parameters. However, a region of the parameters where the residual of the fitting would be good enough and could not be found in this case, since Δ, V, and ε were strongly correlated because Δ was small and |ε| is close to 45°. The fitted parameters of P and the light are listed in Tables 7–3–7 and 7–3–8. In these table, the possible ranges for Δ, V, and ε are indicated.

Table 7–3–7. The fitted parameters of phase shifter.

Data Name	Incident Angle at P	Parameters of Phase Shifter	
		α ($\|r_s/r_p\|$)	Δ(deg) (Retardation)
C79A	79°	1.02±0.02	1~7

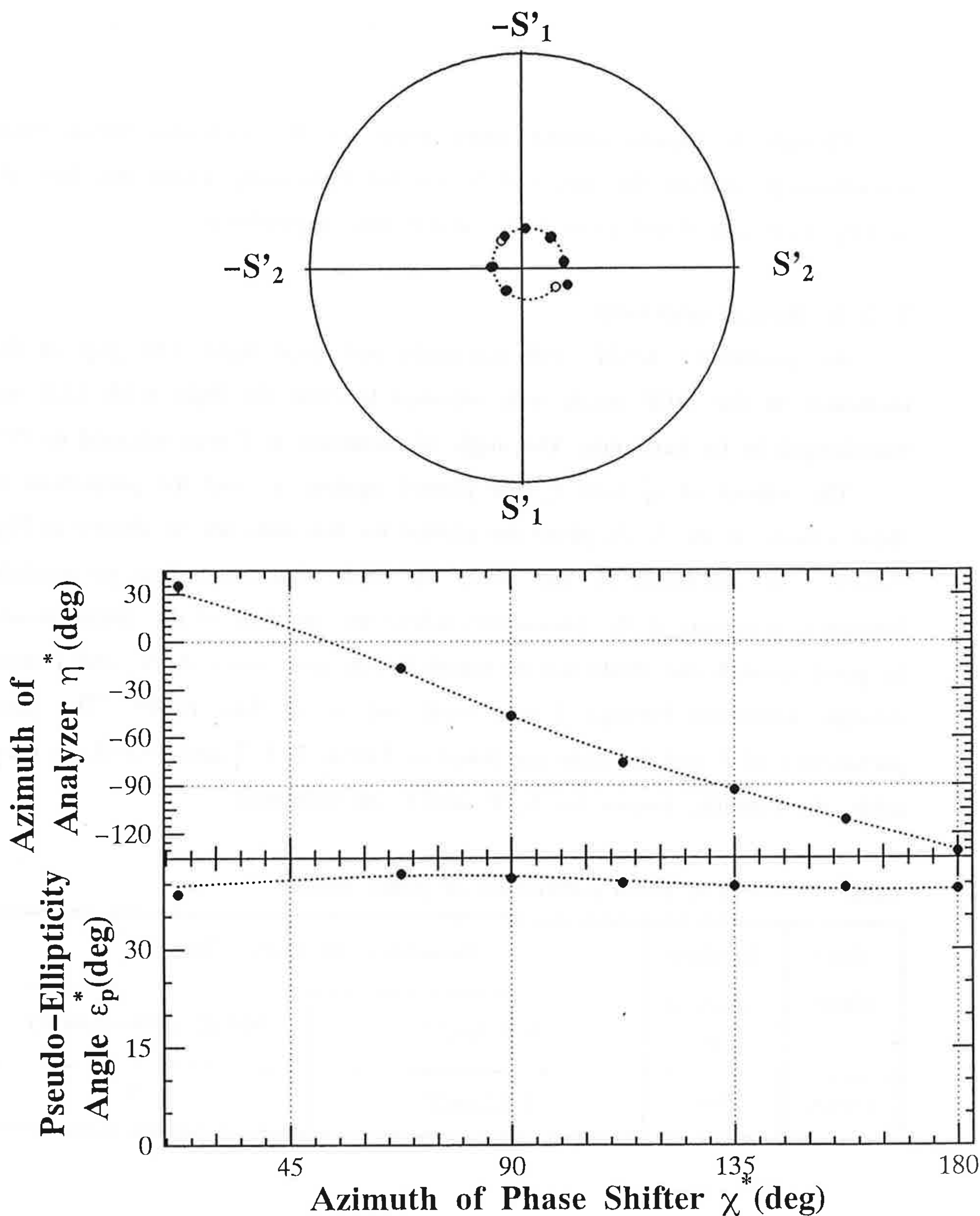

Figure 7–3–9. The values of η^* and ε_p^* of data **C79A** as function of χ^*, and the projection of these values on the S_1–S_2 plane. The solid circles show the measured data. The open circles and the curves show the fitted result.

Table 7–3–8. The fitted parameters of light.

Data Name	Parameters of Light		
	V (Degree of Polarization)	ε(deg) (Ellipticity Angle)	δ(deg) (Azimuth of the Ellipse)
C79A	0.96~0.2	40~16	–43±1

The most reliable value of α at this angle of incidence was bigger than unity (See Sec. 7–2–2). Theoretically Δ is positive at this incident angle at P. In Fig. 7–3–9 , the center of the ellipse is in the region of negative S_2. From this the sign of ε was determined.

The sign of ε, namely, the handedness of the polarization ellipse could be determined by another method, too. In Fig. 7–3–10, the triangles show RAE data of the light reflected from P, which is equivalent to the data of the above RAEP when χ^* equals 180°, and the circles show RAE data without the phase shifter(See Sec. 7–4–2). As is shown, the azimuths corresponding to the minimum intensity are about 135° (–45°). The points of these lights on the Poincaré sphere are near the longitudinal line on the axis of negative S_2. Furthermore, because the contrast factor of the reflected light is slightly smaller than that of the direct light, the point of the reflected light is closer to S_1–S_2 plane than that of the direct light. Since Δ has a positive value, the handedness of the polarization ellipse of the light is determined to be right–handed.

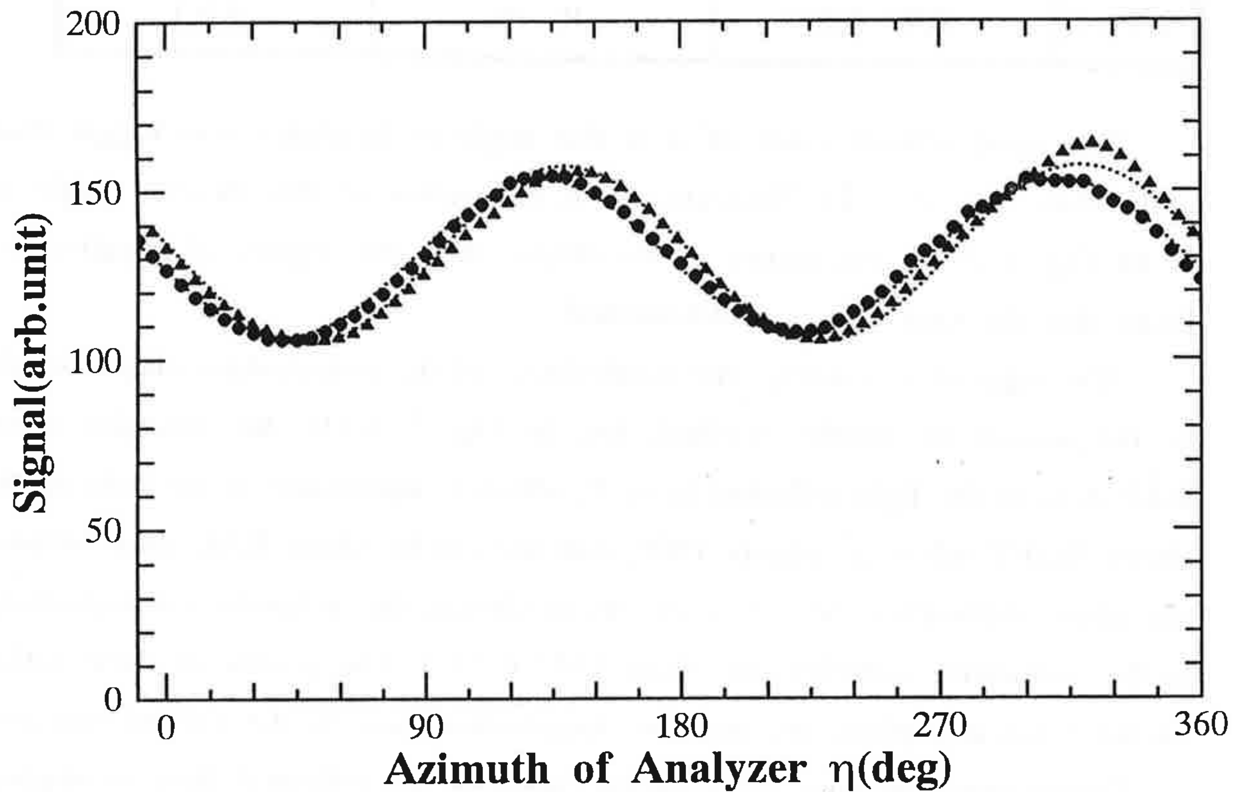

Figure 7–3–10. The detector output as function of η. The triangles show the polarimetry data of the light reflected from P, which is equivalent to the data of the ellipsometry when χ^* equals 180°, the circles show the polarimetry data without P, and the curves show the fitted results.

7-4. Rotating-analyzer ellipsometry (RAE) at BL-28

7-4-1. Linear undulator

We performed RAE for light with 12.8-nm wavelength from the linear undulator, to study the dependence of the polarization state on the gap of the undulator. By changing the gap, we have changed the peak position of the first harmonic in the spectrum of the light emitted from the undulator.

The beam intensity I_{Mon} was detected by measuring the total photoelectron current of the gold mesh set before ELLI. The detection of I_{Mon} does not have any polarization dependence.

The results of the polarization parameters obtained and the measured data are listed in Table 7-4-1. The pseudo-polarization ellipses are also illustrated in Figure 7-4-1. When 12.8 nm equals to the wavelength of the first or the second order light from the undulator, the degree of linear polarization became close to unity. The azimuth of the major axis was not changed within the experimental error in all data.

In this table, I_{Max}/I_{Min}, namely, the ratio between the intensities of the vertical component and the horizontal component was found to be proportional to I_{Mon}. Then I_{Min}, namely, the intensity of the vertical component was suggested to be constant while changing the undulator gap, in other words, changing the beam intensity of the light from the undulator. We interpret that the vertical component was created not by the undulator or the scattering of the optical element, but mainly by the bending magnets located before and after the undulator.

Table 7-4-1. The fitted parameters and the measured data.

Gap (mm)		P_L(Degree of linear polarization)	δ(Azimuth of the Ellipse)	I_{Max}/I_{Min}	I_{Min}(pA) and Applied Voltage to MCP(kV)	I_{Mon} (pA)
121		0.852±0.051	$-2.9^\circ \pm 2.9^\circ$	12.5	11.6(1.32)	68
114	1st	0.983±0.016	$0.1^\circ \pm 1.9^\circ$	113	12.3(1.32)	444
105.5		0.784±0.068	$-1.8^\circ \pm 3.6^\circ$	8.2	8.4(1.32)	49
94.5	2nd	0.968±0.022	$-0.9^\circ \pm 2.0^\circ$	50.2	18.4(1.35)	216
85	3rd	0.905±0.041	$-0.1^\circ \pm 2.6^\circ$	20.1	73.5(1.43)	83
84		0.871±0.051	$-0.1^\circ \pm 2.9^\circ$	14.5	75.4(1.43)	68

7-4-2. Helical undulator

We performed RAE for the 1st harmonic light with 12.8-nm wavelength from the helical undulator under the HUP mode and the HUN mode.

Figure 7-4-2 shows the data of MCP output obtained by rotating A plotted in logarithmic scale. The solid circles show the data of the HUP mode, and the solid triangles show the data of the HUN mode, and the curves show the results of fitting. As is shown, the azimuth of the ellipse is approximately -45° in the HUP mode, and +45° in the HUN mode. These results are discussed in Sec. 8-4.

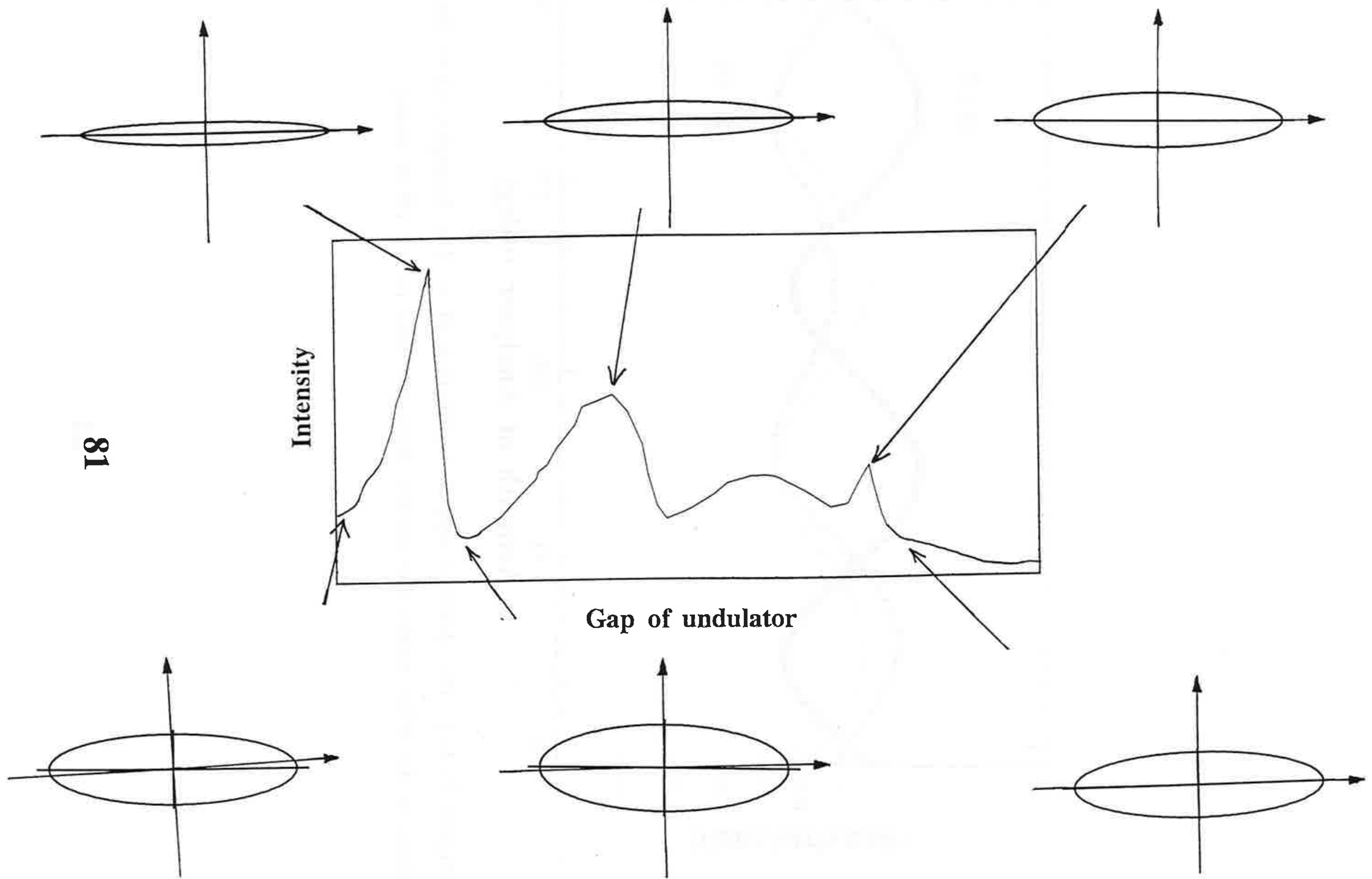

Figure 7–4–1. Changes of the pseudo–polarization ellipse varying the gap of linear undulator.

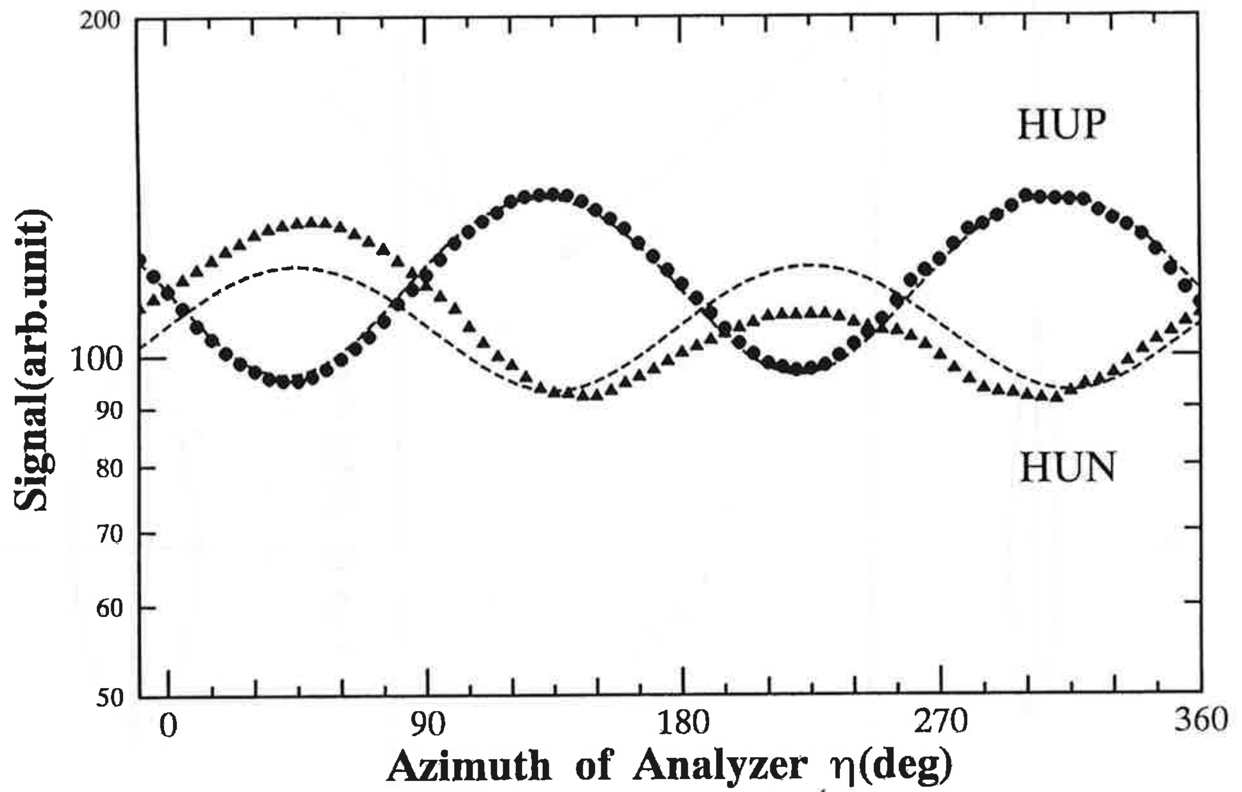

Figure 7–4–2. The detector output as function of η. The triangles show the data in the HUP mode, the circles show the data in the HUN mode.

7-5. Rotating-analyzer ellipsometry (RAE) at BL-18A

At this beamline we have carried out four kinds of RAE on the polarization states of monochromatized light as follows.

(1)The dependence on the vertical observation angle varied by moving the diaphragm.

(2)The dependence on the vertical observation angle varied by tilting the first mirror M_0 of the beamline.

(3)The dependence on the acceptance of the vertical observation angle varied by changing the width of the diaphragm.

(4)The dependence on a portion of the beam cross section cut out.

7-5-1. Dependence on the vertical observation angle varied by moving the diaphragm

We studied the dependence of the polarization state on the vertical observation angle Θ varied by moving the diaphragm (See Fig. 7-1-2). 1-mm diaphragm width corresponds to 0.1-mrad, namely, $0.5-\gamma^{-1}$. If the diaphragm is moved upward, we are able to observe SR emitted above the plane of the positron orbit. Light with 12.8-nm and 14.4-nm wavelength monochromatized by G_1 and G_2 was measured.

Figure 7-5-1 shows the measured P_L, δ, and I_{Mon} as function of the central position of the diaphragm. Four different conditions including diaphragm widths are shown in the figure caption. The behavior of the polarization state, P_L and δ, is almost the same for different conditions. P_L are found to take the maximum value when the central position of the diaphragm was at 0.5 mm. Under this condition, the beam from the monochromator is nearly completely linearly polarized with the electric vector lying in the horizontal plane. Both P_L and δ depend on the vertical observation angle Θ with respect to the plane of the positron orbit. By

---▲--- G1 12.8nm ±0.2mm
---○--- G1 14.4nm ±0.5mm
---△--- G2 12.8nm ±0.5mm
······ Calculation
---●--- G2 14.4nm ±0.5mm

Vertical Observation Angle Θ(mrad)

Linear Polarization P_L(%)

Azimuth of Ellipse δ(deg)

I_{Mon}(pA)

Central Position of Diaphragm(mm)

Figure 7-5-1. Changes in the degree of linear polarization P_L, the azimuth of the major axis δ, and the beam intensity I_{Mon} as function of the central position of the diaphragm.

shifting the origin of the central position of the diaphragm to 0.5 mm and converting that to Θ, we found that the measured dependence of P_L corresponds to the theoretical prediction of emitted SR given by Kitamura[7-3] as shown by the dotted curve. However, the measured dependence of δ does not seem to be explained readily by the calculation. The interpretation is discussed in Sec. 8.

7-5-2. Dependence on the vertical observation angle varied by tilting the first mirror

The observation angle Θ of the emitted SR depends largely on the orientation of the first mirror M_0 of the beamline (See Fig. 7-1-2). That is, if M_0 is inclined upward or downward, we are able to observe SR emitted off plane. We studied the polarization state varying the vertical inclination angle ϕ of M_0. Light with 12.8-nm wavelength monochromatized by G_2 was measured.

Figure 7-5-2 shows the measured P_L, δ, and I_{Mon} as function of ϕ in which the origin of ϕ is arbitrary. At each value of ϕ we realigned the beamline optics to optimize I_{Mon} by adjusting the horizontal tilt of M_0 and the vertical tilt of the M_2. As is shown, when P_L takes the maximum value at 0.075°, the beam is most horizontally linearly polarized. P_L and δ change systematically as in Sec. 7-5-1. However, the change of the intensity of the beam is completely different from the result of Sec. 7-5-1. The intensity increased with decrease of P_L.

We guess two reasons. One is the contamination on M_0 or the thermal distortion of M_0, which was formed at the part exposed to well polarized and very powerful in plane SR. The other reason is that the monochromator was accidentally optimized for an incident optical path, which deviated from the orbit plane, and it is possible that the intensity at the beam monitor is not proportional to the intensity at M_2. This tells us that it is difficult to get good

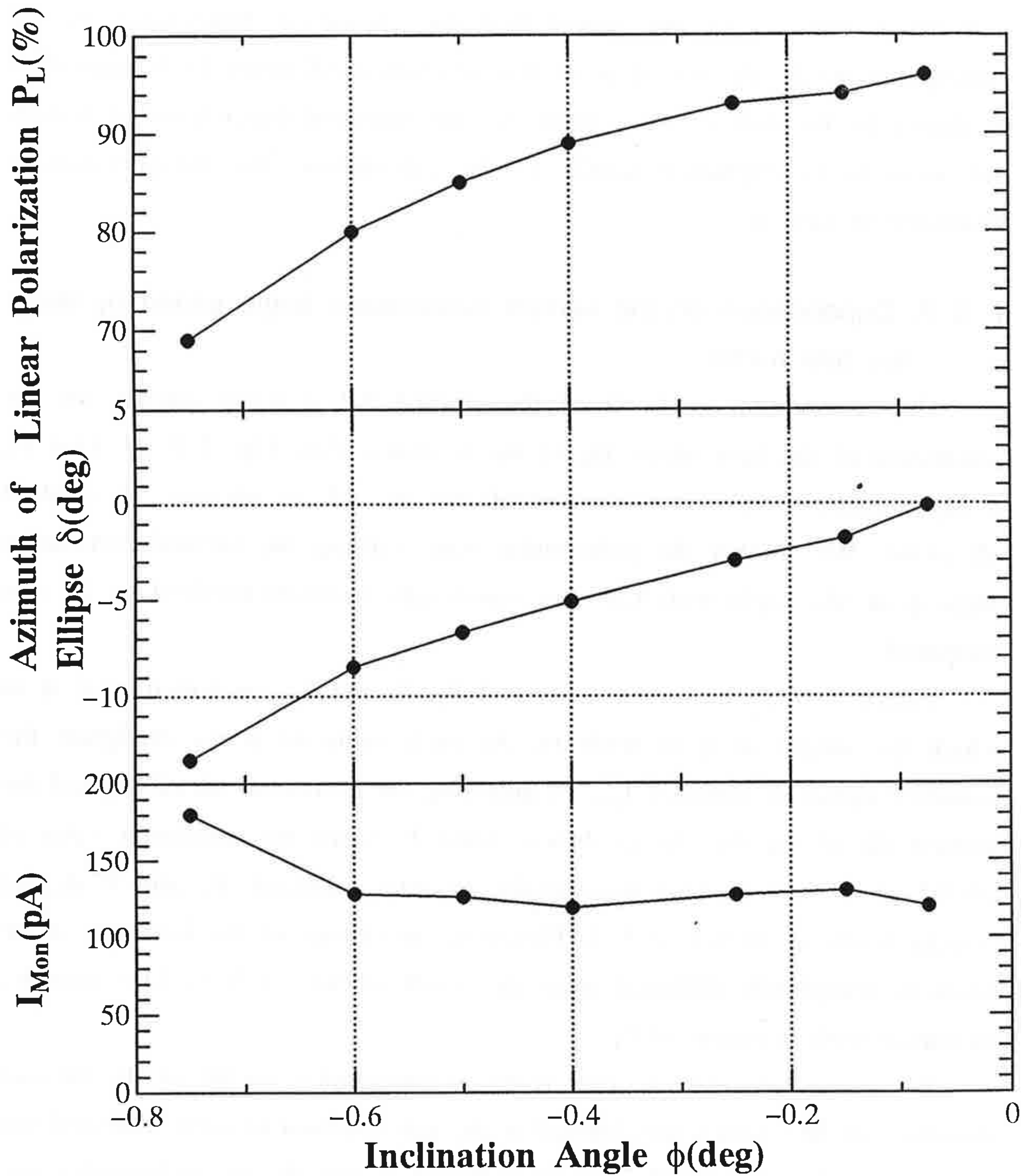

Figure 7-5-2. Changes in the degree of linear polarization P_L, the azimuth of the major axis δ, and the beam intensity I_{Mon} as function of the inclination angle ϕ of M_0. ϕ has an arbitrary origin.

linear polarization only by adjusting the first mirror only by monitoring intensity but without polarization measurement.

7-5-3. Dependence on the acceptance of the vertical observation angle

We have studied the dependence of the polarization state on the vertical acceptance angle Θ_w by changing the width of the diaphragm of the beam line (See Fig. 7-1-2). Light with 12.8-nm wavelength monochromatized by G_2 was measured. 1-mm width of the diaphragm corresponds to 0.1 mrad and 0.5 γ^{-1} of the acceptance angle Θ_w.

Figure 7-5-3 shows P_L, δ, and I_{Mon} as function of Θ_w. P_L kept a value higher than 94% when Θ_w was smaller than 0.1 mrad, and decreased gradually down to 90% until it reaches to 0.8 mrad. δ was not changed within the experimental error. I_{Mon} increased rapidly until Θ_w reaches to 0.2 mrad, and increased slightly when over 0.2 mrad.

7-5-4. Dependence on a portion of the beam cross section

The horizontal and the vertical sizes of the beam cross section at the upstream pinhole of ELLI are 2.0 mm, 0.7 mm, respectively. We have studied the uniformity of the polarization state dependent on the accepted portion of the beam cross section. The central, right, and left portions of the cross section were cut out by the ϕ1-mm pinhole. Light with 12.8-nm wavelength monochromatized by G_2 was measured. The fitted results are shown in Table 7-5-1. Both the degree of linear polarization and the azimuth of the major axis were not changed within the experimental error.

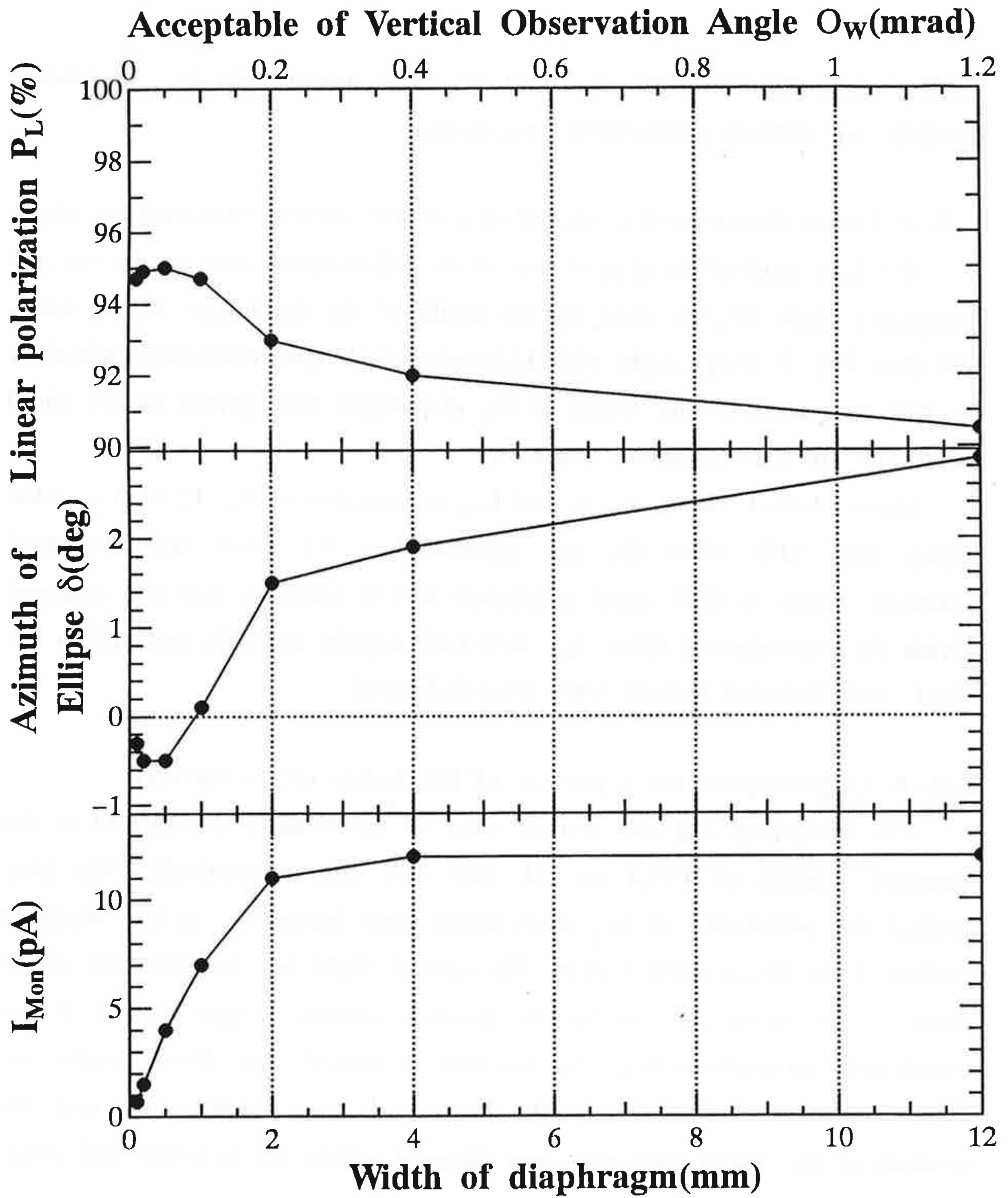

Figure 7-5-3. Changes in the degree of linear polarization P_L, the azimuth of the major axis δ, and the beam intensity I_{Mon} as function of the width of the diaphragm.

Table 7-5-1. The fitted results of the measured data varying the portion of the beam cross section.

Measured portion of the beam cross section	P_L (Degree of Linear Polarization)	δ (Azimuth of the Ellipse)
center	0.961±0.007	0.3°±0.8°
right side	0.960±0.013	−0.6°±1.5°
left side	0.960±0.009	0.5°±1.0°

7-6. Rotating-analyzer ellipsometry (RAE) at INS-SOR BL-1'

The inclination of the major axis of the polarization ellipse of synchrotron radiation (SR) which in the measurements described in Sec. 7-5-1 was dependent on the vertical observation angle. To check this is an intrinsic characteristic of SR or just an effect induced by beamline optics, we performed RAE for a direct beam of SR. The measurement was done using SOR-RING (380 MeV), which is a low energy storage ring and does not emit hard x-rays. The value of γ^{-1} derived from the energy of SOR-RING equals 1.34 mrad.

The polarization measurement was carried out at BL-1' which is a beamline for white SR. Figure 7-6-1 shows the experimental setup. The diaphragm limits the vertical observation angle of SR to within ±1 mrad, namely, ±0.75 γ^{-1}. The movable ϕ2.5-mm pinhole can change the observation angle between ±0.8 mrad, ±0.6 γ^{-1}.

We used a 101-layer Mo/Si multilayer mirror for as analyzer at 38° angle of incidence from normal. The analyzer is mounted on an aluminum triangular holder with ϕ1.5-mm pinhole attached to the shaft end of a vacuum shielded rotary indexer RI for azimuthal angle driving. An Al filter and a photodiode (G2119, HAMAMATSU Co. Ltd.) D are fixed on the holder rigidly and receive the light reflected from A.

The wavelength for maximum reflectance of the analyzer at the above incident angle is 13.0 nm. Therefore we measured quasimonochromatic light with 15.5~13.8-nm wavelength by this system. In this measurement, we observed only the azimuth of the major axis of the polarization ellipse, not the degree of linear polarization.

We studied the azimuth of the major axis by varying the vertical observation angle Θ. The data were obtained for Θ=0 mrad, 0.8 mrad, 2.3 mrad, and -2.6 mrad. We realigned analyzer for each measurement. For Θ=0

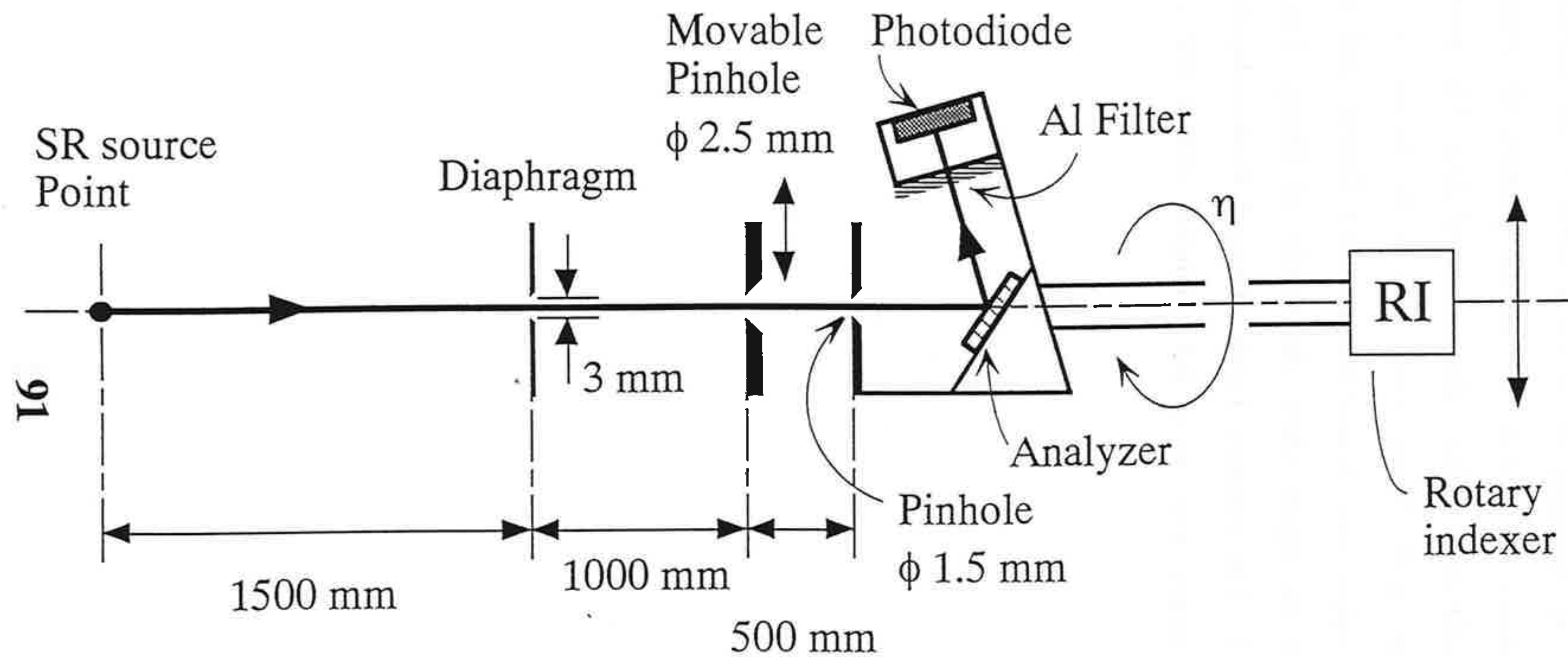

Figure 7-6-1. Side view of the setup of the direct polarization measurement at SOR-RING BL-1'

mrad and 0.8 mrad, we changed Θ by moving the pinhole, and for Θ=2.3 mrad and −2.6 mrad by changing the electron orbit of the storage ring.

Figure 7−6−2 shows some data sets of the photodiode output obtained by rotating A. The solid circles show the measured data. The numbers in the figure shows the value of Θ. Fitting these data to the theory, we determined the azimuths of the major axis δ and the contrast factors and these errors. The dashed curves in the figure show the results of fitting. The results are listed in Table 7−6−1. The contrast factor changed systematically. However the azimuth of the major axis were not changed within the experimental error.

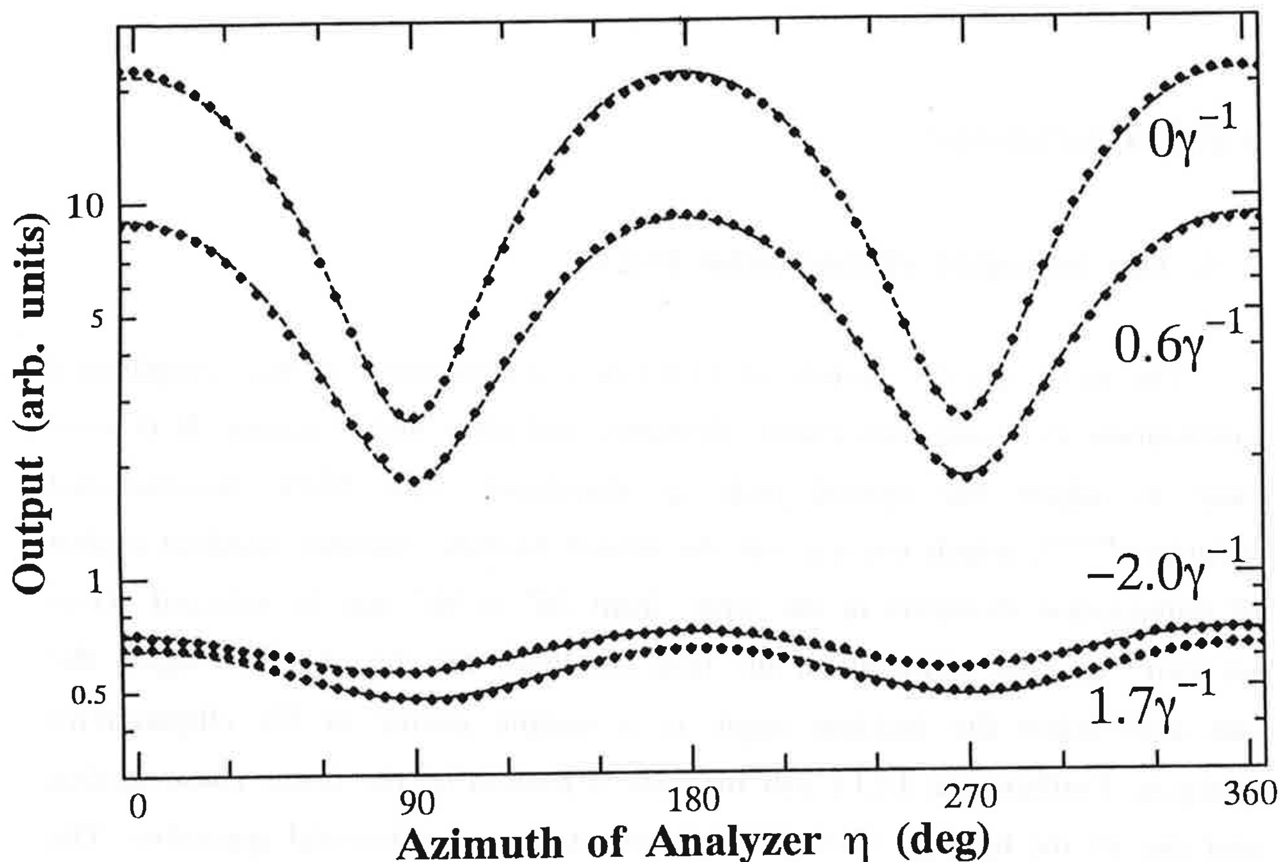

Figure 7-6-2. Detector output at different observation angles Θ. The solid circles show the measured data and the dashed curves show the result of fitting.

Table 7-6-1. The best fitted parameters.

Θ (Vertical Observation Angle)		C_{ont} (Contrast Factor)	δ (Azimuth of the Ellipse)
0mrad	$0\gamma^{-1}$	0.785±0.022	$-0.4^\circ \pm 1.4^\circ$
0.8mrad	$0.6\gamma^{-1}$	0.664±0.026	$0.2^\circ \pm 1.7^\circ$
2.3mrad	$1.7\gamma^{-1}$	0.148±0.027	$2.8^\circ \pm 6.5^\circ$
-2.6mrad	$-2.0\gamma^{-1}$	0.114±0.024	$-2.9^\circ \pm 7.2^\circ$

VIII. Discussion

8-1. The beamline ellipsometer ELLI

The most specific feature of ELLI is a combination of the complicated mechanism for using two mirror elements and ultra high vacuum. It is very easy to adjust the optical axis as compared with VUV conventional polarizers[1C,1R], which use e.g. six Au coated mirrors. Suitable incident angles of polarization elements in the range from 20° to 90° can be selected. Thus we can use the elements in the best condition for the observed light. We can also select the incident angle to a sample mirror in SX ellipsometry analysis. Furthermore ELLI can measure a portion of the beam cross section and can let the light go through to a downstream experimental apparatus. The above features are indispensable for a SR beamline ellipsometer.

The wavelength of the light measurable by ELLI depends on the polarization elements used. Not only multilayer mirrors, but ordinary monolayer mirrors (for example Au coated mirror), transmission type multilayers, and also crystals can be mounted in ELLI.

8-2. Multilayers as polarization elements

The multilayer mirror used in this study performed well as analyzer. Because of its high polarizance, MCP which has a high efficiency could be used as a detector(See Sec. 3-2). Multilayers are dispersive elements and can also be used as a high-cutoff filter for higher order light. Therefore the useful wavelength range of a multilayer analyzer is usually small. However, it was found that the useful range became larger with use of a high efficiency detector, like the MCP used. For the multilayer used, the polarizance was higher than 0.98 in the wavelength range from 10 nm to 20

nm.

On the other hand, the present multilayer mirror could not be used as phase shifter, because the retardation at the incident angle used was too small. However, that is not general problem of multilayers. We hope the future development of multilayers optimized for a phase shifter[8A,8B,8C,8D].

8-3. Analytical method of rotating-analyzer ellipsometry with phase shifter

It was found that our analytical method of RAEP is more effective to the linearly polarized light than to the off-axis SR from a bending magnet. By this method, we could determine the polarization state of the light without detailed information on the phase shifter used.

However, the polarization state of the light from the helical undulator which is close to circular polarization could not be accurately determined. One reason is that the retardation of the phase shifter used was too small. The other reason is that the present analysis method is insensitive to light which is close to perfect circular polarization.

In future, to measure perfectly circularly polarized light we should perform the polarization measurement with compensator which is a phase shifter of which the polarization characteristics known.

8-4. The major axis of the polarization ellipse (δ) and the degree of linear polarization (P_L) of the light emerging from the monochromator at a bending magnet beamline

From rotating analyzer ellipsometry (RAE) for the monochromatized light at the bending magnet beamline, we found that the dependence of δ on the vertical observation angle (Θ) (See Sec. 7-5) is evaluated 5 degree/γ^{-1}.

However, we could not find such a dependence from RAE for the direct white SR (See Sec. 7–6). Therefore this must be due to the optical elements in the beamline.

Generally a reflective surface of medium having absorption has small but positive phase retardation in the glancing angle region. Noticing this, we calculated this effect of phase retardation on the polarization state using the data calculated by Kitamura for light source. Figure 8–1 shows calculated δ for several retardations as function of Θ. If the sign of Θ is positive, the SR emitted above the plane of positron orbit is calculated. As shown in this figure, when the light is left– (right–)handed circularly polarized, the sign of δ is positive (negative). Figure 8–2 shows the calculated P_L as function of Θ. Due to this the retardation, P_L is increased. Consequently, the measured dependence of δ on Θ and the increase of P_L can be explained by this effect of phase retardation of the beamline optics. From RAEP data (See Sec. 7–3–2) we knew the measured degree of polarization of off–axis light is different from that by theoretical prediction. Therefore we did not evaluate the total polarization characteristics of the beamline.

The difference between δ's of the monochromatized light from the helical undulator in the HUP mode and that in the HUN mode can be explained in the same reason (See Sec. 7–4–2).

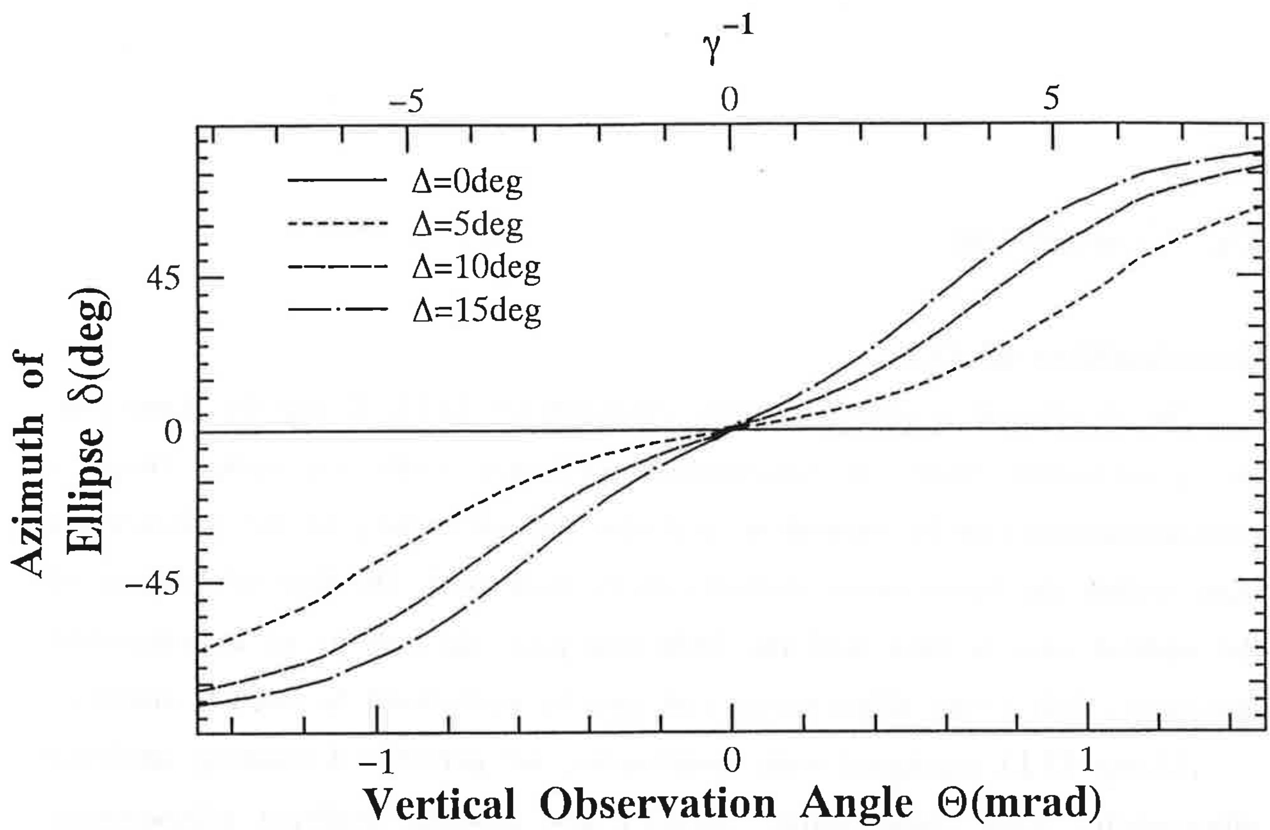

Figure 8–1. The calculated azimuths δ of the polarization ellipse as function of the vertical observation angle Θ for different phase retardations Δ.

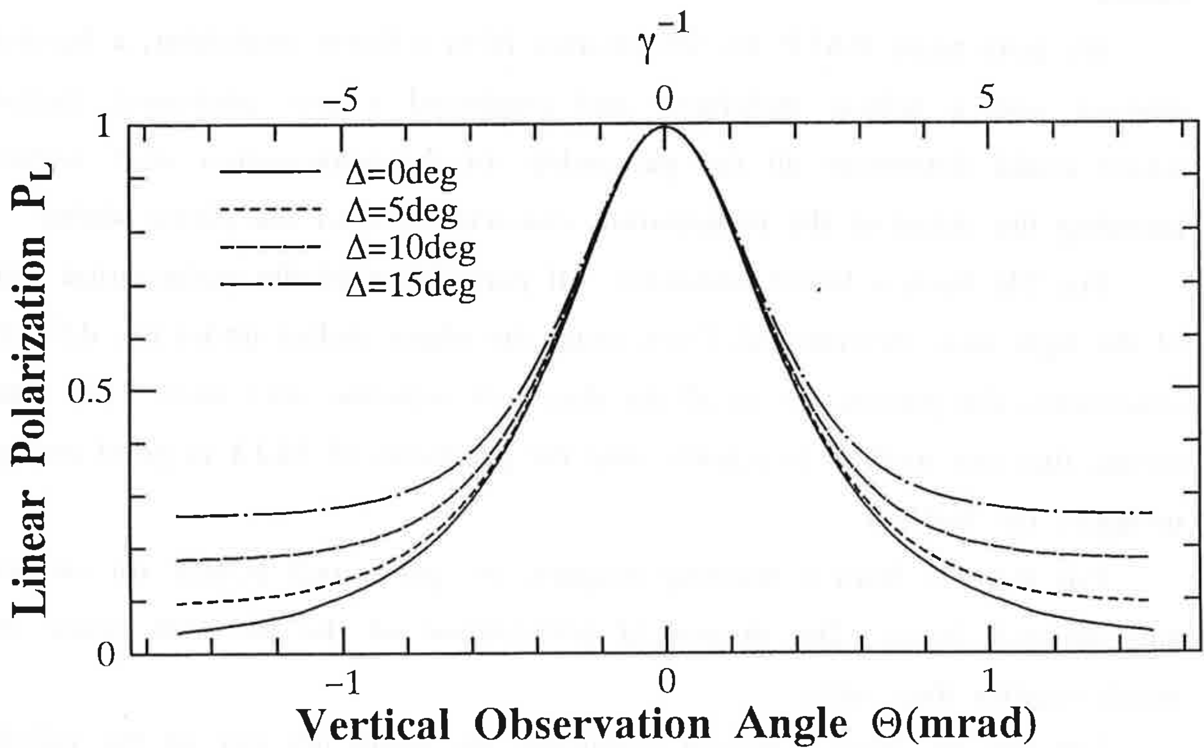

Figure 8–2. The calculated degree of linear polarization P_L as function of the vertical observation angle Θ for different phase retardations Δ.

IX. Conclusion

Construction of ELLI

We developed a novel beamline ellipsometer ELLI. Using the apparatus, the polarization state of synchrotron radiation (SR) emerging from a monochromator can be measured, and also the uniformity of the polarization state within the beam cross section can be measured. On–line adjustment of the optical axis is easy and the light can pass through to an experimental apparatus. Soft x–ray ellipsometry can also be performed to sample mirrors.

Using ELLI equipped with multilayers, we performed rotating–analyzer ellipsometry with phase shifter (RAEP) and rotating–analyzer ellipsometry (RAE) for SR of 12.8–nm wavelength. We obtained results as described below.

RAEP

We performed RAEP for SR emitted from a linear undulator, a bending magnet, and a helical undulator, and employed a new analytical method which could determine all the parameters of the polarization state without knowing the detail of the polarization characteristics of the phase shifter.

For SR from a linear undulator, all parameters of the polarization state of the light were determined. Even using the phase shifter under the different conditions, the parameters in all the data sets coincide very well. This result means that our method is reliable and the precision of ELLI is good enough to apply the method.

For the SR from a bending magnet, we performed RAEP for on–axis and off–axis beam. The degree of polarization of the off–axis beam was much smaller than unity.

For the SR from a helical undulator, we could not get all the reliable results of the polarization state due to the following reasons. Our method is

essentially insensitive to circular polarization when the phase retardation of the polarizer is small. To determine all the parameters of the polarization state with higher accuracy, we should measure more accurately the parameters of the phase shifter in advance or we should develop a phase shifter with larger phase retardation. However, we could determine the handedness of the polarization ellipse. It agrees with the handedness of the positron motion in the undulator.

RAE

It was concluded from RAE data for the SR from the undulator that the vertical component of the intensity did not depend on the gap of undulator, namely, on the total intensity from the undulator. This means that the vertical component comes mainly from the bending magnets radiation, which sandwich the undulator.

It was found that the degree of linear polarization of the monochromatized light from the bending magnet is dependent on the vertical observation angle, which agrees with theoretical predictions quantitatively. It was also found that the polarization of the light is dependent on the vertical observation angle especially, appearing as the inclination of the major axis of the polarization ellipse. On the other hand, direct SR light from the bending magnet was found to be independent of the vertical observation angle. Thus it was concluded that the above inclination is caused by the optical elements of the monochromator. The inclination could be explained as the effect of the retardation due to the optical elements of the beamline. The effect was found also in the monochromatized light from the helical undulator.

Any nonuniformity of the polarization state within the beam cross section was not detected.

X. Acknowledgements

I express my sincere appreciation to Prof. T. Miyahara for his kind and invaluable guidance. I am much indebted to Dr. M. Yamamoto for encouragement and helpful suggestions throughout my work. I would like to express my thanks to Dr. Y. Kagoshima and Dr. S. Muto for their help to set up the system for measurement at BL–28A, to Dr. S. Suzuki and Dr. T. Kinoshita for their help during measurement at BL–18A, and to Prof. Y. Kamiya and Dr. T. Koseki for their help using SOR–RING. I am grateful to Dr. Yanagihara and all other members of the soft x–ray laboratory (Res. Inst. Sci. Meas., Tohoku Univ.) for their helpful discussions and supply good multilayers. My gratitude is also given to the staff in the Photon Factory for their assistance on the performance of my experiment.

Finally, I heartily thank my wife and my parents who always encouraged me and gave me unfailing support.

1993 *Hiroaki Kimura*

This work has been performed under the approval of the Photon Factory Program Advisory Committee (proposal No. 91–154). Another part of work was carried out by a joint research between the Institute for Solid State Physics and the University of Tokyo. This work was supported in part by a Grant–in–Aid for Scientific Research on Priority Area "X–Ray Imaging Optics", No. 63420023 from the Ministry of Education, Science, and Culture, Japan.

XI. References

[1A] U. Heinzmann, J. Phys. **B13**, 4353 (1980).

[1B] S. Yamamoto and H. Kitamura, Jpn. J. Appl. Phys. **26**, L1613 (1987).

[1C] T. Koide, T. Shidara, M. Yuri, N. Kandaka, K. Yamaguchi, and H. Fukutani, Nucl. Instr. and Meth. A **308**, 635(1991).

[1D] E. Spiller, In Proceed. of IX Intern. Conf. of Intern. Commission of Optics, Santa Monica, CA, 581(1972).

[1E] H. Kimura, T. Maehara, M. Yamamoto, M. Yanagihara, W. Okamoto, S. Mitani and T. Namioka, Photon Factory Activity Report #8, 241(1990).

[1F] A. Khandar and P. Dhez, SPIE **563**, 158(1985).

[1G] E.S. Gluskin, S.V. Gaponov, P. Dhez, P.P. Ilyinsky, N.N. Salashchenko, Yu.M. Shatunov, and E.M. Trakhtenberg, Nucl. Instr. and Meth. A **246**, 394(1986).

[1H] A. Khandar, P. Dhez, and M. Berland, SPIE **688**, 176(1986).

[1I] P. Dhez, Nucl. Instr. and Meth. **A261**, 66(1987).

[1J] Yu.M. Alexandrov, A.I. Fedorenko, V.V. Kondratenko, M.O. Koshevoi, I.V. Kozhevnikov, V.A. Murashova, A.A. Rupasov, A.S. Shikanov, A.V. Vinogradov, M.N. Yakimenko, and N.N. Zorev, Rev. Sci. Instrum. **60(7)**, 2124(1989).

[1K] M. Yamamoto, M. Yanagihara, H. Nomura, K. Mayama, and H. Kimura, Rev. Sci. Instrum. **63(1)**, 1510(1992).

[1L] H. Kimura, M. Yamamoto, M. Yanagihara, T.Maehara, and T. Namioka, Rev. Sci. Instrum. **63(1)**, 1379(1992).

[1M] K. Codling and R.P. Madden, J. Appl. Phys **36(2)**, 380(1965).

[1N] G. Rosenbaum, B. Feuerbacher, R.P. Godwin, and M. Skibowski, Appl. Opt. **7**, 1917 (1968).

[1O] U. Heinzmann, B. Osterheld, and F. Schäfers, Nucl. Instr. and Meth. **195**, 395(1982).

[1P] M. Schledermann and M. Skibowski, Appl. Opt. **10**, 321 (1971).

[1Q] W.B. Westerveld, K.Becker, P.W. Zetner, J.J. Corr, and J.W. McConkey, Appl. Opt. **24(14)**, 2256(1985).

[1R] A. Gaupp and W. Peatman, SPIE **733**, 272 (1986).

[1S] T. Koide, T. Shidara, M. Yuri, N. Kandaka, H. Fukutani, and K. Yamaguchi, Rev. Sci, Instrum. **63(1)**, 1458(1992).

[1T] T. Ishikawa, K. Hirano, and S. Kikuta, J. Appl. Cryst. **24**, 982(1991).

[2A] J.M. Bennett, and H.E. Bennett, "Handbook of Optics", W.G. Driscoll and W. Vaughan, eds., McGraw & Hill, N. Y. Chap. 10.

[2B] W.A. Shurcliff, "POLARIZED LIGHT PRODUCTION AND USE", Harvard Univ. Press. (1962).

[5A] H. Domeki, H. Satomi and I. Kusunoki, Rev. Sci. Instrum. **63(8)**, 3913(1992).

[7A] Y. Kagoshima, S. Muto, T. Miyahara, T. Koide, S. Yamamoto, and H. Kitamura, Rev. Sci. Instrum. **63(1)**, 1289(1992).

[7B] S. Suzuki, T. Kashiwakura, A. Kakizaki, T. Kinoshita, A. Harasawa, J. Fujii, S. Suga, M. Fujisawa, H. Kato, S. Sato, and T. Ishii, Activity Report of SRL–ISSP. 1989, p.60–63.

[7C] H. Kitamura(National Laboratory for High Energy Physics, Tsukuba, Japan) private communication, a graph is given in Insertion Device Handbook, (Photon Factory, Tsukuba, 1990), p. 80.

[8A] J. B. Kortright and J. H. Underwood, Nucl. Inst. and Meth. A **291**, 272(1990).

[8B] J. B. Kortright, H. Kimura, V. Nikitin, K. Mayama, M. Yamamoto, and M. Yanagihara, Appl. Phys. Lett. **60(24)**, 2963(1992.

[8C] H. Nomura, K. Mayama, T. Sasaki, M. Yamamoto and M. Yanagihara, SPIE **1720**, 395(1992).

[8D] H. Kimura, M. Yamamoto, H. Nomura, K. Mayama, and M. Yanagihara, Summaries of papers presented at the Physics of X–ray Multilayer Structures Topical Meeting for Optical Society of America(Jackson Hole, USA 1992), p. 174.